



# MONASH University

**The Investigation of Red Cell Mutants  
Identified in an ENU Mutagenesis Screen**

Ashlee Jade Conway

ID: [REDACTED]

A thesis submitted for the degree of Doctor of Philosophy at

Monash University in 2018,

Central Clinical School

Australian Centre for Blood Diseases

## **Copyright notice**

© Ashlee Jade Conway (2018)

I certify that I have made all reasonable efforts to secure copyright permissions for third-party content included in this thesis and have not knowingly added copyright content to my work without the owner's permission.

---

## Abstract

Erythropoiesis is defined as the generation of mature erythrocytes, or red blood cells, from haematopoietic progenitors. There are a number of genes, molecular pathways, and cellular processes within erythropoiesis which can be disrupted by inheritable mutations and result in diseases of the red cell, such as anaemia. Clinical outcomes of human anaemic disorders range in severity from asymptomatic to fatal, prompting the need to develop effective clinical treatments which target dysfunctional erythroid pathways. Although animal-based experiments have widely contributed to the fundamental understanding of inheritable anaemias, many underlying mechanisms of red cell pathology still remain elusive. The chemical mutagen N-ethyl-N-nitrosourea (ENU) has proven to be highly effective in genome-wide forward genetic screens for the study of organ-specific diseases in model organisms, such as mice. In order to identify novel regulators of erythropoiesis, we have undertaken a series of dominant and recessive ENU screens that has generated three mouse strains with unique red cell phenotypes. This thesis details the investigations of those mutant mice, which not only offer new insights into the genes and molecular mechanisms underlying erythropoiesis, but also present new experimental models of human red cell diseases.

Using ENU mutagenesis to identify red cell phenotypes in mice, three vital erythropoietic pathways have been reviewed in this study. Firstly, the haem biosynthesis pathway is crucial for the production of haemoglobin, and defects within the enzymes of this pathway can manifest in humans as a rare condition known as porphyria. Hereditary coproporphyria, a rare subtype of this disease, is highly heterogeneous in clinical manifestation, prompting the need to develop better therapeutic approaches with the help of animal models. Using ENU mutagenesis, we have identified the first murine model of hereditary coproporphyria, called RBC16, with a phenotype analogous to the human disease.

Anaerobic glycolysis is the fundamental energy-synthesising pathway within enucleated red blood cells. Mutations which disrupt the enzymes of this pathway can manifest as severe haemolytic anaemias with fatal clinical outcomes. Triosephosphate isomerase (TPI) deficiency is the rarest and most severe glycolytic enzymopathy, for which no treatment or long-term management strategy has been developed. This study describes a recessive ENU mutagenesis screen which identified a mouse mutant, RBC19, found to be a novel model of TPI deficiency. Using this model, we have demonstrated the effectiveness of a bone marrow transplant in rescuing the red cell phenotype and glycolytic defects, the results of which have translatable implications towards the clinical management of TPI deficiency.

Lastly, iron metabolism is a complex multifaceted pathway involving many genes, hormones, and transcription factors. The erythroid-specific transferrin receptor is central to this process, and mutations that occur within this receptor have shown to cause anaemic phenotypes in experimental models. A novel ENU mutagenesis mutant mouse, RBC21, offers a unique perspective on transferrin receptor function and its role in red cell pathology. New technology has allowed us to visualise for the first time the effects of various transferrin receptor mutations on protein structure, expression, and function on a single-cell level.

---

## Publications during enrolment

**Conway, A.J.**, Brown, F.C., Fullinfaw, R.O., Kile, B.T., Jane, S.M. and Curtis, D.J., (2017). A mouse model of hereditary coproporphyrinemia identified in an ENU mutagenesis screen. *Disease Models & Mechanisms*, 10(8), pp.1005-1013.

**Conway, A.J.**, Brown, F.C., Burgio, G., Morton, C.J., Jane, S.M. and Curtis, D.J., (2018). Bone marrow transplantation corrects haemolytic anaemia in novel ENU mutagenesis mouse model of TPI deficiency. *Disease Models & Mechanisms*, 11(5), pp. dnm-034678.

**Conway, A.J.**, Brown, F.C., Rank, G., Kile, B.T., Morton, C.J., Jane, S.M. and Curtis, D.J., (2018). Characterisation of *Tfr* mutant mice with microcytic phenotypes. *Blood Advances*, 2(15) pp. 1914-1922.

^Brown, F.C., **Conway, A.J.**, Cerruti, L., Collinge, J.E., McLean, C., Wiley, J.S., Kile, B.T., Jane, S.M. and Curtis, D.J., (2015). Activation of the erythroid K-Cl cotransporter Kcc1 enhances sickle cell disease pathology in a humanized mouse model. *Blood*, 126(26), pp.2863-2870.

*^Data from this publication will not be discussed in this thesis.*

---

## Thesis including published works: Declaration

I hereby declare that this thesis contains no material which has been accepted for the award of any other degree or diploma at any university or equivalent institution and that, to the best of my knowledge and belief, this thesis contains no material previously published or written by another person, except where due reference is made in the text of the thesis.

This thesis is comprised of 3 original papers published in peer-reviewed journals. The core theme of the thesis and accompanying papers is *ENU mutagenesis mouse models of red cell defects*. The ideas, development, and writing up of all the papers in the thesis were the principal responsibility of myself, the student, working within the Australian Centre for Blood Diseases under the supervision of Associate Professor David Curtis and Professor Stephen Jane.

The inclusion of co-authors reflects the fact that the work came from active collaboration between researchers and acknowledges input into team-based research.

I declare my contribution to the work involved to produce each chapter of this thesis, and the publications which arose from those results, to be the following:

**Chapter 3:** 75%

**Chapter 4:** 85%

**Chapter 5:** 80%

I acknowledge the important contributions of others to the results presented here for the following chapters:

Thesis Chapter	Publication Title	Status <i>(published, in press, accepted or returned for revision, submitted)</i>	Nature and % of student contribution	Co-author name(s), nature and % of co-author's contributions	Co-author(s) Monash student?
Three	<i>A mouse model of hereditary coproporphyrria identified in an ENU mutagenesis screen.</i>	Published	75% Research, experiments, manuscript writing.	Fiona Brown (10%): Research, experiments, manuscript editing. Robert Fallinfaw (3%): Chemical analyses. Ben Kile (2%): Concept, animal handling. David Curtis (5%): Senior author, concept, manuscript writing/editing. Stephen Jane (5%): Senior author, concept, manuscript editing.	N N N N N
Four	<i>Bone marrow transplantation corrects haemolytic anaemia in novel ENU mutagenesis mouse model of TPI deficiency.</i>	Submitted (Published at time of Thesis pass)	85% Research, experiments, manuscript writing.	Fiona Brown (5%): Animal handling, experiments, manuscript editing. Gaetan Burgio (2%): Concept, animal handling. Craig Morton (1%): Protein analysis. David Curtis (5%): Senior author, concept, manuscript writing. Stephen Jane (2%): Senior author, concept, manuscript editing.	N N N N N
Five	<i>Characterisation of</i>	Submitted	80% Research,	Fiona Brown (10%): Animal handling, experiments, manuscript editing.	N



---

## Acknowledgements

The past four years have only been made possible thanks to a number of dear friends and colleagues at the Australian Centre for Blood Diseases. My time there as both an undergraduate and postgraduate student has been incredibly enjoyable, and the mentorship I received has come from devoted supervisors, researchers, technicians, and fellow students who have each played an integral role in the success of this final product. Particularly to my supervisor, A/Professor David Curtis: your guidance, patience, and honesty has been fundamental to my growth and development and I could not be more grateful for all the time you have dedicated towards me over these years. To Professor Stephen Jane also, thank you for providing me with the opportunity to undergo my PhD in such a vibrant and ambitious lab.

There are many fellow lab members I need to thank who have collectively helped keep me sane during this degree, by not only by providing enormous amounts of entertainment but also freely offering their unforgettable practical and academic advice. I would like to thank firstly Dr Fiona Ward, my undergraduate supervisor and predecessor, who helped me rapidly accumulate the skills to become an independent researcher. Other members of the Red Cell group have each provided fantastic guidance and friendship, including Dr Cedric Tremblay, Dr Stefan Sonderegger, Loretta Cerruti, Jesslyn Saw, Dr Sung Chiu, and all of the ACBD students who came and went in between. You all helped bring a vibrant energy to the lab that made it an absolute pleasure to be there.

Special thanks also goes to our collaborators, without whom our publications would not have been possible, as well as the technical help of external facilities such as the AGRF, Australian Phenomics Network, and animal house staff at ARL and PAC.

Lastly, I dedicate this piece with unconditional love to my parents, Karen and Paul, and my brother Mitch, who can make me laugh until I cry. Without you all this crazy adventure would not have been possible. You are all the light at the end of my tunnel.

*This research was supported by an Australian Government Research Training Program (RTP) Scholarship, formerly known as the Australian Postgraduate Award (APA).*

---

## Table of Contents

Copyright notice .....	2
<b>Abstract</b> .....	3
Publications during enrolment .....	5
Thesis including published works: Declaration.....	6
Acknowledgements .....	9
Table of Contents .....	11
List of figures .....	13
List of tables .....	14
Abbreviations.....	15
<b>CHAPTER ONE: Introduction</b> .....	19
1.1 Erythropoiesis.....	20
1.1.1 The haematopoietic stem cell and erythroid progenitors.....	20
1.1.2 Erythropoiesis during development .....	21
1.1.3 Iron .....	22
1.1.4 Haem .....	24
1.1.5 Energy requirements of the red cell .....	26
1.2 Clinical and experimental approaches in the study of red cell diseases .....	27
1.2.1 Mice as model organisms.....	27
1.2.2 ENU mutagenesis as a method of forward genetics .....	29
1.2.3 Limitations of ENU mutagenesis .....	30
1.2.4 Application of ENU mutagenesis in the study of erythropoiesis .....	32
1.3 Project outline.....	33
1.4 Introductory figures and tables .....	35
<b>CHAPTER TWO: Materials and Methods</b> .....	46
2.1 Buffers, solutions, and basic reagents .....	47
2.2 Additional commercial kits .....	48
2.3 Antibodies.....	50
2.4 Experimental animals .....	51
2.5 Blood and cell preparation techniques .....	51
2.6 Additional techniques and experimental methods.....	53
2.7 Sequencing and analysis .....	56
2.8 Statistical analysis .....	57
<b>CHAPTER THREE: A mouse model of hereditary coproporphyrinemia identified in an ENU mutagenesis screen</b> .....	58

<b>CHAPTER FOUR: Bone marrow transplantation corrects haemolytic anaemia in a novel ENU mutagenesis mouse model of TPI deficiency .....</b>	<b>68</b>
<b>CHAPTER FIVE: Characterisation of Tfr mutant mice with microcytic phenotypes.....</b>	<b>77</b>
Discussion and future directions .....	87
References.....	89

---

## List of figures

1.1 The haematopoietic hierarchy.....	36
1.2 Cells of the erythroid lineage.....	37
1.3 Primitive versus definitive erythropoiesis.....	38
1.4 The acquisition of iron.....	39
1.5 The transferrin receptor cycle.....	40
1.6 Regulators of iron absorption.....	41
1.7 The porphyrin biosynthesis pathway.....	42
1.8 Anaerobic glycolysis.....	43
1.9 Forward vs. reverse genetics.....	44

---

## List of tables

1.1 The porphyrias.....	45
1.2 The RBC mutants.....	46
2.1 Antibodies used for Western blotting.....	51
2.2 Antibodies used for flow cytometry.....	51
2.3 Experimental mouse strains used throughout this study.....	52

---

## Abbreviations

AGRF	Australian Genomics Research Facility
APC	Allophycocyanin
ATP	Adenosine triphosphate
bp	Base-pair
BSA	Bovine serum albumin
BSGC	Buffered saline glucose citrate
cDNA	Complementary DNA
cGy	Centigray
Copro I (CI)	Coproporphyrinogen I
Copro III (CIII)	Coproporphyrinogen III
CPOX	Coproporphyrinogen oxidase
C-terminal	Carboxy terminal
dH <sub>2</sub> O	Distilled water
DMSO	Dimethyl sulphoxide
DNA	Deoxyribonucleic acid
dsDNA	Double-stranded DNA
EDTA	Ethylenediaminetetra-acetic acid
ELISA	Enzyme-linked immunosorbent assay
ENU	N-ethyl-n-nitrosourea
FACS	Florescent activated cell sorting
FBE	Full blood examination
Fe <sup>+2</sup>	Ferrous iron
Fe <sup>+3</sup>	Ferric iron
FITC	Fluorescein isothiocyanate

g	Gram
G	Gauge
GAPDH	Glyceraldehyde-3-phosphate dehydrogenase
gDNA	Genomic DNA
Hb	Haemoglobin
HbA1c	Glycosylated haemoglobin
HCP	Hereditary coproporphyrria
IgG	Immunoglobulin G
kb	Kilo-base
kDa	Kilo Dalton
kg	Kilogram
L	Litre
M	Molar
Mb	Megabase
mg	Milligram
mL	Millilitre
mM	Micromolar
mol	Mole
mRNA	Messenger RNA
ng	Nanogram
NHS-biotin	N-hydroxysuccinimido biotin
nm	Nanometre
nmol	Nanomole
N-terminal	Amino terminal
PB	Phenobarbital
PBS	Phosphate buffered saline
PCR	Polymerase chain reaction

PE	Phycoerythrin
pH	$\text{Log}_{10}[\text{H}^+]$
Proto	Protoporphyrinogen
qPCR	Quantitative PCR
RMH	Royal Melbourne Hospital
RNA	Ribonucleic acid
RPM	Revolutions per minute
RPMI	Roswell Park Memorial Institute medium
SA	Streptavidin
TAE	Tris acetate EDTA
TBS	Tris buffered saline
TBST	Tris buffered saline-Tween 20
Tf	Transferrin
TfR(1)	Transferrin receptor (1)
TfR2	Transferrin receptor 2
TPI	Triosephosphate isomerase
U	Unit (enzyme)
Uro	Uroporphyrinogen
UV	Ultraviolet
V	Volts
<i>xg</i>	Relative force
$\alpha$	Alpha
$\beta$	Beta
$\gamma$	Gamma
$\delta$	Delta
$\kappa$	Kappa
$\epsilon$	Epsilon
$\zeta$	Zeta

$\mu\text{g}$

Microgram

$\mu\text{L}$

Microlitre

$\mu\text{M}$

Micromolar

$\mu\text{mol}$

Micromole

---

## CHAPTER ONE

### Introduction

Erythropoiesis is the process of generating mature red blood cells (RBC) from the haematopoietic stem cell (HSC); a vital cellular program that ultimately allows oxygen exchange and the transport of nutrients through the bloodstream to tissues. Mutations which occur in the erythropoietic pathway and affect the development or function of RBCs often result in the manifestation of clinical disease, particularly anaemia. Anaemia is a global health concern that is estimated to affect up to 25% of the world's population, and varies greatly in clinical presentation and outcome, from asymptomatic to fatal. Observations in humans and experimental studies in animal models have identified a number of hereditary mutations in the genes that regulate erythropoiesis as being causative to the underlying pathology of particular anaemias, however, many patients still present with red cell conditions of unknown aetiology, suggesting there are many genes, pathways, hormones, and feedback mechanisms regulating erythropoiesis yet to be identified. Additionally, rare and complicated anaemias remain difficult to diagnose and treat, prompting the need to generate reliable animal models that recapitulate these conditions in order to establish better clinical treatments. Forward genetics screens, using the mutagen N-ethyl-nitrosourea (ENU), has become a powerful tool in genome-wide studies of specific organ systems, such as erythropoiesis. The application of this method in mouse models has proven to be vital in the further understanding of mammalian red cell development and in the generation of novel animal models of human red cell diseases.

## 1.1 Erythropoiesis

### 1.1.1 The haematopoietic stem cell and erythroid progenitors

The haematopoietic stem cell (HSC) is the pluripotent, self-renewing stem cell of the bone marrow from which all blood cells are derived<sup>1</sup>. Haematopoiesis defines the HSC's role in the collective generation and maintenance of all blood components, including white blood cells (leukocytes), platelets (thrombocytes), and red blood cells (erythrocytes) (Figure 1.1). Through complex, multifaceted processes, HSCs give rise to progenitor cells which gradually lose their pluripotency and self-renewal capacity, and eventually commit to one of the definitive blood cell lineages<sup>2</sup>.

Erythroid progenitor cells emerge from the myeloid lineage<sup>3</sup>. This begins with the common myeloid progenitor (CMP), responsible for generating all myeloid cell types. A more restricted progenitor, the megakaryocyte-erythroid progenitor (MEP) cell, derives from the CMP and subsequently undergoes step-wise maturation to become an RBC within the bone marrow (Figure 1.2). The first definitive erythroid cell to emerge from this precursor is the erythroid blast-forming unit (BFU-E), and subsequently the erythroid colony-forming unit (CFU-E), which can be grown in culture in the presence of the hormone erythropoietin (Epo)<sup>4</sup>. The first morphologically recognisable erythroid cell to appear is the proerythroblast. It is the first erythroblast to express transferrin receptor (TfR or CD71) on its cell surface for the purpose of iron uptake<sup>5</sup>. From this precursor, the basophilic erythroblast emerges, as does the erythroid-specific cell surface marker, glycophorin A (Ter-119). Morphologically this cell is smaller in size with a denser nucleus than the proerythroblast, and the cytoplasm appears highly acidic due to the rapid synthesis of haemoglobin. A reduction in size and condensation of the nucleus continues on as the cell matures into the polychromatic erythroblast, immunologically characterised as Ter-119<sup>+</sup>CD71<sup>mid</sup>. The orthochromatic normoblast is the last stage of development before the erythroid cell loses its nucleus via enucleation. This process expels the compacted, polarised nucleus from the cell to increase the intracellular space where oxygen exchange will later occur. The remaining enucleated cell, known as a reticulocyte, still retains some ribosomal machinery. Reticulocytes are present in the bloodstream in low

percentages (2-3%), but must expel their remaining RNA to become fully functional, oxygen-carrying erythrocytes. Immunologically, the mature RBC is characterised as Ter-119<sup>+</sup>CD71<sup>low</sup>.

### 1.1.2 Erythropoiesis during development

Mammals—particularly humans and mice—share overlapping developmental programs throughout embryogenesis, including many aspects of erythropoiesis<sup>6</sup>. In both organisms, there are unique waves of blood cell formation that supply the embryo with oxygen-carrying cells through various stages of development. The two main erythropoietic programs, termed *primitive* and *definitive* erythropoiesis, differ in progenitor cell expansion, site of development, and globin synthesis to suit the needs of the growing embryo (Figure 1.3)<sup>7</sup>.

Primitive erythropoiesis begins as early as embryonic day 7.5 (E7.5) in the mouse, and approximately 2.5 weeks post-gestation in humans. In the yolk sac, blood islands arise in the mesodermal layer, where haemangioblasts supply the embryo with the earliest proerythroblasts. In contrast to HSC-derived erythroblasts, these precursors remain nucleated and only offer minimal oxygen-carrying capacity during early embryonic development. By approximately day E10.5 in mice, or 4 weeks in humans, the emergence of the mesoderm-derived aorta-gonad-mesonephros (AGM) initiates definitive erythropoiesis by supplying the first self-replicating HSCs capable of generating all blood cell lineages<sup>7</sup>. Prior to the formation of bone marrow, erythroblasts must migrate to the foetal liver to expand and mature, a process which occurs by E12.5 in mice or 6 weeks post-gestation in humans. During foetal liver erythropoiesis, globin switching also occurs to supply the embryo with more adult-like haemoglobins with greater oxygen-carrying efficiency<sup>8</sup>.

Eventually the bone marrow becomes the primary site of definitive erythropoiesis<sup>7</sup>, which begins in humans at approximately 18 weeks' post-gestation but does not occur in mice until birth. The liver and other extramedullary organs with blood-developing capacity, such as the spleen, are not used as major sites of erythropoiesis in the adult unless severe injury or blood loss occurs, or in cases of

particular dyserythropoietic diseases, when the bone marrow alone cannot supply sufficient numbers of RBCs<sup>9</sup>.

### 1.1.3 Iron

Iron is one of the most abundant metals in the body and is used by many cells for various molecular processes. Due to its oxygen-binding capacity, it plays a well-known role in red blood cell function, and, if in excess or lacking, can cause pathological diseases such as haemochromatosis<sup>10</sup> or iron deficiency anaemia (IDA)<sup>11</sup>, respectively. Since the body has limited iron-storing capacity, iron is required from the diet, which is best found in red meat, dark leafy greens, and beans. Iron absorption takes place across the duodenum, where enterocytes allow the uptake of ferrous ( $\text{Fe}^{+2}$ ) iron through the DMT-1 portal at the apical membrane<sup>12</sup>. At the basal membrane, iron enters the bloodstream through ferroportin. There, the copper-dependant ferroxidase, hephaestin, converts ferrous iron into its ferric ( $\text{Fe}^{+3}$ ) form, which then allows it to bind to its carrier protein, transferrin (Tf), and circulate to cells which require and utilise iron (Figure 1.4). The other major source of the body's iron comes from macrophages, which digest old red blood cells as they pass through the spleen and recycle their components, such as iron, which is released back into the bloodstream via the ferroportin channel also<sup>13</sup>.

Iron-bound Tf (Fe-Tf), carrying up to two atoms of iron per molecule, binds to the transferrin receptor (TfR), a transmembrane glycoprotein encoded by two genes: TfR1 (CD71) and TfR2<sup>14</sup>. TfR1 is expressed on multiple cells but is the major surface protein of haemoglobin-producing erythroblasts, while TfR2 expression is mostly localised to hepatocytes of the liver. TfR1 plays a more senior role in cellular iron uptake (Figure 1.5). The receptor functions as a homodimer and possesses two binding regions capable of binding two transferrin molecules<sup>15</sup>. During steady state, receptor binding regions are occupied by the iron-regulatory haemochromatosis protein (HFE). TfR1 has a much higher affinity for Fe-Tf than HFE at biological pH (approx. 7.4), and so HFE is outcompeted and displaced when Fe-Tf is present. The Tf-TfR complex then enters the cell via receptor-mediated endocytosis, within a clathrin-coated pit, to form an endosome. A reduction in

pH (approx. 5.5) allows iron to disassociate from its carrier protein, but keeps Tf anchored to the TfR<sup>15</sup>. The metalloreductase, STEAP3, then converts ferric iron back into a more soluble ferrous form, allowing iron to leave the endosome and enter the cytosol, where it is subsequently used in the synthesis of haem, or stored as ferritin. The empty Tf-TfR complex is cycled back to the cell surface, where empty Tf (apo-Tf) disassociates from the receptor and returns to the circulation.

The displaced HFE molecule is part of a well-controlled feedback loop with TfR2 that tightly regulates iron uptake to prevent iron overload (Figure 1.6)<sup>16</sup>. In high iron conditions, free HFE binds to TfR2 and triggers the assembly of a large protein complex at the cell surface of hepatocytes. This complex involves known iron-regulatory molecules such as hemojuvelin (HJV) and bone morphogenic protein 6 (BMP6). The formation of this complex triggers downstream intracellular signalling that prompts the synthesis of the iron-regulatory hormone, hepcidin<sup>16,17</sup>. Hepcidin subsequently binds to and inhibits ferroportin, blocking iron absorption from the diet or from being released by macrophages. Upon depletion of cellular iron stores, the lack of oxygen tension in tissues initiates the hypoxia-driven synthesis of erythropoietin (Epo) in the kidney. Epo drives the synthesis of a bone marrow-derived hormone, erythroferrone (Erfe)<sup>18</sup>, which negatively regulates hepcidin. The inhibition of hepcidin reopens ferroportin channels and allows iron absorption to resume.

Iron itself is a key regulator of protein synthesis. Several genes regulating the iron metabolism pathway, including TfR1, Tf, ferritin, ferroportin, and hepcidin, contain sequence-specific iron responsive elements (IREs)<sup>19</sup>. IREs direct the binding of iron regulatory proteins (IRPs) to the 5' or 3' untranslated regions (UTR) of mRNA transcripts, resulting in RNA stabilisation or degradation, depending on the body's needs<sup>19</sup>. In high iron conditions, IRPs inhibit the translation of mRNAs encoding DMT-1 and ferroportin, to help reduce the amount of iron entering the bloodstream. During low iron stores, IRPs increase synthesis of TfR1, leading to enhanced expression on the cell surface, and reduces transcription of ferritin or Tf. These complex mechanisms and overlapping regulatory pathways highlight the importance of maintaining balanced iron levels in the body.

Multiple clinical conditions that can manifest as a result of excessive or insufficient iron levels. Haemochromatosis, or iron-overload, can be acquired or can stem from inherited mutations in one of the many regulatory elements of iron metabolism pathway<sup>10,16</sup>. Common genes responsible for the pathogenesis of haemochromatosis include those encoding HFE, hepcidin, HJV, and TfR2. Mutations in these genes are typically loss-of-function, and when mutated, the ability to detect high intracellular iron levels is lost. If iron concentrations persistently exceed the body's daily needs, iron can become deposited in tissues, such as the joints, heart, liver, and pancreas, causing cirrhotic damage to organs. Avoidance of high iron foods and regular phlebotomies is the best clinical management strategy, sometimes in combination with iron chelating agents<sup>10</sup>. In contrast, poor dietary intake of iron or malabsorption can result in iron deficiency anaemia, believed to account for 50% of all cases of anaemia globally<sup>11</sup>. Vegetarians, pregnant or menstruating women, and patients with underlying bleeding disorders are highly susceptible to developing IDA. Pallor, lethargy, and dizziness are common symptoms of IDA, but this can progress to difficulties in swallowing, nail and hair brittleness, tachycardia, or developmental delays in children if left untreated. Oral iron therapy is typically the first stage of addressing low iron stores<sup>20</sup>. Intramuscular injections of iron are available for more severe cases, as well as intravenous iron or blood transfusions to replenish iron pools more rapidly. However, there are an increasing number of patients with microcytosis and suspected IDA who do not respond to iron therapy<sup>20</sup>. These rare cases highlight the possibility of inherited iron metabolic defects within erythropoietic genes that are yet to be identified in humans.

#### **1.1.4 Haem**

Haem is the prosthetic cofactor of the haemoglobin molecule that binds iron and allows gas exchange to take place between RBCs and other tissues<sup>21</sup>. It is an organic compound that belongs to a class of porphyrins, made of four modified pyrroles that form heterocyclic rings, each held together by methane bridges. It is this iron-conjugated ringed molecule that gives haemoglobin, and ultimately red blood cells, their distinctive red colour. The majority of the body's haem (70%) is

synthesised in bone marrow erythroblasts for use in haemoglobin, while the remainder is largely generated in hepatocytes for integration into non-haemoglobin proteins, such as myoglobin, cytochromes, and enzymes such as peroxidases.

Haem is synthesised by the porphyrin biosynthesis pathway, which takes place in the mitochondria and cytosol of cells via a series of irreversible enzymatic reactions (Figure 1.7)<sup>21</sup>. This begins with the rate-limiting porphyrin precursor,  $\delta$ -aminolevulinic acid (ALA), synthesised in the mitochondria by aminolevulinic acid synthase (ALAS). In the cytosol, two molecules of ALA are dimerised into porphobilinogen (PBG) by the ALA deaminase (ALAD) enzyme, generating the first ringed pyrrole. PBG is then condensed into a series of porphyrins by subsequent enzymatic reactions, generating uroporphyrinogen III, coproporphyrinogen III, and protoporphyrinogen IX, in linear succession. The last of these decarboxylating reactions generates protoporphyrin IX. When iron is integrated into the centre of the protoporphyrin IX structure, it becomes ferrous protoporphyrin, or haem. Haem, in turn, regulates its own synthesis pathway by completing a feedback loop with ALAS, limiting the enzyme's function or protein transcription to ensure haem is not over-produced<sup>21</sup>.

Loss-of-function mutations can occur in any of the seven enzymes involved in porphyrin biosynthesis, diminishing haem production and causing excessive accumulation of porphyrin intermediates. This clinically presents as a condition called porphyria, for which there are several subtypes depending on which enzyme is affected (Table 1.1)<sup>22</sup>. The porphyrias are a highly heterogeneous collection of diseases that can be autosomal recessive, dominant, or X-linked in inheritance. They are typically rare in incidence; the most common occurring form of porphyria seen in humans, porphyria cutanea tarda, which occurs due to autosomal dominant mutations in the *UROD* enzyme gene, has an incidence of 1:25,000<sup>22</sup>. Other subtypes, such as ALAD deficiency porphyria, have had less than 10 known reported clinical cases. Each porphyria varies enormously in penetrance, clinical presentation, onset, severity, and triggers, but typically emerges during adolescence with intermittent bouts of abdominal pain, nausea, discoloured urine, skin blisters, and peripheral nervous symptoms. Biochemically, high concentrations of unmetabolised porphyrins are detected in the urine, faeces, and blood. If left untreated or poorly managed, the

condition can progress to severe pain, seizures, tachycardia, renal failure, and paralysis. Symptoms are experienced in waves, referred to as 'crises', and are usually brought on by environmental or endogenous factors which hyperactivate porphyrin synthesis<sup>22</sup>. The ALAS enzyme is particularly responsive to environmental triggers, including alcohol, drugs (particularly barbiturates), iron, and hormones (such as progesterone). Patients who therefore take particular medications, as well as women, are more susceptible to experiencing porphyric crises than others with the same genetic mutation. Inhibitors of ALAS include glucose and haem. Intravenous glucose or dextrose, as well as the haem-based pharmaceutical, heme arginate (Normosang)<sup>23</sup>, can be administered to patients suffering moderate to severe porphyric crises to dampen symptoms. Otherwise, avoidance of triggers and maintaining a high-carbohydrate diet are currently the only long-term management strategies for patients with porphyria. Research into better treatment options for the porphyrias, such as gene therapy and ALAS inhibitors, is currently underway<sup>24</sup>.

### **1.1.5 Energy requirements of the red cell**

Like all cells, RBCs require energy in the form of ATP (adenosine triphosphate), and cofactors such as NADH, to perform basic cellular functions. While gas exchange occurs passively, other red cell homeostatic mechanisms, such as a membrane deformability, antioxidant reactions, and ion pump operation, are ATP-dependant<sup>28-30</sup>. Two signature cellular mechanisms result in the production of ATP: glycolysis—the anaerobic pathway—and oxidative phosphorylation, which is oxygen-dependant. Since RBCs lack mitochondria, they are restricted to glycolysis as the only pathway to obtain ATP. Glycolysis consists of a series of reversible enzymatic reactions that converts one molecule of glucose into two molecules of pyruvate and two molecules of ATP (Figure 1.9)<sup>31</sup>. Typically, pyruvate is funnelled into the oxidative phosphorylation pathway to generate more ATP through the electron transport chain. In RBCs, pyruvate is reduced to lactate by lactate dehydrogenase (LDH), and then excreted from the body as waste.

The enzymes involved in glycolysis reactions are considered housekeeping proteins (eg: GAPDH) due to their ubiquitous expression, high stability, and near-perfect catalytic kinetics<sup>30</sup>. Inheritable

mutations can occur within almost any of these housekeeper genes, but due to the red cell's total dependence on glycolysis as its energy source, metabolic enzymopathies have a more profound effect on RBCs over other tissues. Glycolytic enzymopathies often present clinically as non-spherical haemolytic anaemias, which ranges from mild to fatal in severity<sup>30</sup>. The most common deficiency in humans is glucose-6-phosphate dehydrogenase (G6PD) deficiency: an X-linked condition that affects the pentose-phosphate pathway, adjacently linked to glycolysis<sup>32</sup>. Haemolytic anaemia is a common clinical finding, although it has no long-term impact on patient lifespan and is controllable by avoiding specific foods that trigger the enzymes of this pathway, such as fava beans. Mutations in other enzymes, such as hexokinase, pyruvate kinase, or triosephosphate isomerase (TPI) are far rarer and can be associated with more severe pathology, including jaundice, lethargy, susceptibility to infections, splenomegaly, and, particularly in cases of TPI deficiency, neurodegeneration and death in early childhood<sup>30,33</sup>. In these haemolytic conditions, the red cell lifespan (typically 120 days in humans) is dramatically reduced, and RBCs are destroyed by the spleen faster than the bone marrow can replace them. If not countered by regular blood transfusions or reversed using a haematopoietic stem cell transplantation (HSCT), the haemolytic anaemia can prove to be fatal. Due to the rarity of these conditions, and the elusiveness of red cell metabolism, further research into metabolic diseases is needed in order to establish novel therapeutic options.

## **1.2 Clinical and experimental approaches in the study of red cell diseases**

### **1.2.1 Mice as model organisms**

The identification of many genes and regulators of erythropoiesis have largely come from the study of patients or families with pathological red cell phenotypes. Pallor or jaundice, changes to red cell indices or morphology, and the quantification of products in the serum and urine are traditionally used to diagnose red cell conditions, such as anaemia<sup>34</sup>. Advancements in gene sequencing techniques have also proven incredibly beneficial for the identification of new mutations responsible for red cell diseases in humans<sup>35</sup>. The use of animal models, such as mice, has also

had a profound impact on the identification of novel genes or alleles that govern erythropoiesis, as well as the understanding of underlying molecular mechanisms that contribute to human pathology.

The house mouse (*mus musculus*) shares more than 85% genetic homology to humans in terms of protein-coding genes. Their genome was entirely mapped in 2002<sup>36</sup>, allowing researchers to easily manipulate, edit, delete, and transpose almost any segment of their genome. The function of single genes can be studied at a complete systemic level with the use of mouse models, which can ultimately lead to the identification of new molecular mechanisms involved in cellular pathways and the design of novel therapies that target those mechanisms.

There are two directions in which mouse genetics and phenotypes can be ultimately studied: forward or reverse (Figure 1.10). Reverse genetics is the more traditional method, in which a known gene of interest is edited, mutated, inserted, or deleted from the genome, and the resulting mouse phenotype is observed and catalogued<sup>37</sup>. While this approach has demonstrated the importance of many genes in their role in disease origin and progression, it requires previous knowledge of the existence of the gene of interest, and is often considered a biased method that forces researchers to expect a definitively noticeable outcome in the animal's phenotype. Many methods of reverse genetics are also costly and time-consuming, and the resulting outcomes are not guaranteed to phenocopy human diseases. Forward genetics is an unbiased method in which random mutagenesis creates organisms with distinct phenotypes, which are then genetically sequenced in order to locate the underlying mutation responsible<sup>38</sup>. Prior knowledge of the gene's existence or function is not required; forward genetics can therefore be utilised in the rapid identification of new genes or alleles. Experimentally, the process of random mutagenesis is relatively cheap and simple, and can generate large litters of phenotypically fascinating progeny that can then be screened for particular traits of interest. With advances in gene sequencing technology, such as next-generation sequencing (NGS) techniques, gene identification following forward genetic screening is also becoming faster and cheaper to perform. For the purpose of identifying novel genes regulating specific pathways such as erythropoiesis, forward genetics is an ideal experimental method to use on mouse models.

## 1.2.2 ENU mutagenesis as a method of forward genetics

Many methods of forward genetics have been employed to induce spontaneous phenotypes in model organisms. Exposure to radiation or chemotherapeutic agents have been widely used to initiate random base-pair mutations, splice variants, deletions, and chromosomal rearrangements in DNA, generating interesting phenotypes in model plants and animals<sup>39</sup>. Amongst the chemical mutagens often used in mice is the alkylating agent, *N*-ethyl-*N*-nitrosourea (ENU)<sup>38,40</sup>. The properties of ENU have been well-characterised and it is considered ideal for forward genetics studies for many reasons, such as its calculatable mutation frequency, and the fact that it favourably induces missense or nonsense mutations within coding regions at a high rate (>80%)<sup>41</sup>. These properties not only increase the likelihood of generating a notable phenotype due to a mutant protein product, but also allows high-throughput, cost-effective NGS techniques, such as whole exome sequencing (WES), to be easily utilised in identifying the mutation thereafter. ENU mutagenesis generates heritable mutations at a frequency of about  $1.4 \times 10^{-6}$  per nucleotide site, two orders of magnitude faster than the natural mutation rate<sup>41</sup>. At optimal levels, with the maximum mutagen dose tolerable, a frequency of up to  $6 \times 10^{-3}$  mutations per nucleotide, equivalent to one mutation every 650 gametes, can be obtained in mice<sup>41</sup>.

ENU mutagenesis has been utilised in the identification of novel genes or alleles involved in many pathological processes critical for understanding human diseases, such as diabetes, hearing loss, malarial resistance/susceptibility, haematopoiesis, and neurological defects<sup>42-46</sup>. One major advantage of ENU over reverse genetics methods, such as targeted deletions, is that the presence of a mutant gene can often be more informative than the gene's absence entirely. In knockout animal models, the deletion of an important gene of interest may be unviable and cause embryonic lethality, or if the gene of interest is non-redundant, a phenotype may not develop at all. Since ENU favours base-pair substitutions in coding regions, a mutant gene product is often preserved, allowing a greater analysis of that gene's function<sup>41</sup>. The mutations gained through ENU mutagenesis are also germline and do not require complex editing or manual induction of the

mutation, such as with CRISPR-generated mutants or conditional knockout models, which are expensive, biased, and time-consuming. ENU can also result in gain-of-function mutations as well as loss-of-function, expanding the breadth of understanding in functional genomics<sup>40</sup>.

Dominant and recessive ENU mutagenesis screens are performed on male mice. The alkylating agent induces mutations within spermatogonial cells by transfer of the chemical's ethyl group to random nucleotides, causing base-pair mismatching<sup>40</sup>. After intraperitoneal injection, male mice are crossed with untreated females to create G<sub>1</sub> progeny, which can be screened for the phenotype of interest in a dominant screen. In a recessive screen, G<sub>1</sub> mice are intercrossed or backcrossed with the original paternal mouse generating G<sub>2</sub> progeny, which may then display a homozygous phenotype of interest. To determine if a phenotype is fully penetrant, selected animals are outcrossed with wildtype mice to assess phenotype heritability. Weak phenotypes may be more penetrable if crossed onto the background of another inbred mouse strain. For instance, ENU mutant mice initially generated on BL/6 backgrounds are later crossed with a BALB/c mouse to intensify their phenotype, since BALB/c mice are more susceptible to the effects of ENU than other strains<sup>47</sup>. Once a stable, inheritable phenotype has been established, the mutant strain can then be characterised and the causative mutation can be identified using NGS techniques. For ENU mutagenesis screens, such as those used in this project, WES was an ideal application due to the higher likelihood (80%) of finding the mutation within a coding region. Bioinformatics then aligned the sequences to the background strain database (g: BL/6) in order to identify the affected gene.

### **1.2.3 Limitations of ENU mutagenesis**

ENU mutagenesis is not without its limitations, and several factors must be considered in the design of a forward genetics screen. The genetic background of the mouse strain can greatly affect the outcome of the experiment: mutability and phenotype strength differs greatly between inbred strains<sup>47</sup>. BALB/c mice, as mentioned, are more susceptible to ethylating mutagens than the BL/6 strain and often display a stronger ENU-induced phenotype. This mixed genetic background later

complicates genetic sequencing and bioinformatics required for the identification of the mutant gene. Similarly, there is a difference in the tolerability of ENU toxicity: FVB/N mice, for example, are more susceptible to high concentrations of the cytotoxic mutagen and require a lower dose<sup>48</sup>. Since ENU mutagenesis is a dose-dependant process, the maximum calculable rate of mutations varies greatly between strains.

The penetrability of the phenotype is also a major hurdle that determines the success of the experiment: phenotypes with low penetrability or which gradually diminish with subsequent generations cannot be further studied and are ultimately lost. In progeny with strong, observable phenotypes, researchers must be mindful that additional mutations will also be present from the initial mutagenised male. A careful breeding strategy must be designed so that mice are bred in favour of only one phenotype. If additional mutations are still present in the cohort at the time of genetic sequencing, multiple false positive results may emerge, making it more difficult to determine with certainty the singular gene responsible for the observed phenotype.

Lastly, despite the randomness of mutagenesis induced by ENU, particular DNA hotspots exist, therefore some genes are far more 'mutable' than others<sup>41,47</sup>. ENU is particularly drawn towards protein-coding exons, as open euchromatin is more susceptible to ethylation than tightly-packed heterochromatin, therefore large genes with more exons are more likely to be targeted. On a nucleotide level, ENU is more likely to induce transversions of thymine (T) more than any other nucleotide, particularly when surrounded by G/C-rich regions. This pattern of mutation does not match the pattern generally observed in human disease, in which glycine (G) or cysteine (C) residues are more likely to be involved in monogenic diseases due to the high rate of base-pair mismatching of methylated CpG islands<sup>41,47</sup>. This reduces the probability that mutagenesis screens will generate animal models of human diseases with identical genetic profiles. Therefore, given these biases of chemical mutagenicity and epigenetic regulation, not all genes will be targeted equally. In fact, it is predicted that <10% of the organism's total genome can be targeted by ENU, leaving a substantial proportion inaccessible by this method<sup>41</sup>.

### 1.2.4 Application of ENU mutagenesis in the study of erythropoiesis

Over the course of several years in our laboratory, a series of genome-wide forward genetics screens using ENU have been performed on mice generate a library of phenotypically distinct mutant mouse strains with red cell defects (Table 1.2). These red blood cell (RBC) mutants, numbered in order of discovery, were phenotyped by their red cell mean corpuscular volume (MCV), which, if more than three standard deviations above or below the average population, were classified as macrocytic or microcytic RBC mutants, respectively. To date, a total of 17 RBC mutant strains have been identified through these screens. Their corresponding mutations have all been identified using a combination of gene mapping, Sanger sequencing, and WES, depending on the availability of the sequencing technology at the time.

The majority of RBC mutants were found to harbour autosomal dominant mutations which appeared in the G<sub>1</sub> population (RBC6, RBC12, RBC13), some which also produced viable homozygotes with a more severe phenotype than their heterozygous littermates (RBC10). Unsurprisingly, a vast majority of the mutations identified were found within erythroid-specific genes that were responsible for, or contributed to, RBC development, such as red cell membrane formation (RBC2)<sup>49</sup>, globin synthesis (RBC13, RBC14)<sup>50</sup>, and iron metabolism (RBC6<sup>51</sup>, RBC7). Some mutations were more ubiquitous, but nonetheless affected RBC function, including genes that control cellular salt regulation (RBC10)<sup>52</sup> and endocytosis (RBC12)<sup>53</sup>. As a result, many RBC mutants were found to be accurate models of human red cell diseases, such as hereditary spherocytosis (RBC2) and  $\beta$ -thalassemia (RBC13, RBC14), while others offered new molecular functions for known genes (RBC12). Taken together, ENU mutagenesis can effectively identify novel genes or alleles that regulate erythropoiesis, and generate accurate models of human red cell diseases.

### 1.3 Project outline

This thesis contains the details and results obtained from the characterisation of three novel RBC mutant mouse lines identified in independent ENU mutagenesis screens: RBC16, RBC19, and RBC21 (Table 1.2). Each mutant model, derived from a unique founder mouse, was phenotyped by MCV, and subsequent gene mapping or WES isolated the causative genetic mutation. These studies have identified novel autosomal dominant and recessively inherited red cell defects, displaying both microcytic and macrocytic anaemia, offering unique insights into human red cell diseases. The results of the characterisations of each mutant RBC strain are presented here in the form of three scientific articles (see *Thesis including published works*), which have either been published by peer-reviewed scientific journals (RBC16)<sup>54</sup> or have been submitted for publication during enrolment (RBC19, RBC21)<sup>55,56</sup>.

The hypothesis for this project was as follows:

*That RBC mutant mice, identified in ENU mutagenesis screens, will reveal novel genes or alleles that regulate erythropoiesis, and will offer new insights into the pathological mechanisms that contribute to human red cell diseases.*

For each RBC mutant strain (RBC16, RBC19, and RBC21), three key aims were addressed in this project:

- 1. To characterise the RBC mutant's haematological, developmental, and physiological phenotype.*
- 2. To identify the causative mutation in the RBC mutant that resulted in that phenotype.*
- 3. To utilise the RBC mutant in further understanding the molecular mechanisms of erythropoiesis and the pathogenesis of human red cell diseases.*

The expected outcomes of this project included the anticipation of identifying novel genes or alleles that regulated erythropoiesis through phenotypic characterisation and genetic sequencing of these novel RBC mutant strains. We also expected these mutant mice to contribute towards the further

understanding of human red cell defects, either by identifying a new pathological role for a known red cell gene, or presenting as a phenotypically comparable model of a human red cell disease.

## 1.4 Introductory figures and tables

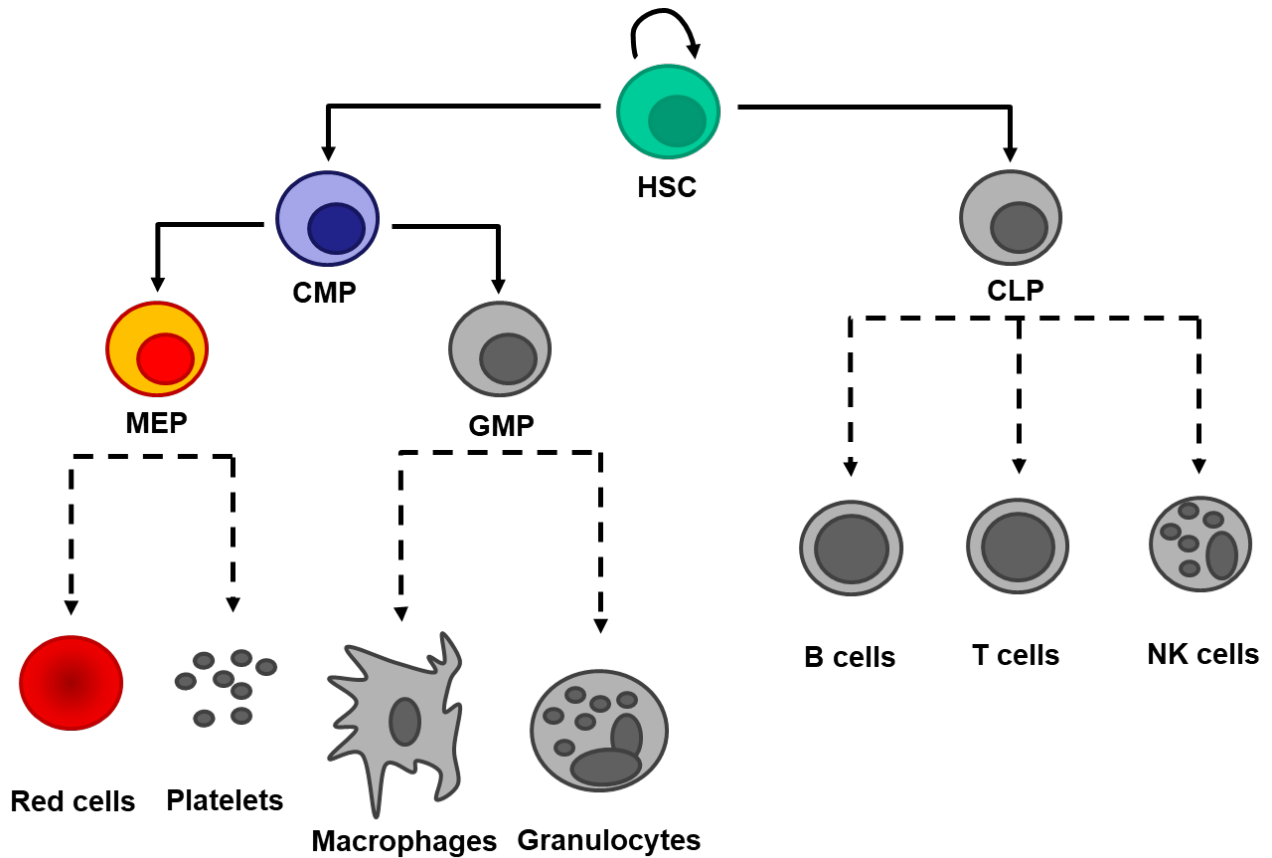


**Figure 1.1: The haematopoietic hierarchy**

A basic schematic depicting the order of haematopoiesis and the origin of blood cells. The self-renewing haematopoietic stem cell (HSC) can divide and differentiate into any of the blood cells via restricted progenitor cells, which each gradually lose their pluripotency as they mature into a specific cell lineage. The two main arms of haematopoiesis are the myeloid and lymphoid lineages, which emerge from the common myeloid progenitor (CMP) and common lymphoid progenitor (CLP) respectively. The megakaryocyte-erythroid progenitor (MEP) is further restricted to the generation of just platelets and red blood cells, while the granulocyte-macrophage progenitor (GMP) gives rise to the granulocytic leukocytes.

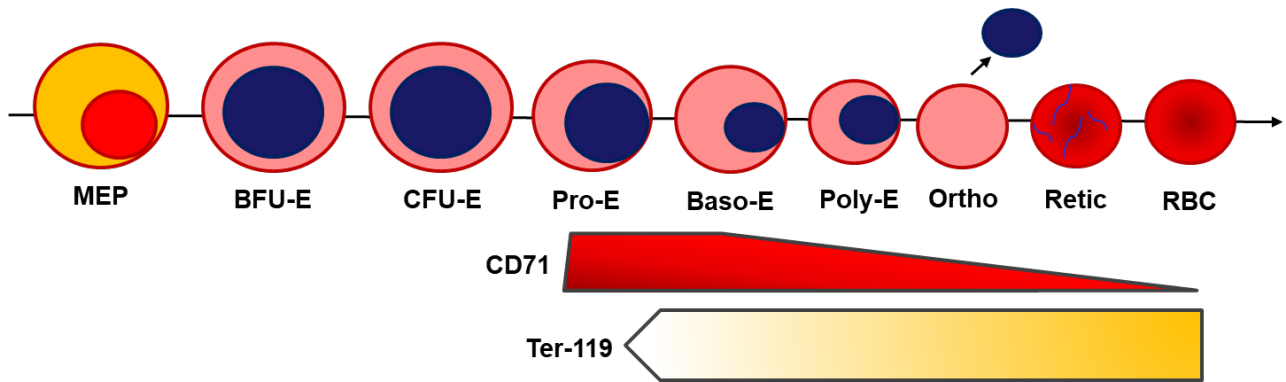


**Figure 1.2: Cells of the erythroid lineage**

Erythropoiesis is the specific pathway that gives rise to mature erythroblasts (RBCs) from the HSC. The MEP progenitor commits to the erythroid lineage with the formation of blast-forming units (BFU-E) and colony forming units (CFU-E). The proerythroblast (Pro-B) is the first microscopically recognisable erythroid cell, and is the first to express the iron receptor marker, CD71. At the basophilic erythroblast (Baso-E) stage, the surface marker Ter-119 is also detectable. As erythroblasts mature, they become smaller in size and condense their nucleus, which is ultimately ejected from the cell at the orthochromatic normoblast (Ortho) stage to increase the cell's oxygen-carrying abilities. The reticulocyte (Retic) is the first erythroid cell visible in circulation, but still carries fragments of RNA. These too are removed from the cell to form the mature, enucleated RBC.

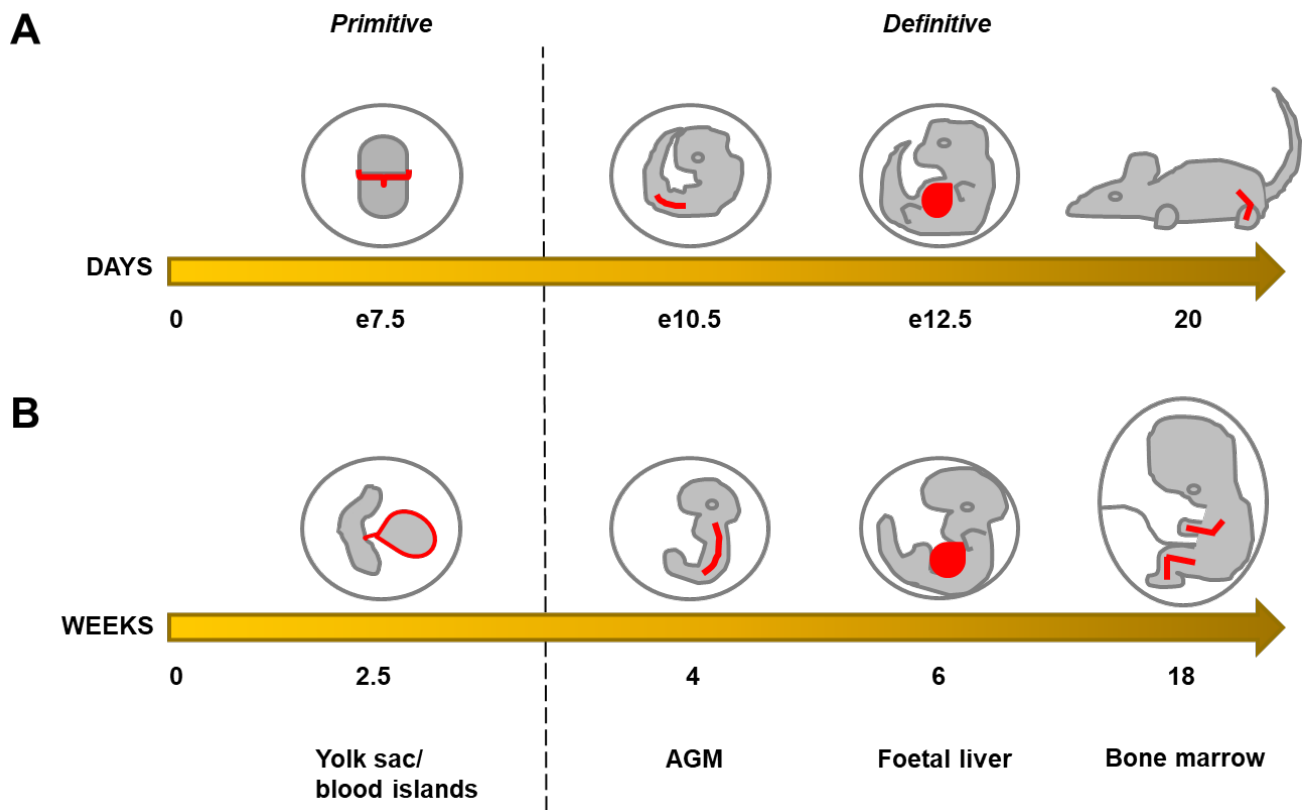


**Figure 1.3: Primitive versus definitive erythropoiesis**

The site of blood cell generation (red highlight) changes throughout embryogenesis, as seen in a comparison of mouse (A), and human (B) development. Primitive erythropoiesis takes place exclusively in the yolk sac and blood islands, which forms erythroid-like hemangioblasts from the mesodermal layer. Definitive erythropoiesis begins with the formation of the aorta-gonad-mesonephros (AGM), where the first HSCs begin to expand. The foetal liver eventually becomes the major site of erythroblast expansion and RBC formation, and acts as the primary blood-supplying organ prior to the formation of the bone marrow. The bone marrow becomes the main site of blood cell development much earlier in humans than mice, and remains the site of definitive

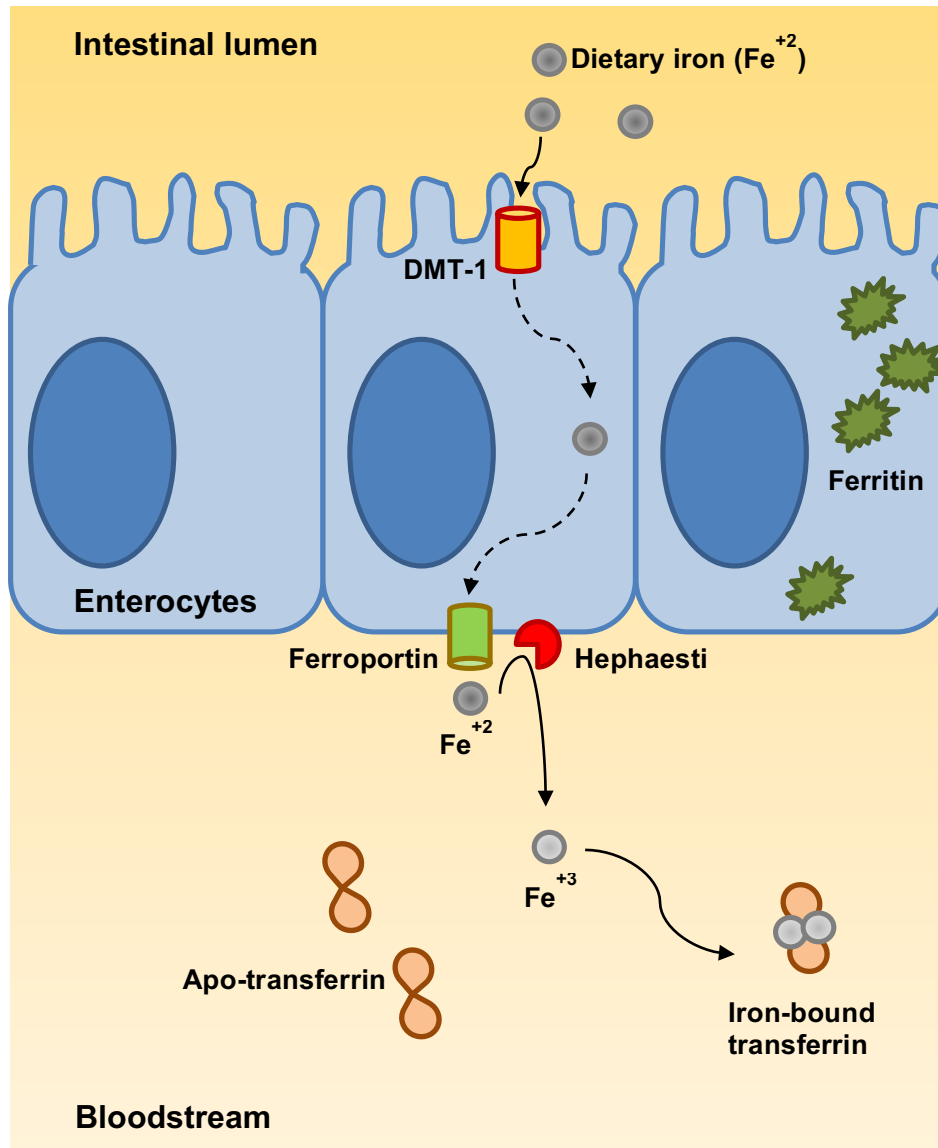


**Figure 1.4: The acquisition of iron**

The main source of the body's iron comes from the diet, where iron-rich foods (red meat, etc) are digested in the lumen of the gastrointestinal track. Enterocytes of the duodenum allow the passage of iron into the bloodstream. Iron enters through the apical membrane via the DMT-1 portal, and pass out through the basal membrane via ferroportin. Iron must travel through the circulation bound to a carrier protein, transferrin. Before it can bind to transferrin, the enzyme hephaestin must convert iron into its ferric ( $Fe^{+3}$ ) form. Enterocytes, and many other cells, can also store iron internally in the form of ferritin.

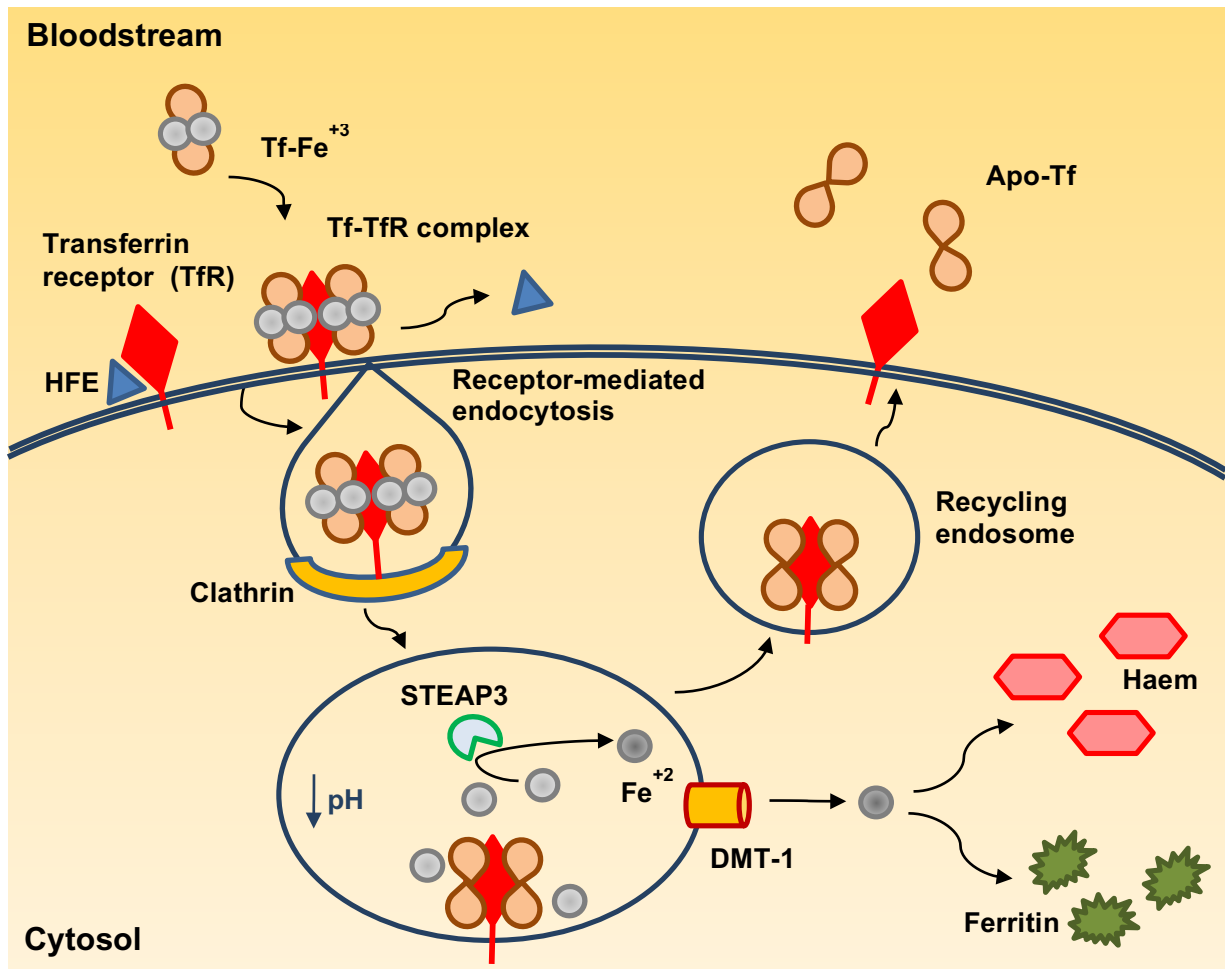


**Figure 1.5: The transferrin receptor cycle**

Iron is incorporated into cells via receptor-mediated endocytosis. Iron circulates the bloodstream bound to its carrier protein, transferrin ( $\text{Tf-Fe}^{+3}$ ), which binds with high affinity to the transferrin receptor (TfR), expressed on the surface of iron-absorbing cells (eg: erythroblasts). The Tf-TfR complex is then endocytosed within a clathrin-coated pit to form an endosome. A drop in pH allows iron to disassociate from Tf. It is then converted back into its ferrous form ( $\text{Fe}^{+2}$ ) by the enzyme STEAP3, before leaving the endosome via the DMT-1 portal. Iron can then be utilised in the production of metalloproteins (eg: haem) or be stored intracellularly as ferritin. The Tf-TfR complex is then recycled back to the cell surface, and empty (apo-) Tf, for which the receptor has low affinity, detaches from the TfR and returns to the circulation.

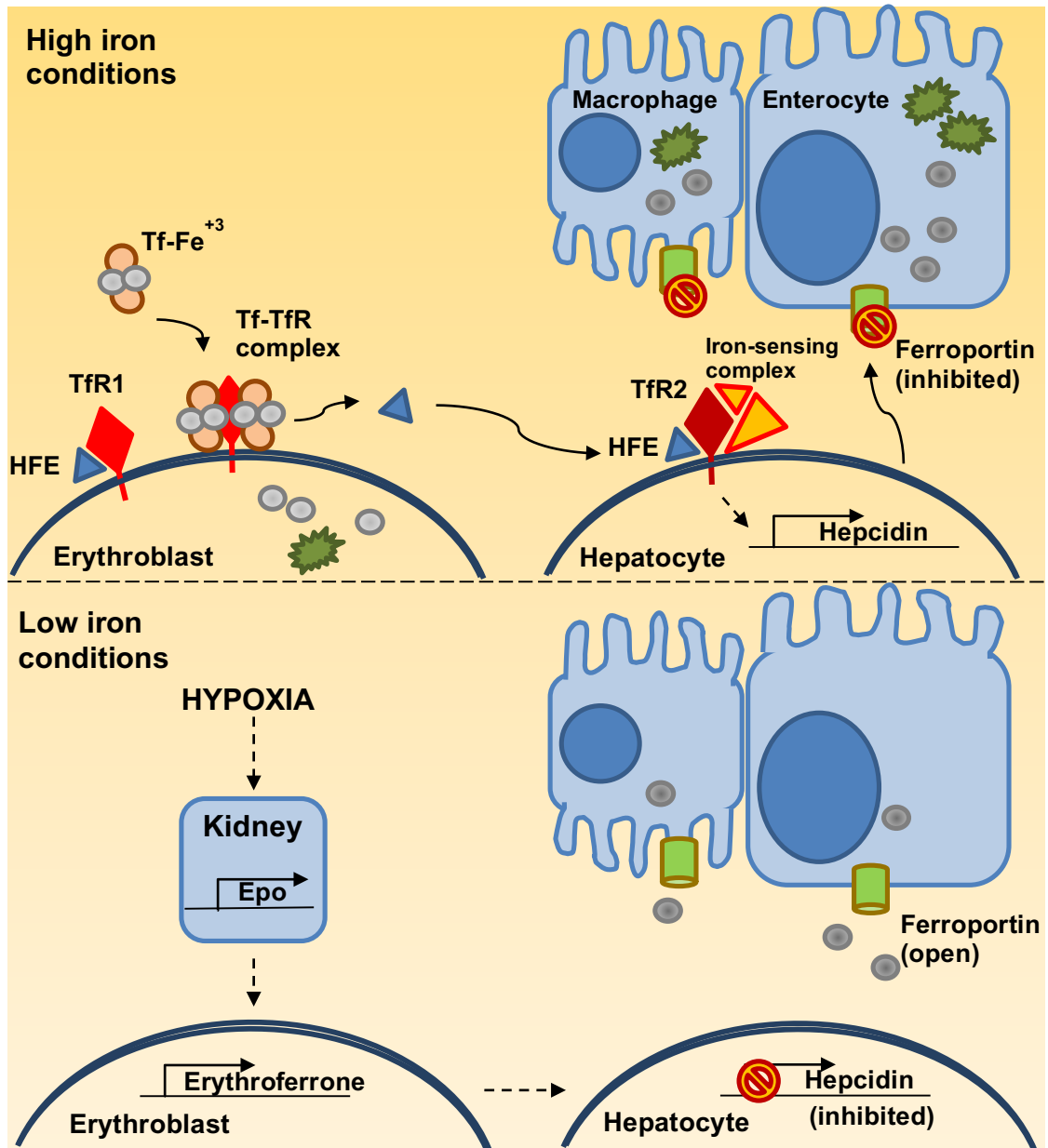


**Figure 1.6: Regulators of iron absorption**

Iron metabolism and absorption is a tightly regulated mechanism largely mediated by the actions of the hormones hepcidin and erythroferrone. During transferrin uptake, iron-bound Tf outcompetes the HFE molecule for a similar binding position on the transferrin receptor 1 (TfR1) dimer on the surface of iron-absorbing cells (eg: erythroblasts). The free HFE molecule binds to the TfR2 receptor, found mostly on the surface of hepatocytes. This triggers the hepatocyte to produce the hormone hepcidin, which is excreted from the liver and acts on cells that express ferroportin, such as enterocytes and macrophages. Hepcidin inhibits ferroportin, halting more iron from entering into circulation. When iron stores fall, the bone marrow is triggered to produce the hormone erythroferrone. Erythroferrone inhibits the function of hepcidin, reopening ferroportin and allowing iron to enter the bloodstream once more.

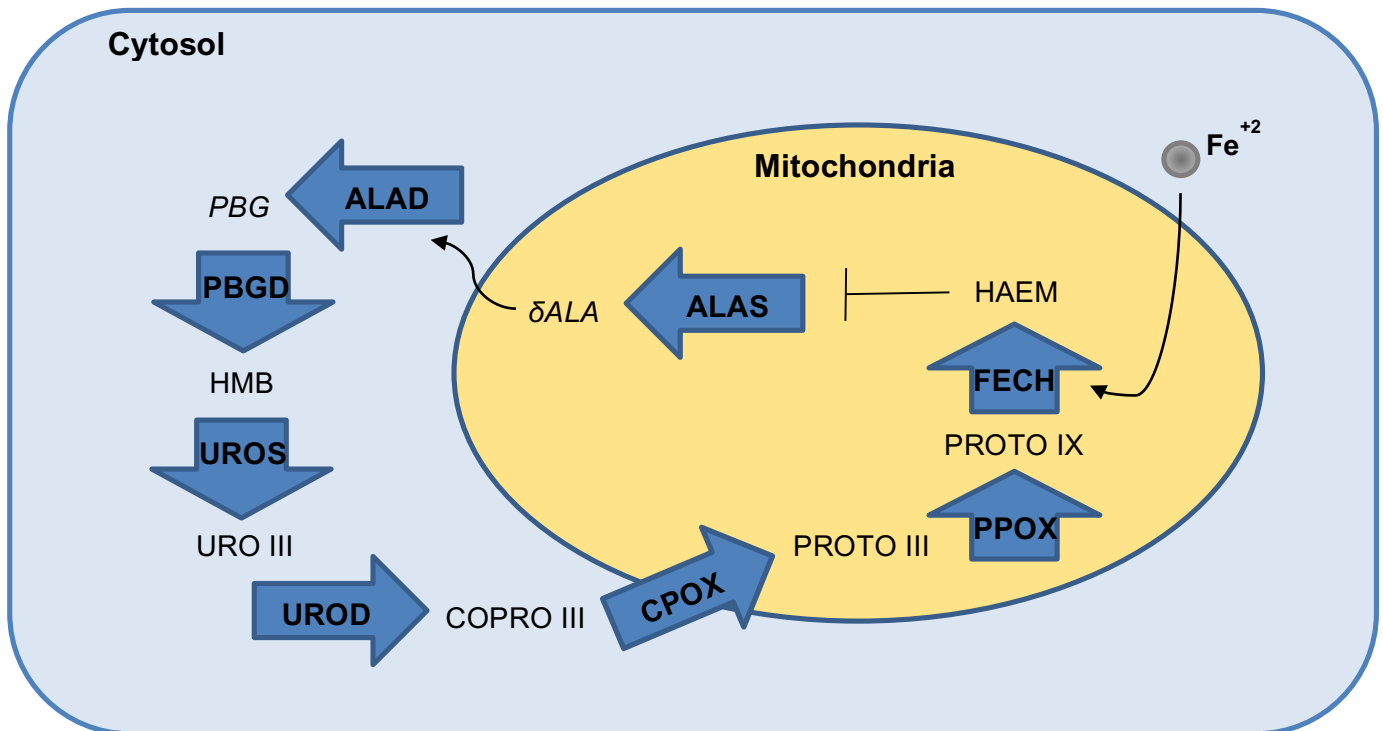


**Figure 1.7: The porphyrin biosynthesis pathway**

The porphyrin biosynthesis pathway generates haem from porphyrin precursors in the cytosol and mitochondria of various cell types (erythroblasts, hepatocytes, etc) through a series of linear enzymatic reactions. Porphyrin precursors (ALA and PBG) are synthesised into porphyrins in a step-wise manner in the cytosol and subsequently the mitochondria once again. In the final step of the biosynthesis pathway, iron ( $\text{Fe}^{+2}$ ) enters the mitochondria and is incorporated into the last porphyrin to become haem. Haem completes a feedback loop by directly inhibiting the first enzyme, ALAS.

Abbreviations: ALAD: ALA deaminase; PBGD: PBG deaminase; HMB: hydroxymethylbilane; UROS: uroporphyrinogen III synthase; URO III: uroporphyrinogen III; UROD: uroporphyrinogen decarboxylase; COPRO III: coproporphyrinogen III; CPOX: coproporphyrinogen oxidase; PROTO III: protoporphyrinogen III; PPOX: protoporphyrinogen oxidase; PROTO IX: protoporphyrin IX; FECH: ferrochelatase.

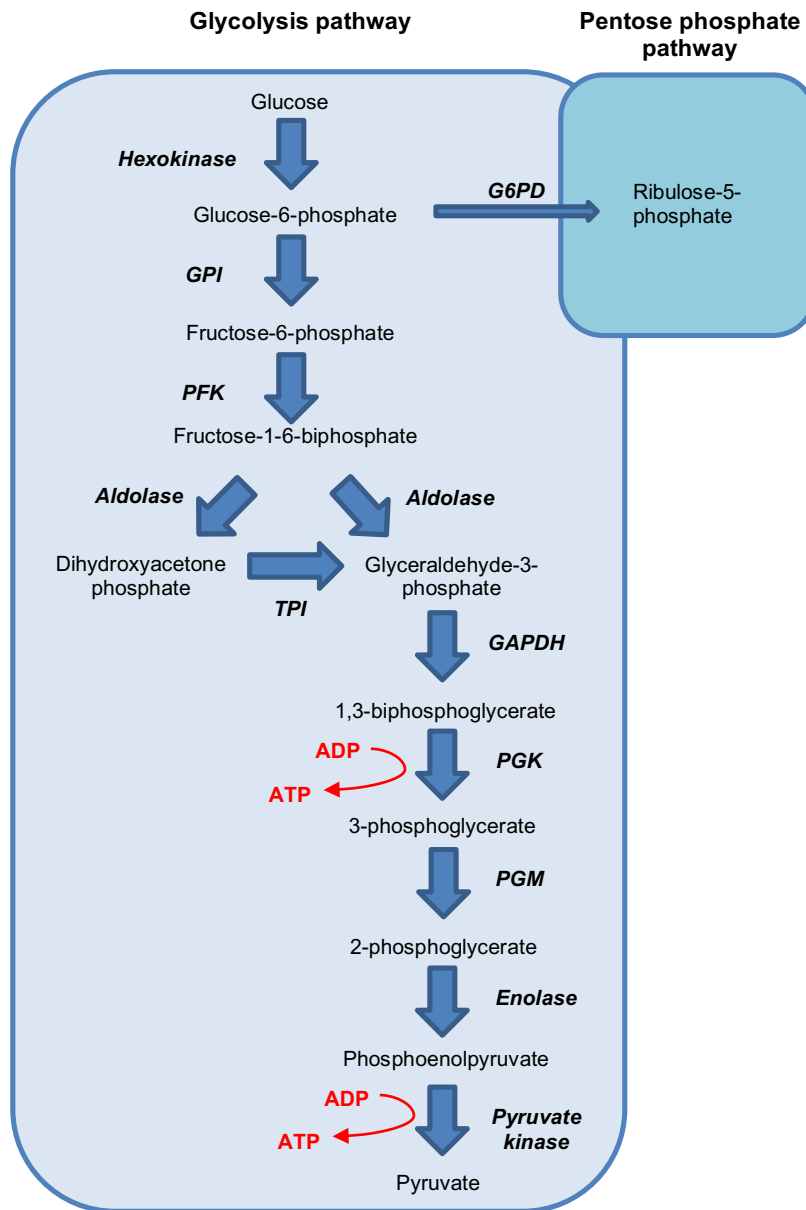


**Figure 1.8: Anaerobic glycolysis**

The enzymatic reactions of glycolysis take place in the cytosol of all cells and do not require oxygen or mitochondrial machinery. The outcome of glycolysis is the synthesis of two molecules each of pyruvate and ATP per molecule of glucose. In the red blood cell, glycolysis is the only metabolic pathway available for the synthesis of ATP. Mutations that occur in any of the glycolytic enzymes can result in metabolic diseases, which often present as haemolytic anaemias.

Abbreviations: G6PD: glucose-6-phosphate dehydrogenase; GPI: phosphoglucose isomerase; PFK: phosphofructose kinase; TPI: triosephosphate isomerase; GAPDH: glyceraldehyde-3-phosphate hydrogenase; PGK: phosphoglycerate kinase; PGM: phosphoglycerate mutase.

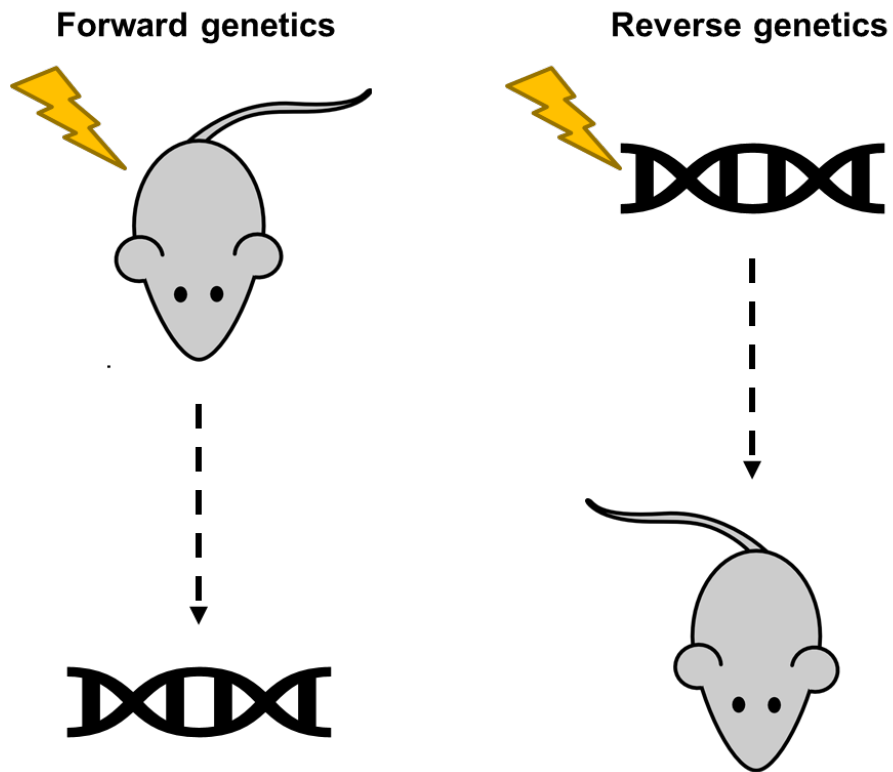


**Figure 1.9: Forward vs. reverse genetics**

The two traditional methods of gene studies in model organisms, such as mice, is through forward or reverse genetics. In forward genetics, the animal is manipulated in a way that will cause a random genetic mutation, such as by exposure to a chemical agent or radiation, producing a phenotype of interest. Researchers then endeavour to search the animal's DNA in order to find what genetic mutation caused that phenotype. In reverse genetics, the DNA is targeted and a gene of interest is edited, inserted, or deleted. Researchers then observe the animal to see what phenotype develops as a result of that genetic mutation.

**Table 1.1: The porphyrias**

<b>Porphyria</b>	<b>Affected enzyme</b>	<b>Symptoms</b>	<b>Excreted products</b>
<b>ALAD deficiency porphyria</b>	ALAD	Neurovisceral crises	δALA
<b>Acute intermittent porphyria</b>	PBGD	Neurovisceral crises	δALA, PBG
<b>Congenital erythropoietic porphyria</b>	UROS	Photosensitivity	Uro I, Copro I
<b>Porphyria cutanea tarda</b>	UROD	Photosensitivity	Uro I, Uro III
<b>Hereditary coproporphyria</b>	CPOX	Neurovisceral crises, photosensitivity	δALA, PBG, Copro III
<b>Variegate porphyria</b>	PPOX	Neurovisceral crises, photosensitivity	δALA, PBG, Proto III
<b>Erythropoietic porphyria</b>	FECH	Photosensitivity	Proto IX, ZnPP

The porphyrias are a collection of inheritable diseases that result from mutations in one of the enzymes of the haem biosynthesis pathway. Mutations can be autosomal dominant, recessive, or X-linked. While patient symptoms frequently overlap and are quite heterogenous in appearance and severity, each subset of porphyria has distinct porphyrin products that accumulate in the urine, faeces, or blood. These biochemical markers can be quantified and are required in order to provide an accurate diagnosis.

Abbreviations: ALAD: aminolevulinic acid deaminase; δALA: d-aminolevulinic acid; PBGD: PBG deaminase; PBG: porphobilinogen; UROS: uroporphyrinogen III synthase; URO: uroporphyrinogen III; UROD: uroporphyrinogen decarboxylase; COPRO: coproporphyrinogen III; CPOX: coproporphyrinogen oxidase; PPOX: protoporphyrinogen oxidase; PROTO: protoporphyrin; FECH: ferrochelatase; ZnPP: zinc protoporphyrin.

**Table 1.2: The RBC mutants**

<b>Mutant</b>	<b>Heterozygote phenotype</b>	<b>Homozygote phenotype</b>	<b>Gene</b>	<b>Chrom</b>	<b>Publication reference</b>
<b>RBC1, 4, 5, 6, 8, 17</b>	Microcytosis	Lethal (e12.5)	<i>Tfrc</i>	16	51, 56; <i>this thesis</i>
<b>RBC2</b>	Microcytosis	Lethal (8 weeks)	<i>Ank1</i>	8	49
<b>RBC3</b>	Macrocytosis	Lethal (e12.5)	<i>Scf</i>	10	-
<b>RBC7</b>	Microcytosis	Lethal (e12.5)	<i>Steap3</i>	1	-
<b>RBC10</b>	Microcytosis	Microcytosis	<i>Kcc1</i>	8	52
<b>RBC12</b>	Microcytosis	Lethal (8 days)	<i>Dnm2</i>	9	51, 53
<b>RBC13, 14</b>	Microcytosis	Lethal (e18.5)	<i>B-globin</i>	7	50
<b>RBC16</b>	Microcytosis	Lethal (e9.5)	<i>Cpox</i>	16	54; <i>this thesis</i>
<b>RBC19</b>	Macrocytosis	Macrocytosis, haemolytic anaemia	<i>Tpi1</i>	6	55; <i>this thesis</i>
<b>RBC21</b>	Microcytosis	Lethal (18.5)	<i>Tfrc</i>	16	56; <i>this thesis</i>

The RBC mutant mice identified in ENU mutagenesis screens were phenotyped by their red cell mean corpuscular volume (MCV), which classified them as either microcytic or macrocytic mutant strains. Dominant mutations were typically embryonic lethal in homozygosity (RBC6, RBC13, RBC16), while others were autosomal recessive in inheritance and generated a viable homozygous mutant with a more profound red cell phenotype (RBC19). The genetic mutations responsible for each phenotype were initially identified using traditional gene mapping and candidate gene sequencing (RBC1-8), gene mapping in combination with high-throughput sequencing (RBC9-16), and later WES and bioinformatics alone (RBC19 and RBC21). Many RBC mutants were found to be accurate models of congenital human red cell diseases, such as hereditary spherocytosis (RBC2),  $\beta$ -thalassemia (RBC13 and RBC14), hereditary coproporphyrinuria (RBC16), and TPI deficiency (RBC19).

---

## CHAPTER TWO

### Materials and Methods

This chapter outlines the solutions, equipment, materials, and experimental procedures used throughout this thesis. *Note: To avoid repetition, any materials or methods outlined in the published/submitted articles included in this thesis have been omitted from this chapter.*

## 2.1 Buffers, solutions, and basic reagents

Buffers, solutions, and reagents used throughout this thesis were all of analytical grade and purchased from standard distributors, as listed throughout. Solutions are maintained at room temperature unless stated otherwise.

**Agarose gel (0.8%) (electrophoresis):** 0.8g agarose boiled in 100mL TAE, with 3 $\mu$ L ethidium bromide added once cooled.

**BSA (1%) solution:** 1g Bovine Serum Albumin dissolved gently in 100mL PBS, stored at 4°C.

**Buffered saline glucose citrate (BSGC):** 7.0g NaCl, 218g KH<sub>2</sub>PO<sub>4</sub>, 1.2g Na<sub>2</sub>HPO<sub>4</sub>, 2.0g D-glucose, 4.0g Na<sub>3</sub>C<sub>6</sub>H<sub>5</sub>O<sub>7</sub>, dissolved in 1L dH<sub>2</sub>O, pH 7.4, stored at 4°C.

**cOMplete Proteinase inhibitor cocktail (Roche) x50:** 1 tablet dissolved in 1mL dH<sub>2</sub>O, stored at -20°C. Diluted to x1 in dH<sub>2</sub>O before use.

**DNA ladder (x6):** 100 $\mu$ L Lambda DNA/*HindIII* marker, 50 $\mu$ L *PhiX* 174 marker/*HaeIII*, 100 $\mu$ L Blue/Orange x6 DNA loading dye (Promega, Alexandria, Australia), in 350 $\mu$ L dH<sub>2</sub>O.

**FACS block solution (x50):** 1mg/mL IgG from rat serum (Sigma-Aldrich) in PBS. Diluted to x1 in PBS before use. Stored at 4°C.

**FACS buffer:** 2% v/v FBS and 0.2% v/v NaN<sub>3</sub> in PBS, stored at 4°C.

**Neomycin-treated acid water:** 10mL of 10mg/mL neomycin (in saline) added to 1L acidified H<sub>2</sub>O, pH 2.6, using HCl. Stored at 4°C.

**Paraformaldehyde (PFA) (4%):** 50g paraformaldehyde (Sigma-Aldrich), 200 $\mu$ L of 10M NaOH, in 500mL PBS, pH 7.5, stored at -20°C. Diluted to 2% in PBS before use.

**Phosphate buffered saline (PBS):** 2.85g NaHPO<sub>4</sub>.2H<sub>2</sub>O, 0.625g NaH<sub>2</sub>PO<sub>4</sub>.2H<sub>2</sub>O, 149 mM NaCl in 1L dH<sub>2</sub>O, pH 7.4.

**Red cell lysis buffer:** 156 mM NH<sub>4</sub>Cl at pH 7.6, stored at 4°C.

**Sequencing purification buffer:** 2 $\mu$ L of 1M MgSO<sub>4</sub> dissolved in 3mL Milli-Q H<sub>2</sub>O and 7mL ethanol.

**Sodium dodecyl sulphate (SDS) (10%) solution:** 10g SDS in 100mL dH<sub>2</sub>O.

**Sodium acetate:** 3M NaAc, pH 5.2.

**TAE:** 40mM Tris and 1mM EDTA, pH 8.2.

**TBS (x10):** 0.2M Tris, 1.5M NaCl. Working solution (x1 TBST) was prepared by diluting TBS and adding 0.05% Tween 20 (Amresco).

**Tail/ear clip digestion buffer:** 100mM Tris, 200mM NaCl, 5mM EDTA, and 0.2% SDS. 20 $\mu$ L of 20mg/mL Proteinase K (Roche) added prior to use, pH 8.0.

**TE buffer:** 10mM Tris and 1mM EDTA, pH 8.0.

**(Western blot) SLAB buffer (x5):** 5mM Tris HCl, 1% SDS, 2% Glycerol, 0.33%  $\beta$ -mercaptoethanol and 22.5mg/mL bromophenol blue, pH 6.8. Stored at -20°C. Diluted to x1 in dH<sub>2</sub>O before use.

**(Western blot) Separating gel:** 7.2mL Milli-Q H<sub>2</sub>O, 3.8mL separating gel buffer (375mM Tris HCl, pH 8.8, 0.1% SDS), 3.76mL 40% acrylamide, 224 $\mu$ L 10% ammonium persulfate (APS), and 10 $\mu$ L of tetramethylethylenediamine (TEMED) (Sigma-Aldrich). After pouring into the gel cast, a thin layer of isopropanol (roughly 500 $\mu$ L) was added to remove any air bubbles. Isopropanol was washed away thoroughly with dH<sub>2</sub>O once gel was set.

**(Western blot) Stacking gel:** 2.15mL Milli-Q H<sub>2</sub>O, 888 $\mu$ L stacking gel buffer (125mM Tris HCl, pH 6.8, 0.1% SDS), 450 $\mu$ L 40% acrylamide, 35 $\mu$ L 10% APS, and 10 $\mu$ L TEMED. Added to the stacking gel cast and set with a 1.5mm comb (Bio-Rad, California, USA) to create wells in the gel cast. Comb was removed once gel was set.

**(Western blot) Stripping buffer:** 0.1M glycine and 0.05% Tween 20 in TBST, pH 2.25.

**(Western blot) NuPAGE™ transfer buffer (x20):** 10.2g bicine, 13.1g bis-tris (free base), 0.75g EDTA in 125mL dH<sub>2</sub>O, stored at 4°C. Diluted to x1 in dH<sub>2</sub>O before use.

**(Western blot) NuPAGE™ MOPS SDS running buffer (x20):** 104.6g MOPS, 60.0g Tris, 10.0g SDS, 3.0g EDTA in 500mL dH<sub>2</sub>O, stored at 4°C. Diluted to x1 in dH<sub>2</sub>O before use.

## 2.2 Additional commercial kits

Additional commercially-available kits and reagents used throughout this thesis, which are not described in the published/submitted papers, are outlined here. Protocols were followed as per the manufacturer's instructions.

**Amersham electrogenerated chemiluminescence (ECL) kit:** For Western blotting. Available from GE Healthcare Lifesciences (Illinois, USA). Both reagents in the kit are mixed in a 1:1 solution immediately prior to use.

**BigDye™ Terminator v3.1 sequencing kit:** For sequencing/genotyping. Available from Thermo Fischer Scientific (Scoresby, Victoria, Australia).

**DNeasy Blood and Tissue kit:** For DNA extraction of tissues/blood products. Available from Qiagen (Hilden, Germany). Samples were initially digested overnight in 180µL tail/ear clip digestion buffer and 20µL Proteinase K at 56°C.

**QIAquick gel extraction kit:** For gel electrophoresis clean-up of gDNA (see section 2.7). Available from Qiagen.

**RNeasy extraction kit:** For RNA extraction of tissues/blood products. Samples were initially treated with TRIzol (Thermo Fischer Scientific) (see section 2.5) before being transferred to the kit.

**Transcription First Strand cDNA synthesis kit:** For the synthesis of cDNA from RNA. Available from Roche (Basel, Switzerland).

## 2.3 Antibodies

Table 2.1: Antibodies used for Western blotting

<b>Antibody name</b>	<b>Detects</b>	<b>Supplier</b>	<b>Dilution used</b>	<b>Band size</b>	<b>Refer to chapter/reference</b>
Rabbit anti-mouse Coproporphyrinogen oxidase Polyclonal Antibody	CPOX	Protein-Tech	1:5000	37kDa	Chapter 3, Ref 54
Goat anti-mouse Triosephosphate isomerase antibody	TPI	Abcam	1:1000-1:5000	26kDa	Chapter 4, Ref 55
Anti- $\beta$ -Actin HRP conjugate	Actin	Thermo Fischer	1:5000	42kDa	Chapter 4, Ref 55
Anti-GAPDH HRP conjugate	GAPDH	Thermo Fischer	1:1000	36kDa	Chapter 3, Ref 54

Table 2.2: Antibodies used for flow cytometry

<b>Antibody name</b>	<b>Fluorophore</b>	<b>Detects</b>	<b>Supplier</b>	<b>Dilution used</b>	<b>Refer to chapter/reference</b>
CD71	FITC	Transferrin receptor	BD Biosciences	1:50	Chapter 3-5, Ref 54-56
TER-119	FITC or PE	Glycophorin A	BD Biosciences	1:50	Chapter 3-5, Ref 54-56
Thiazole orange	FITC	dsDNA (Reticulocytes)	BD Biosciences	1ng/mL	Chapter 3-5, Ref 54-56
Tf Alexa-Fluor 647	APC	Ligand for CD71	Life Technologies	5mg/mL	Chapter 5, Ref 56

Streptavidin	PE	Secondary for biotin- conjugated cells	BD Biosciences	1:50	Chapter 4, Ref 55
--------------	----	---	-------------------	------	----------------------

## 2.4 Experimental animals

Table 2.3: Experimental mouse strains used throughout this study

<b>Strain name</b>	<b>Affected gene</b>	<b>Source</b>	<b>Refer to chapter/ reference</b>
BALB/c	Wildtype	BIO21	Chapter 3, Ref 54
SJL	Wildtype	WEHI	Chapter 4, Ref 55
C57BL/6	Wildtype	BIO21	Chapter 5, Ref 56
RBC16	<i>Cpox</i>	WEHI Mutagenesis screen	Chapter 3, Ref 54
RBC19	<i>Tpi1</i>	WEHI Mutagenesis screen	Chapter 4, Ref 55
RBC6	<i>Tfr</i>	WEHI Mutagenesis screen	Chapter 5, Ref 56
RBC21	<i>Tfr</i>	WEHI Mutagenesis screen	Chapter 5, Ref 56

## 2.5 Blood and cell preparation techniques

**Blood sampling:** Small volumes of blood (<10µL) were extracted from tail vein venepuncture.

Mice were briefly placed under a heating lamp (maximum 30 minutes) to dilute blood vessels. Mice were then secured in a cone and a 23G needle, flushed with BSGC, was used to puncture the tail vein. Larger volumes of blood (20-50µL) were obtained via submandibular venepuncture with the mouse secured in a scruff hold. Very large volumes of blood (100-500µL) were obtained from cardiac puncture performed on euthanised mice (via CO<sub>2</sub>) using a 23G needle flushed with BSGC. All blood was collected in EDTA tubes and kept at 4°C.

**Bone marrow and organ extraction:** Bone marrow was harvested from the femurs of euthanised adult mice using 23G needles, and flushed with 1mL PBS repeatedly into Eppendorf tubes. Organs

were partially or wholly dissected from euthanised mice and kept in ice-cold PBS in Eppendorf tubes or in 10mL polystyrene round-bottom tubes. Samples were kept on ice or stored at 4°C.

**Foetal liver cell extraction:** Foetal livers were harvested from e14.5 mouse embryos. Embryos were collected from euthanised female mice and placed into 6-well plates filled with ice-cold PBS. Foetal livers were extracted from individual embryos and gently homogenised by repeated pipetting using a 1mL syringe and an 18G drawing needle. Cells were then passaged gently through a 40µm nylon strainer and washed twice in PBS using centrifugation at 300xg for 5 minutes at 4°C.

**RNA extraction:** RNA was extracted from tissue samples (bone marrow, etc) using the (Thermo Fischer Scientific) TRIzol method. A known number of homogenised cells were repeatedly pipetted in 1mL TRIzol (Thermo Fischer Scientific) in Eppendorf tubes to induce lysis. 200µL chloroform was then added to the sample and allowed to sit for 15 minutes at room temperature. Samples were then centrifuged at 500xg for 15 minutes to induce phase separation, and the upper aqueous phase, containing the RNA, was extracted into fresh tubes. RNA samples then underwent a modified phenol:chloroform cleaning process using the RNeasy extraction kit (see section 2.2). The final product was eluted into 50-100µL RNase-free H<sub>2</sub>O and stored at -80°C.

**Serum preparation:** EDTA-treated whole blood (>50µL) was centrifuged at 10,000 RPM for 15 minutes to separate serum from other blood products. Serum was extracted by pipetting the acellular upper layer into Eppendorf tubes and frozen at -20°C until use. Serum samples with evidence of haemolysis were discarded.

**Western blot cell preparation:** Bone marrow or tissue samples were collected from euthanised mice (as above) and homogenised in cold PBS using a 40µL nylon strainer to obtain a single-cell suspension. A maximum of  $1 \times 10^6$  cells were washed three times in PBS using centrifugation set to 350xg for 5 minutes at 4°C. Cells were then vortexed and pipetted thoroughly in SLAB buffer (see

section 2.1). Samples were heated for 5 minutes at 100°C prior to use, or otherwise stored at -20°C.

## 2.6 Additional techniques and experimental methods

Additional techniques and methods used throughout this thesis, which are not described in the published/submitted papers, are outlined here.

**Blood film and histology staining:** For blood films, a small volume (<10µL) of EDTA-treated whole blood was smeared onto SuperFrost® microscope slides (Menzel-Glaser, Braunschweig, Germany) and air dried. Blood smears were stained with May-Grumwald Giemsa solution, then cover-slipped using DePex mounting medium. For histology, organs or whole embryos were harvest from euthanised mice and fixed in 2% PFA for 24 hours. Samples were then transferred to 70% ethanol and underwent sectioning, embedding, and staining by the Monash Histology Platform (Clayton, Victoria, Australia), where they were stained in Hematoxylin & Eosin (H&E) solution. Stained slides were then cover-slipped using DePex mounting medium. Blood smears and histology slides were examined under a light microscope.

**Bone marrow and foetal liver transplantations:** Live animal transplantations were performed on adult recipient mice subjected to a single dose of lethal irradiation (950 cGy) using a cesium-137  $\gamma$ -emitting irradiator (Gamma Cell 40, MSD Nordion, Ontario, Canada). Donor mice (or e14.5 embryos) were euthanised and bone marrow (or foetal liver) was harvested and made into a single-cell suspension (see section 2.5) under sterile conditions.  $1 \times 10^6$  live donor cells, as well as  $2 \times 10^5$  supporting spleen cells, were counted, washed, and resuspended in 200µL sterile PBS. Irradiated recipient mice were held in a cone and injected intravenously via the tail vein with donor cells using a 0.3mL Ultra-Fine insulin syringe (BD Sciences). Recipient mice were kept on neomycin-treated acid water for 14 days following transplantation to avoid infections.

**Cell counts:** Non-blood cell samples (single cell suspensions of bone marrow, tissue, etc) were counted using the Muse<sup>®</sup> Cell Analyzer (Merck), which automatically calculated the viable cell number from the volume and dilution factor.

**Flow cytometry and gating for erythroid cell sub-populations:** Flow cytometric protocols were largely focused on erythroid cell populations using TER-119 and CD71 antibodies (see section 2.3). A known number of cells ( $1 \times 10^6$  –  $5 \times 10^6$ ) from single cell suspensions were placed in 5mL polystyrene round bottom tubes (Falcon) in 100uL PBS. Cells were incubated in FACS blocking solution for 5 minutes on ice to prevent non-specific antibody binding. The necessary antibodies were then added and cells were left to incubate in the dark on ice for 30-45 minutes.

Compensation controls were also prepared. Following staining, cells were washed twice by centrifugation at 500xg for 5 minutes. If a secondary antibody was required (SA), it was added to the pre-stained cells and left to incubate in the same conditions as stated, then washed twice as stated. Cells were resuspended in 200µL PBS with 1µL propidium iodide (PI) (Sigma-Aldrich), added to recognise dead cells. Flow cytometry was performed on the FACSCalibur<sup>™</sup> (BD Sciences) and analysis was conducted using the FlowJo<sup>®</sup> software (BD Sciences). Erythroid populations were gated on live (PI-negative) cells and divided into erythroid subsets as per Socolovski, 2001<sup>56</sup>, which distinguishes early erythroblasts (TER-119<sup>lo</sup>CD71<sup>hi</sup>), polychromatic erythroblast (TER-119<sup>hi</sup>CD71<sup>hi</sup>), orthochromic normoblasts (TER-119<sup>hi</sup>CD71<sup>mid</sup>) and mature erythroid cells (TER-119<sup>hi</sup>CD71<sup>lo</sup>).

**Reticulocyte counts:** The percentage of circulating reticulocytes in whole blood samples was determined by flow cytometry (see above) using the additional stain, Thiazole orange (TO). 1-2µL of EDTA-treated whole blood was suspended in 90µL PBS and 10µL BSA 1% buffer, and stained with TER-119 and TO, as per the protocol above. A single-stain sample lacking TO was used as the 0% control. Stained samples were analysed on the FACSCalibur<sup>™</sup>, which selected for live TER-119+ cells. Cells which were deemed TO+ were counted as reticulocytes. The total percentage of reticulocytes was therefore taken as the fraction of cells deemed TER-119+TO+ divided by the total TER-119+ cells in the sample.

**Real-time quantitative PCR:** RT-qPCR was performed on cDNA generated from 1 µg RNA samples using the First Strand cDNA kit (see section 2.2). PCR was performed on the LightCycler<sup>®</sup> 480II (Roche) using the SYBR<sup>®</sup> Green protocol in a 96-well plate. Samples were tested in duplicate, where each test reaction contained 2 µL cDNA, 0.5 µL each forward and reverse primers, and GoTaq<sup>®</sup> Master Mix (Promega, Wisconsin, USA). Standard curves for each test gene and a housekeeping gene were also prepared, where duplicate wells containing decreasing concentrations of wildtype cDNA in nuclease-free water (1:1, 1:5, 1:25, 1:125) were generated, and added to the PCR reaction mixture. The reaction then underwent a number of cycles, including an incubation cycle (95°C for 5 minutes), 45-50x amplification cycles (95°C for 10 seconds, 57°C for 10 seconds, 72°C for 10 seconds), and a melting curve (95°C for 10 seconds, 65°C for 10 seconds, 97°C continuously). Analysis was performed using the LightCycler<sup>®</sup> software (LCS48 1.5.1.62). The quality of the run was determined by the presence of a single peak per gene target, and also by the linearity of the standard curve. Relative expression of the target gene versus the housekeeping gene in each sample was then extrapolated from the standard curves and calculated. See results chapters for more information on individual projects, including primer lists.

**Western blotting:** To examine protein content in a cell sample, separated by size, Western blotting was employed. 20 µL of cell lysates prepared in SLAB buffer (see section 2.5) were loaded into the wells of an acrylamide-based gel, made up of a separating and stacking gel (see section 2.1). 15 µL of a protein ladder (Precision Plus Protein<sup>™</sup> WesternC, Bio-Rad) was also added to one of the lanes. The loaded gel was then placed in a mini-PROTEAN Tetra Cell tank (Bio-Rad) filled with running buffer (see section 2.1) and allowed to run for 30 minutes at 80V, then at 130V until the loading dye had run to the bottom of the gel. The gel-separated proteins were then transferred onto a polyvinylidene difluoride (PVDF) membrane (GE Healthcare Life Sciences), soaked in methanol and then washed in transfer buffer (see section 2.1). The gel was clamped firmly to the PVDF membrane in a transfer cassette and placed in a tank filled with transfer buffer, a magnetic stirring bead, and an ice block. The transfer was performed at 4°C in a cold room on a magnetic spinner, at 100V for 2 hours. The membrane was then removed from the transfer tank, washed

briefly in dH<sub>2</sub>O, and blocked in 2% skim milk at room temperature for 1 hour. The membrane was then saturated in the appropriate primary antibody, diluted in 5% BSA (see Table 2.1), overnight at 4°C. The following day, the stained membrane was washed in TBST five times for 5 minutes each. The membrane was then stained in the appropriate secondary antibody, diluted in 5% skim milk, for 1 hour at 4°C. Again, the membrane was washed five times in TBST. The stained membrane was then exposed to 1mL of the combined ECL kit reagents (see section 2.2) for one minute and dried with tissue before imaging. Imaging of the proteins was performed on the ChemiDoc™ Touch Imaging System set to chemiluminescence, with exposure times adapted for each protein for optimal clarity. If stripping was required, the membrane was washed in stripping buffer (see section 2.1) for 10 minutes, washed five times in TBST, then blocked again using 2% skim milk at room temperature for 1 hour. Antibody staining and imaging processes then proceeded as above. The densities of imaged bands were analysed using the Image Lab software (Bio-Rad).

## 2.7 Sequencing and analysis

Laboratory techniques used for next generation sequencing preparation and data processing used throughout this thesis, which are not described in the published/submitted papers, are outlined here.

**Sample preparation for whole exome sequencing (WES):** Genomic DNA for WES was prepared in each study from the tails of adult mice (RBC16, RBC19) or e14.5 embryos (RBC21) using the DNeasy extraction kit (see section 2.2). The quantity and quality of the gDNA was tested using the Nanodrop 1000 photospectrometer (Thermo Fischer), where high quality gDNA was determined to have an A260/A280 ratio between 1.8 and 2.0 at an absorbance of 260nm. Gel electrophoresis was also used to ensure gDNA was not degraded (i.e.: a clear band larger than 12kb with no smearing). Two samples of gDNA per mouse strain were then sent to the Australian Genome Research Facility (AGRF) to undergo WES using the Illumina Hi-Seq platform. See results chapters for more information on individual projects.

**Bioinformatics and analysis results:** Bioinformatics was performed for each project by AGRF, which aligned reads obtained from sequencing to the reference sequence of each mouse strain, based on its genetic background (C57BL/6, BALB/c, or SJL). Possible mutations identified by incorrect base-pairs within the sequence were flagged for review and further investigated. Only mutations identified in coding regions or splice sites, and which appeared in both test samples, were considered. Online genome browsers, such as Ensembl ([www.ensembl.org](http://www.ensembl.org)) and the National Centre for Biotechnology Information ([www.ncbi.nlm.nih.gov/genome](http://www.ncbi.nlm.nih.gov/genome)) were utilised to investigate the possible function or disease relevance of each candidate gene. Mutations identified within genes with known erythroid function, or with known human disease relevance, were prioritised and subjected to Sanger sequencing to confirm the mutation. See results chapters for more information on individual projects, including sequencing primers.

## **2.8 Statistical analysis**

Unless stated otherwise, all experiments were conducted on at least three animals per genotype, with a minimum of two independent experiments. Where applicable, results were expressed as the mean  $\pm$  standard deviation. For the determination of a statistical difference, a two-tailed student's t-test was employed, where  $p < 0.05$ , or as defined in figure legends.

---

## CHAPTER THREE

### **A mouse model of hereditary coproporphyria identified in an ENU mutagenesis screen**

The following chapter describes the first complete set of results obtained for this thesis, which have been published in the form of a research article in a peer-reviewed scientific journal during enrolment (see *Thesis including published works*), and recognises the leading author as Ashlee J. Conway. The hypotheses, aims, and expected outcomes of this thesis are each discussed in this chapter, and additional content specific to the article (methods, references, etc) are also supplied. The article has not been altered from its original published format.

## RESEARCH ARTICLE

# A mouse model of hereditary coproporphyria identified in an ENU mutagenesis screen

Ashlee J. Conway<sup>1</sup>, Fiona C. Brown<sup>1</sup>, Robert O. Fullinfaw<sup>2</sup>, Benjamin T. Kile<sup>3</sup>, Stephen M. Jane<sup>1,4</sup> and David J. Curtis<sup>1,\*</sup>

## ABSTRACT

A genome-wide ethyl-N-nitrosourea (ENU) mutagenesis screen in mice was performed to identify novel regulators of erythropoiesis. Here, we describe a mouse line, RBC16, which harbours a dominantly inherited mutation in the *Cpox* gene, responsible for production of the haem biosynthesis enzyme, coproporphyrinogen III oxidase (CPOX). A premature stop codon in place of a tryptophan at amino acid 373 results in reduced mRNA expression and diminished protein levels, yielding a microcytic red blood cell phenotype in heterozygous mice. Urinary and faecal porphyrins in female RBC16 heterozygotes were significantly elevated compared with that of wild-type littermates, particularly coproporphyrinogen III, whereas males were biochemically normal. Attempts to induce acute porphyric crises were made using fasting and phenobarbital treatment on females. While fasting had no biochemical effect on RBC16 mice, phenobarbital caused significant elevation of faecal coproporphyrinogen III in heterozygous mice. This is the first known investigation of a mutagenesis mouse model with genetic and biochemical parallels to hereditary coproporphyria.

**KEY WORDS:** Ethyl-N-nitrosourea, Hereditary coproporphyria, CPOX, Anaemia

## INTRODUCTION

The porphyrias are a collection of hereditary disorders characterised by a deficiency in one or more of the enzymes within the haem biosynthesis pathway (Kauppinen, 2005). Hereditary coproporphyria (HCP) is an acute hepatic disorder that stems from a dominantly inherited mutation in the gene encoding the sixth haem enzyme coproporphyrinogen III oxidase (*CPOX*) (Siegesmund et al., 2010). This enzyme is responsible for the conversion of coproporphyrinogen III into protoporphyrinogen IX in the mitochondria of haem-synthesising cells. More than 65 mutations within the *CPOX* gene have been characterised in humans so far, encompassing missense, nonsense, frameshift and insertion/deletion mutations, each with variable penetrance, enzyme functionality and clinical manifestation

(Bissell and Wang, 2015). Clinically, porphyria usually emerges in adolescence with acute attacks triggered by factors that activate hepatic enzymes, such as fasting, alcohol, sulphonamide antibiotics, and hormones such as progesterone (Bissell and Wang, 2015). Biochemically, HCP presents with a marked increase in porphyrin precursors, such as porphobilinogen (PBG), as well as porphyrins, notably coproporphyrinogen III, which accumulate and are detected in urine and faeces in high concentrations during episodic attacks, but can be normal or only marginally elevated during latent periods. Avoidance of known triggers is so far the only approach to managing the acute hepatic porphyrias. Symptoms can be alleviated with substances that inhibit haem biosynthesis, such as glucose loading (Anderson et al., 2005) or the administration of haem arginate (Besur et al., 2014). A liver transplant has been shown to be curative in some subtypes of porphyria (Singal et al., 2014).

Animal models representing the hereditary porphyrias have been generated for all porphyria subtypes except for HCP and aminolevulinic acid dehydratase deficiency porphyria (ADP) (Richard et al., 2008; Homedan et al., 2015; Medlock et al., 2002; Phillips et al., 2011). These animal models have been vital for the understanding of mitochondrial biosynthesis pathways and the development of novel gene replacement therapies. Through an ethyl-N-nitrosourea (ENU) mutagenesis screen to identify novel regulators of erythropoiesis, we have generated a novel mouse strain harbouring a nonsense mutation in *Cpox* (W373X), resulting in a microcytic hypochromic red blood cell phenotype. This mouse strain is the first reported model of hereditary coproporphyria with parallels to the human condition.

## RESULTS

### Characterisation of a mouse strain with microcytic anaemia

Using ENU mutagenesis to identify novel genes regulating erythropoiesis, we identified a mouse line (RBC16) with a microcytic anaemia (Table 1). Fifty per cent of progeny born from the founder mouse mated with a wild-type mouse displayed a reduced mean corpuscular volume (MCV), indicating that the phenotype was autosomal dominant and fully penetrant. Red cell distribution width (RDW) was markedly increased in heterozygotes, while platelet counts and white cell counts were normal. Peripheral blood smears revealed microcytic hypochromic red cells and abundant target cells (Fig. 1A). RBC16 heterozygotes (+/M) had enlarged spleens with increased red pulp (Fig. 1B) and flow analysis of spleen cells revealed a substantial increase in early erythroblast expansion (Fig. 1C). No notable pathology was identified in the liver (data not shown). Increased spleen size suggested the possibility of haemolysis; however, reticulocyte counts (Table 1) and red cell half-life (Fig. 1D) were both normal. In addition, whole blood haem in the red cells of heterozygotes was found to be significantly reduced (Fig. 1E), while serum ferritin was markedly elevated (Fig. 1F). RBC16 heterozygous mice therefore presented

<sup>1</sup>Australian Centre for Blood Diseases, Monash University and Clinical Haematology, Alfred Health, Melbourne 3004, Australia. <sup>2</sup>Porphyria Reference Laboratory, Biochemistry Department, Royal Melbourne Hospital, Parkville 3050, Australia. <sup>3</sup>ACRF Chemical Biology Division, The Walter and Eliza Hall Institute of Medical Research, Parkville 3052, Australia. <sup>4</sup>Central Clinical School, Monash University, Melbourne 3004, Australia.

\*Author for correspondence (david.curtis@monash.edu)

© B.T.K., 0000-0002-8836-8947; S.M.J., 0000-0003-2968-359X; D.J.C., 0000-0001-9497-0996

This is an Open Access article distributed under the terms of the Creative Commons Attribution License (<http://creativecommons.org/licenses/by/3.0>), which permits unrestricted use, distribution and reproduction in any medium provided that the original work is properly attributed.

**Table 1. Full blood examination of RBC16 mice**

	Female		Male	
	+/+	+/M	+/+	+/M
No. of mice	32	28	21	36
RCC ( $\times 10^{12}/l$ )	9.93 $\pm$ 1.2	10.69 $\pm$ 0.8*	10.4 $\pm$ 0.5	10.66 $\pm$ 1.0
Hb (g/dl)	15.2 $\pm$ 1.3	13.7 $\pm$ 1.2*	15.3 $\pm$ 0.8	13.5 $\pm$ 1.4*
HCT (%)	51.9 $\pm$ 5.1	46.8 $\pm$ 4.5*	53.9 $\pm$ 3.5	46.6 $\pm$ 5.2*
MCV (fl)	51.5 $\pm$ 2.8	43.8 $\pm$ 2.9*	51.9 $\pm$ 2.1	43.8 $\pm$ 2.3*
MCH (pg)	15.0 $\pm$ 0.6	13.0 $\pm$ 0.5*	14.7 $\pm$ 0.4	12.7 $\pm$ 0.5*
MCHC (g/dl)	29.1 $\pm$ 2.2	29.8 $\pm$ 2.4	28.5 $\pm$ 1.6	28.9 $\pm$ 2.0
RDW (%)	19.3 $\pm$ 1.3	24.9 $\pm$ 1.2*	19.2 $\pm$ 1.1	24.6 $\pm$ 1.3*
WBC ( $\times 10^9/l$ )	8.66 $\pm$ 2.0	9.79 $\pm$ 2.4	8.77 $\pm$ 1.4	9.69 $\pm$ 3.1
Platelets ( $\times 10^9/l$ )	840 $\pm$ 236	907 $\pm$ 240	1108 $\pm$ 167	1036 $\pm$ 301
Reticulocytes (%)	3.3 $\pm$ 1.9	2.6 $\pm$ 1.1	3.2 $\pm$ 1.6	3.6 $\pm$ 1.2

Blood parameters obtained from 7-week-old wild-type (+/+) and RBC16 heterozygous (+/M) mice. All values are means $\pm$ s.d. Two-tailed Student's *t*-test: \**P*<0.05 compares wild-type values to heterozygotes of the same gender.

with microcytic anaemia more suggestive of a defect in haem iron than globin chain synthesis.

### RBC16 mice have a mutation of the haem biosynthetic pathway gene *Cpox*

The ENU-induced mutation was mapped by crossing RBC16<sup>+M</sup> mice (C57BL/6 background) with wild-type Balb/c mice as previously described (Brown et al., 2013). Genome-wide and fine-mapping of single nucleotide polymorphisms (SNPs) was performed on animals displaying low MCV, which localised the mutation to a region lying between 56.46 Mb and 60.98 Mb on chromosome 16 (Fig. 2A). Custom genome capture of the 3.43 Mb genomic interval was combined with massively parallel sequencing of DNA from a RBC16<sup>+M</sup> mouse (based on low MCV) using the Illumina HiSeq platform. This identified a G to A substitution at position c.1118 in exon 5 of *Cpox* (NM\_007757.2), predicted to produce an immediate stop codon in place of a highly-conserved tryptophan at amino acid 373 (W373X) (Fig. 2B). Sanger sequencing of genomic DNA extracted from multiple presumed heterozygotes, identified by low MCV, confirmed this mutation. Sanger sequencing of cDNA, generated from the bone marrow of *Cpox*<sup>c.1180G>A</sup> heterozygotes (denoted as *Cpox*<sup>+W373X</sup> hereafter), did not detect the nucleotide substitution (Fig. 2B), suggesting that the truncated transcript had undergone degradation. In addition, quantitative real-time (Q)PCR demonstrated a 50% reduction in *Cpox* mRNA expression (Fig. 2C), and western blotting of liver lysates confirmed a similar loss of total CPOX protein (Fig. 2D). Overall, the absence of detectable mRNA and 50% reduction in protein suggested the W373X mutation was a functional null allele.

Intercrossing of heterozygous *Cpox*<sup>+W373X</sup> mice did not yield a third phenotype in adult progeny, suggesting embryonic lethality of homozygotes. Genotyping of embryos showed that homozygous mutants did not survive beyond embryonic day (E) 9.5 (Table 2). Microscopic examination of E9.5 homozygous embryos showed severe developmental delays, including underdeveloped phalangeal arch structures, lack of prominent forelimb bud, and an open rostral neural tube (Fig. 2E). A vascularised yolk sac was visible in the homozygotes with evidence of blood cell formation, suggesting that homozygous mutants did not die as a result of an inability to produce blood.

### *Cpox*<sup>+W373X</sup> mice display a mild hereditary coproporphria phenotype

The hallmark biochemical feature of HCP is elevated porphyrins, notably coproporphyrinogen III and uroporphyrinogen, in the urine

and faeces of affected individuals. Analysis of *Cpox*<sup>+W373X</sup> female mice, using HPLC, revealed a three- to four-fold increase in porphyrins, particularly coproporphyrinogen III, in the urine (Fig. 3A) and faeces (Fig. 3B) in comparison to wild-type mice. Male heterozygotes, however, did not show elevated porphyrins, and were subsequently excluded from further tests. In the faeces, the ratio of the two coproporphyrinogen isomers (CIII:CI) was significantly elevated in female heterozygotes (Fig. 3C), which is highly specific for the diagnosis of HCP (Allen et al., 2005). Despite elevated levels of porphyrins, urinary porphobilinogen (PBG) was normal in female *Cpox*<sup>+W373X</sup> mice (Fig. 3D), suggesting a dormant HCP phenotype. Thus, the *Cpox*<sup>+W373X</sup> mouse strain had some, but not all, of the biochemical features of hereditary coproporphria.

### Fasting does not induce crisis

In patients with porphyria, fasting can trigger an acute crisis by activation of hepatic enzymes. In particular, the activity of the enzyme aminolevulinic acid synthase (ALAS-1) is believed to be a crucial driver of clinical crises by supplying haem-synthesising cells with the rate-limiting porphyrin precursor, 5-aminolevulinic acid (ALA) (Handschin et al., 2005). To determine if fasting increases porphyrin production and induces clinical crises in *Cpox*<sup>+W373X</sup> mice, females were fasted for 15 h on two consecutive days and urine was collected. Despite fasting, mice remained clinically well and urinary porphyrins (uroporphyrinogen and coproporphyrinogen III) did not significantly increase (Fig. 4A). In the faeces, the CIII:CI ratio also remained unchanged (Fig. 4B). There was a three-fold increase in the porphyrin precursor, PBG, in the urine but this was observed equally in wild-type and *Cpox*<sup>+W373X</sup> mice (Fig. 4C). To understand why fasting did not increase porphyrins, liver mRNA transcription levels of *Alas1* and *Cpox* were analysed via quantitative real-time (Q)PCR. As expected, fasting induced a three- to four-fold increase in *Alas1* expression in both wild-type and *Cpox*<sup>+W373X</sup> mice (Fig. 4D). *Cpox* mRNA levels also increased proportionally, with fasting levels in *Cpox*<sup>+W373X</sup> mice remaining approximately half that of wild-type mice (Fig. 4E). Thus, fasting did not induce the clinical or biochemical changes of a porphyric crisis.

### Phenobarbital elevates faecal coproporphyrinogen III in *Cpox*<sup>+W373X</sup> mice

Phenobarbital is a potent porphyrinogenic agent and common crisis stimulant, used in experimental animal models to induce acute porphyric attacks in various porphyria subtypes (Lindberg et al., 1996; Yasuda et al., 2014). Therefore, to induce the maximum porphyric stress, female *Cpox*<sup>+W373X</sup> mice and age-matched wild-type females were treated daily with phenobarbital for 4 days, followed by analysis of urinary and faecal porphyrins. Faecal coproporphyrinogen III levels in the faeces were significantly elevated in heterozygous *Cpox*<sup>+W373X</sup> mice following exposure to phenobarbital (Fig. 5A), accompanied by a significant elevation in the CIII:CI ratio (Fig. 5B). However, urinary porphyrins were not significantly increased above baseline levels following phenobarbital treatment (Fig. 5C). Urinary PBG showed an identical three-fold increase in both wild-type and *Cpox*<sup>+W373X</sup> mice (Fig. 5D). Phenobarbital had a different effect on induction of *Alas1* and *Cpox* mRNA compared with fasting, with a more potent activation of liver mRNA expression of *Alas1* (10- to 20-fold) than *Cpox* (two-fold) (Fig. 5E,F). In summary, the more potent induction of *Alas1* by phenobarbital was able to increase faecal coproporphyrin III in *Cpox*<sup>+W373X</sup> mice.

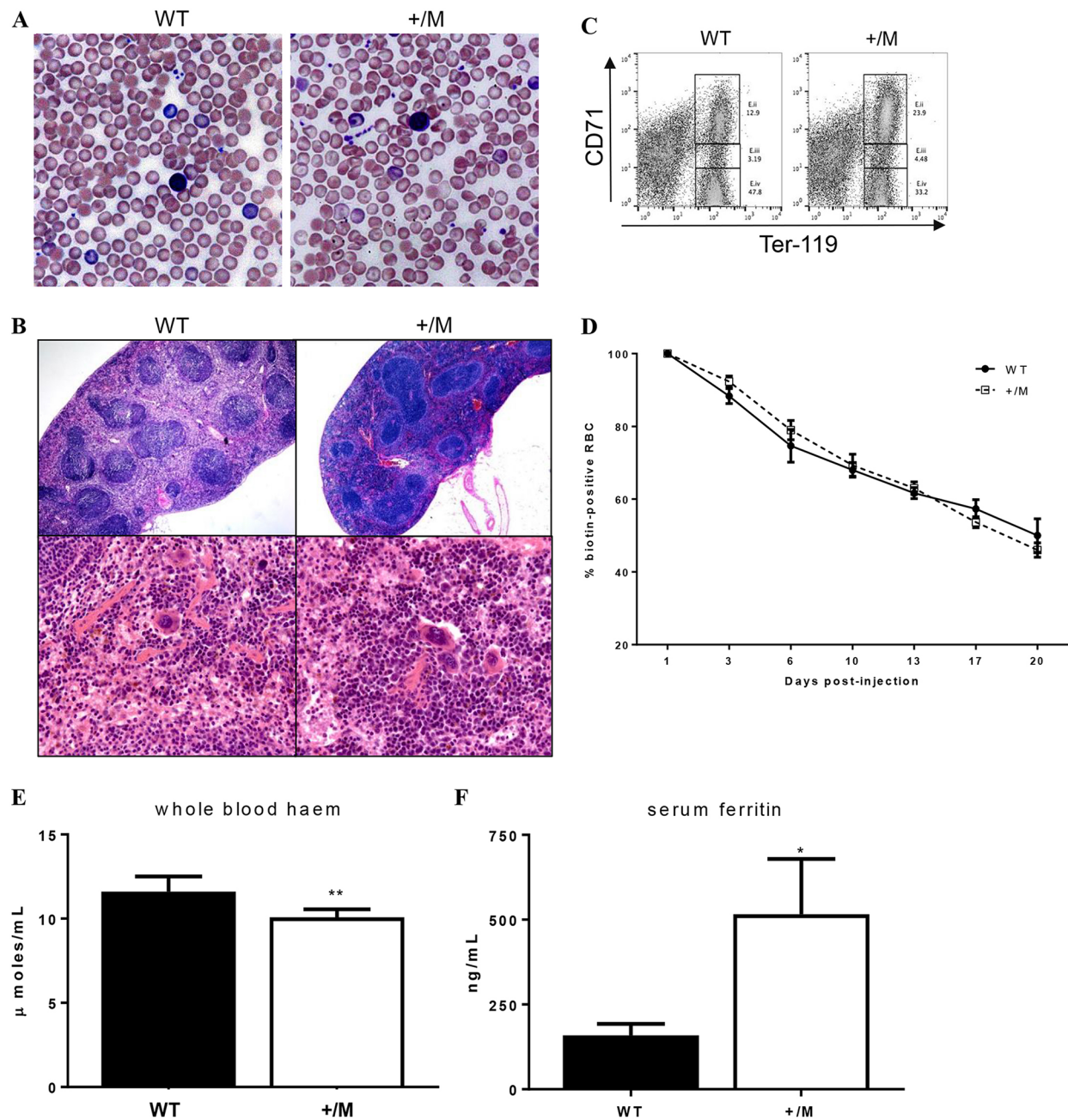


**Fig. 1. Phenotype of the RBC16 mouse mutant.** (A) Peripheral blood smears of 7-week-old wild-type (WT) and RBC16 heterozygous (+/M) mice show microcytic hypochromic red cells and prominent target cells. (B) H&E staining of sectioned spleens harvested from 4-month-old wild-type and heterozygous mice at both low ( $\times 40$ ) and high ( $\times 200$ ) magnification. (C) FACS plot of spleen cells stained with Ter-119 and CD71. Gated Ter-119<sup>+</sup> CD71<sup>hi</sup> cells reveal a significant increase in early erythroblast (E.i) populations in the mutant. (D) Red cell half-life measured *in vivo* using biotinylation;  $n=4$ . Whole blood haem (E) and serum ferritin (F) quantification. Values are mean $\pm$ s.d.;  $n=4$ . \* $P<0.05$ , \*\* $P<0.01$ .

## DISCUSSION

The prosthetic haem molecule is a vital component of haemoglobin, myoglobin and cytochromes. Haem is synthesised largely in the bone marrow, but also in hepatocytes and other cells, through a series of linear irreversible enzymatic reactions that occur in the cytosol and mitochondria. Coproporphyrinogen III oxidase (CPOX) is the sixth enzyme in the haem biosynthesis pathway, responsible for the conversion of coproporphyrinogen III into protoporphyrinogen IX. Mutations that aberrantly affect the function or production of this enzyme result in the manifestation of the disease hereditary coproporphyria (HCP), one of the acute

hepatic porphyrias (Kauppinen, 2005). Using ENU mutagenesis, we have generated a novel mouse mutant, *Cpox*<sup>+/*W373X*</sup>, harbouring a base-pair mutation in *Cpox* that results in a premature stop codon in place of a tryptophan at amino acid 373 of exon 5. cDNA analysis and mRNA expression levels suggest this mutation likely results in the degradation of the truncated transcript, therefore reducing the total CPOX protein by 50% in the heterozygote. Anaemia manifests due to insufficient haem availability, while porphyrins, such as uroporphyrinogen and coproporphyrinogen III, are excreted in the urine and faeces in excess because of a blockage in the haem biosynthesis pathway. The *Cpox*<sup>+/*W373X*</sup> mouse presents with

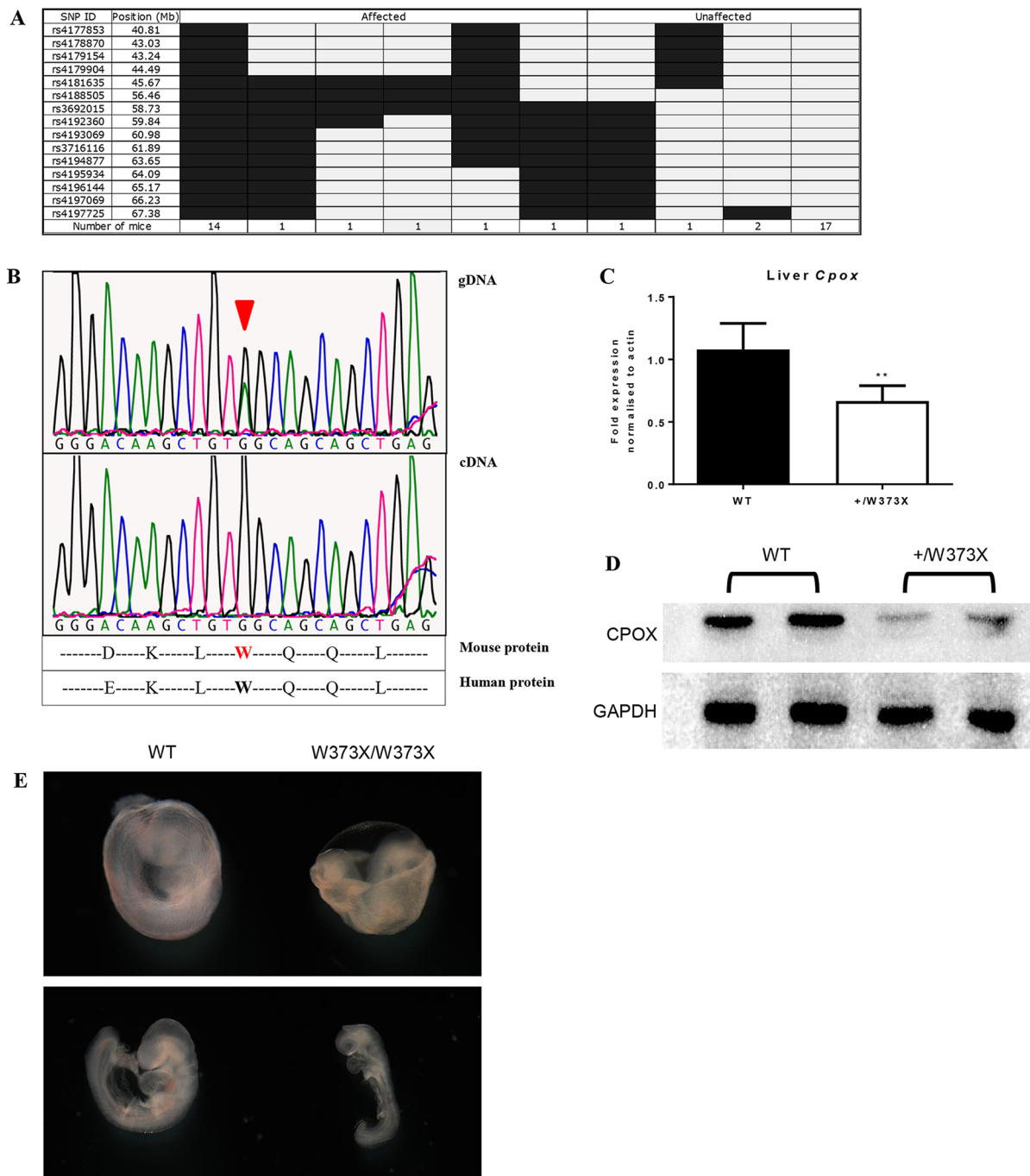


**Fig. 2. Characterisation of the W373X mutation.** (A) Fine SNP mapping of 40 mice at 15 SNP markers localised the RBC16 mutation between 56.46 Mb and 60.98 Mb on chromosome 16. Light grey indicates homozygous for Balb/c; dark grey indicates heterozygous for Balb/c and C57BL/6. (B) Sanger sequencing of heterozygous RBC16 gDNA shows the G→A substitution in *Cpox* (arrowhead), whereas in heterozygous cDNA, only the wild-type sequence is visible. (C) Quantitative RT-PCR for *Cpox* mRNA expression in the liver. Values are mean±s.d.,  $n=4$ ; \*\* $P<0.005$ . (D) Western blot of the CPOX protein from liver lysates of WT and +/W373X mice. (E) Wild-type (WT) and homozygous (W373X/W373X) embryo littermates dissected at day 9.5, showing yolk sac (top) and whole embryo formation (bottom).

biochemical abnormalities that are specific for the diagnosis of HCP, including an increase in the ratio of coproporphyrin III:I isomers, but does not display an increase in early porphyrin precursors, namely PBG. This suggests that *Cpox*<sup>+/W373X</sup> mice display a latent porphyric phenotype. Interestingly, these biochemical changes were only witnessed in female *Cpox*<sup>+/W373X</sup> mice, which excrete far more porphyrins than age-matched males with an identical mutation. This disparity mimics what is observed

clinically in many porphyrias, where female patients often endure acute attacks more frequently and with greater severity than males with the same mutation due to the periodic flux of progesterone levels (Andersson et al., 2003).

Fasting is known to be capable of precipitating symptoms of acute crises in porphyria as a result of the direct activation of ALAS-1 (Handschin et al., 2005). After two consecutive bouts of overnight fasting, *Cpox*<sup>+/W373X</sup> female mice did not show any signs of a

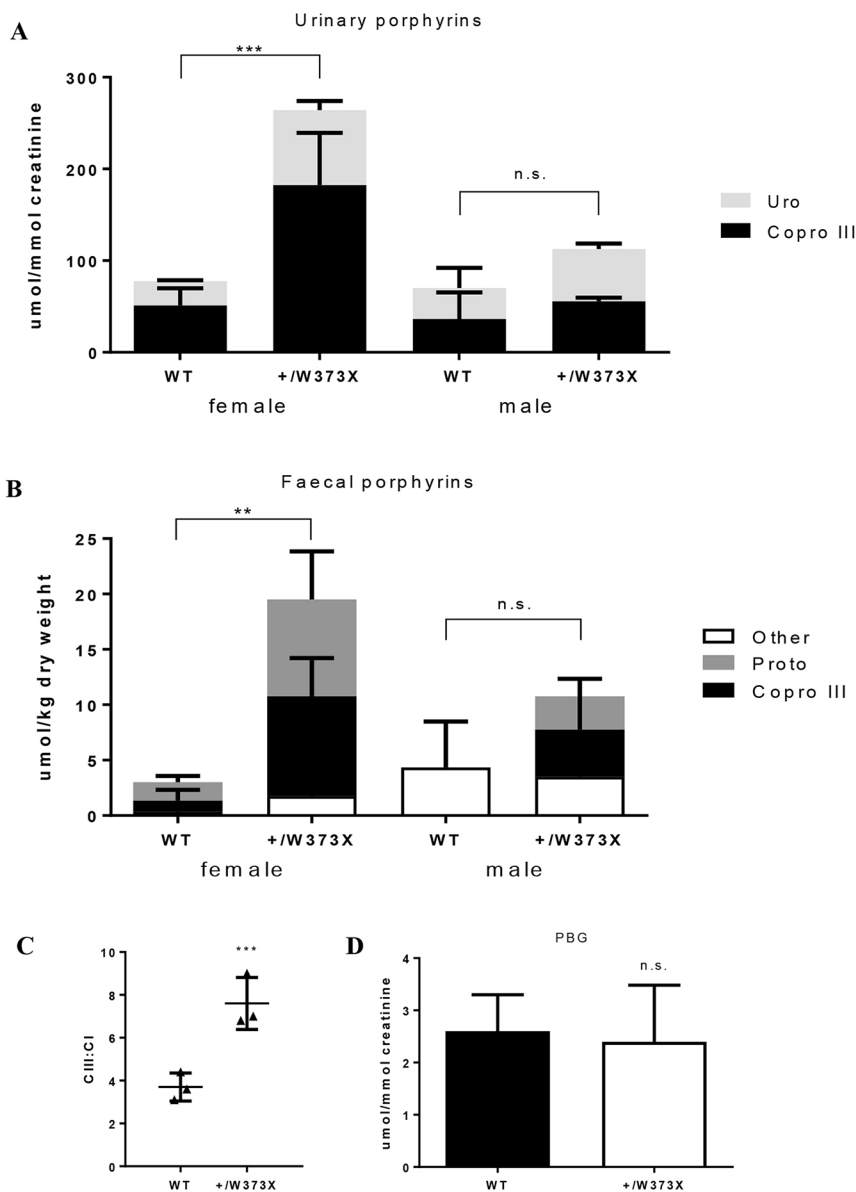
**Table 2. Timed pregnancy data of RBC16 mice**

	+/+	+/M	M/M
E8.5	3 (20%)	7 (46.7%)	5 (33.3%)
E9.5	8 (21%)	25 (65.8%)	5 (13.2%)
E10.5	5 (31.3%)	11 (68.8%)	0 (0%)
E11.5	5 (35.7%)	9 (64.3%)	0 (0%)

Timed pregnancies of RBC16 heterozygous intercrosses showing number of progeny generated and percentage per genotype at each embryonic day examined. No viable homozygous fetuses (M/M) were found beyond day E9.5, indicating that homozygosity of the RBC16 mutation was lethal.

clinical crisis, and biochemical analysis of porphyrins and porphyrin precursors showed no significant changes. The mRNA expression levels of *Alas1* and *Cpox* appear central to this observation. Fasting induced an expected increase in *Alas1* expression, which provides more rate-limiting porphyrin precursor (ALA) to haem-synthesising cells. At the same time, there was a proportional increase in *Cpox* mRNA. Working under the hypothesis that the W373X mutation does not generate a

functional mutant protein, the increase in wild-type CPOX enzyme, matching increased ALA availability, is likely to have inhibited a subsequent build-up of porphyrins and prevented an acute crisis from developing in *Cpox*<sup>+/W373X</sup> mice. An increase in CPOX enzyme activity may also have contributed to these findings, which remains to be determined. Phenobarbital was used as a more acute porphyrinogenic agent and was able to precipitate some, but not all, biochemical signs of a porphyric crisis. Following 4 days of increasing doses of phenobarbital, the level of faecal coproporphyrinogen III was significantly elevated, along with a further increase in the CIII:CI ratio. In the urine, the change in porphyrins was less notable, and PBG remained normal. On a molecular level, we once again observed how changes in *Alas1* and *Cpox* transcription could have influenced these observations. *Alas1* mRNA expression was dramatically amplified following phenobarbital treatment – 10- to 20-fold greater than pre-treated levels – while *Cpox* mRNA transcription saw only a two-fold increase. This disproportionate production of the ALA precursor, met by insufficient CPOX enzyme, is likely to be linked to the

**Fig. 3. Porphyrin studies in *Cpox*<sup>+/W373X</sup> mice.**

(A) Baseline urinary and (B) faecal porphyrins of 5-month-old RBC16 wild-type (WT) and heterozygous (+/W373X) mice of each gender. 'Other' represents porphyrins too low in concentration to accurately distinguish. (C) Isomer ratio of faecal coproporphyrin III to I (CIII:CI) and (D) baseline urinary PBG levels measured in female wild-type (WT) and heterozygous (+/W373X) mice. Values are mean±s.d.; n=3. \*\*P<0.01, \*\*\*P<0.001, n.s., not significant.

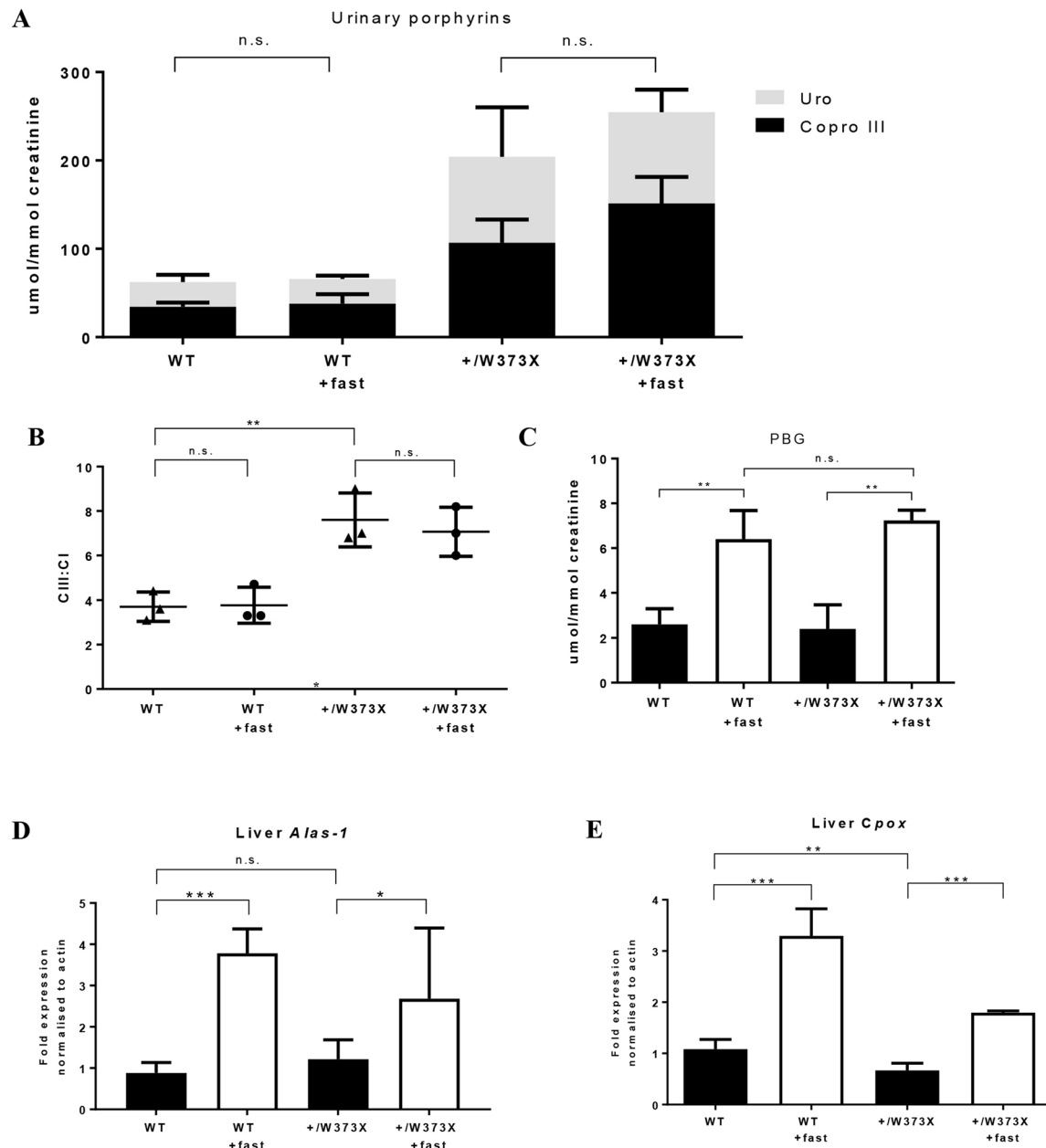


**Fig. 4. Effects of fasting on female *Cpx*<sup>+/W373X</sup> mice.** (A) Urinary porphyrins of 4-month-old RBC16 wild-type (WT) and heterozygous (+/W373X) female mice measured before and after (+fast) fasting period. (B) Isomer ratio of faecal coproporphyrin III to I (CIII:CI) measured before and after (+fast) fasting period. (C) Urinary PBG quantification before and after (+fast) fasting period. (D) Quantitative RT-PCR for *Alas-1* and (E) *Cpx* mRNA expression in the liver before and after (+fast) fasting period. Values are mean±s.d.; n=3 for A-C and n=4 for D,E. \**P*<0.05, \*\**P*<0.01, \*\*\**P*<0.001, n.s., not significant.

excessive build-up of faecal coproporphyrinogen III witnessed in *Cpx*<sup>+/W373X</sup> female mice. The minimal effect of phenobarbital treatment on urinary porphyrins is still under investigation. The *Cpx*<sup>+/W373X</sup> mouse strain is therefore susceptible to some, but not all, porphyrinogenic triggers, the outcome of which appears to be linked to ALAS-1 activity.

The haematological abnormalities present in the *Cpx*<sup>+/W373X</sup> mouse strain represents an unexpected phenotype that is not typically identified in HCP. Haem deficiency was evident in the *Cpx*<sup>+/W373X</sup> mice. This is known to suppress globin synthesis (Iolascon et al., 2009), resulting in microcytic red cells that lack sufficient haemoglobin, while splenomegaly is induced as a compensatory mechanism of extramedullary erythropoiesis. The additional increase in serum ferritin levels in heterozygotes

represents a defect in iron-to-haem loading that requires further investigation. As ENU mutagenesis results in many mutations in experimental animals (Hitotsumachi et al., 1985), it is possible that additional genetic loci are responsible for the haematological phenotype witnessed in the *Cpx*<sup>+/W373X</sup> mouse strain. This could be further investigated by crossing the *Cpx*<sup>+/W373X</sup> mouse onto multiple genetic backgrounds, to determine whether the red cell phenotype, as well as its responsiveness to porphyrinogenic triggers, is genetically transferable. With regards to the embryo lethality observed in homozygous *Cpx*<sup>W373X/W373X</sup> mutants, while red blood cells were visible in the yolk sac, it is likely that they are functionally deficient, although this may be adjacent to the gross developmental irregularities seen in day 9.5 homozygotes. Embryonic growth retardation, including limb and cranial

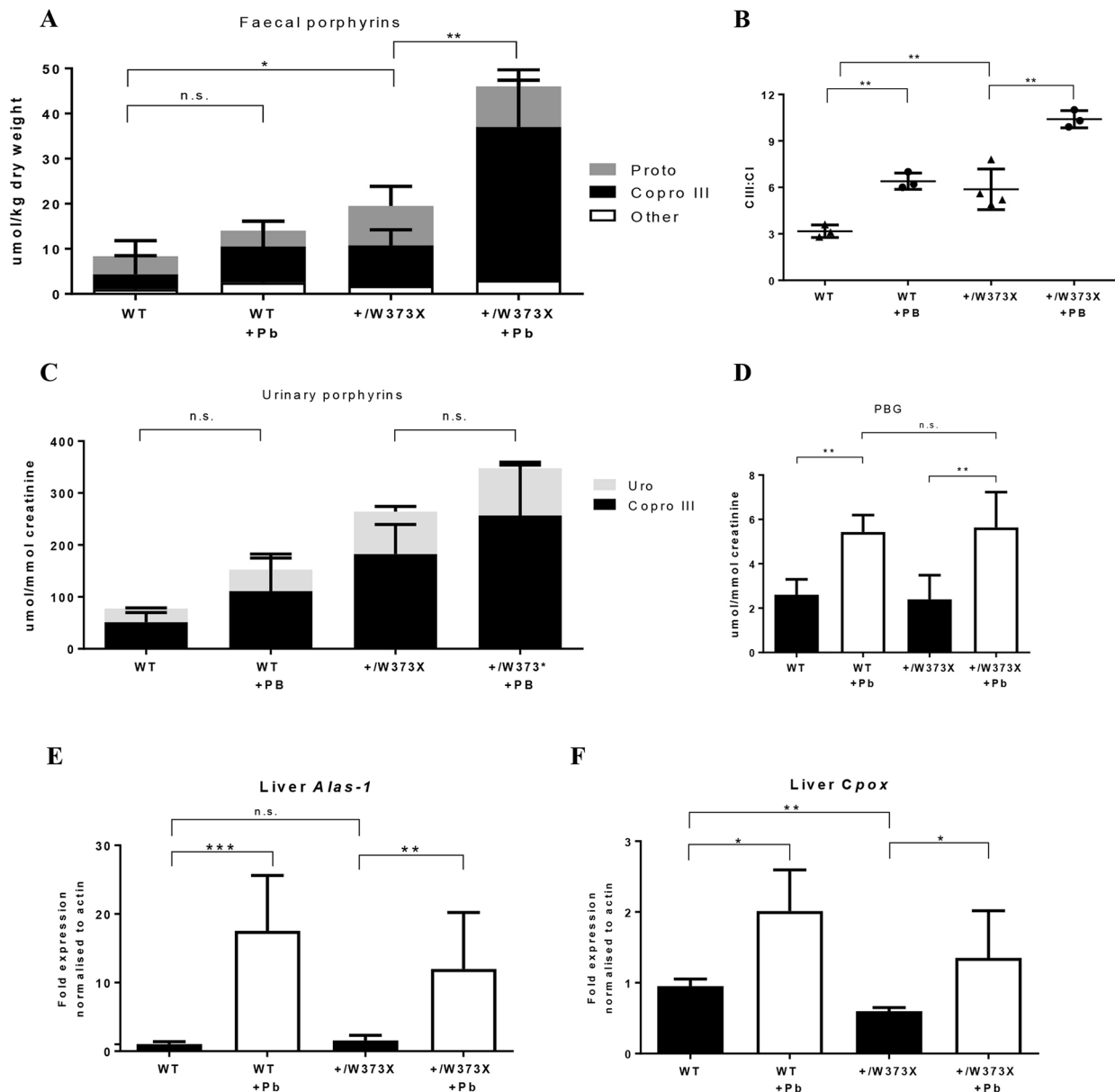


**Fig. 5. Effects of phenobarbital treatment on female *Cpxw*<sup>+W373X</sup> mice.** (A) Faecal porphyrins of 4-month-old wild-type (WT) and heterozygous (+W373X) female mice measured before and after (+Pb) phenobarbital treatment. 'Other' represents porphyrins too low in concentration to accurately distinguish. (B) Isomer ratio of faecal coproporphyrin III to I (CIII:CI) measured before and after (+Pb) phenobarbital. (C) Urinary porphyrins of wild-type (WT) and heterozygous (+W373X) female mice measured before and after (+Pb) phenobarbital treatment. (D) Urinary PBG quantification of wild-type (WT) and heterozygous (+W373X) female mice measured before and after (+Pb) phenobarbital treatment. (E) Quantitative RT-PCR for *Alas1* and (F) *Cpxw* mRNA expression in the liver before and after (+Pb) phenobarbital treatment. Values are mean±s.d.; n=3 for A-C and n=4 for D,E. \**P*<0.05, \*\**P*<0.01, \*\*\**P*<0.001, n.s., not significant.

abnormalities, has been observed in murine models with haem iron defects that diminish the free haem pool (Keel et al., 2008). This suggests that haem plays a non-erythropoietic role in embryogenesis, which may contribute to the developmental abnormalities and lethality observed in *Cpxw*<sup>W373X/W373X</sup> embryos. It also interesting to note that the *Cpxw*<sup>+W373X</sup> mouse does not present with a hereditary cataract phenotype, in comparison to the established Nakano mouse model, which harbours a missense mutation in *Cpxw* with autosomal recessive inheritance and presents with increased accumulation of coproporphyrinogen III in the lenses of homozygous mice (Nakano et al., 1960). While the underlying mechanism defining porphyrins and lens pathology remains unknown in this model, it again suggests that haem plays a

variety of roles in physiological development that are yet to be fully determined.

The heterogeneity of HCP in humans and lack of a genotype-phenotype relationship is still a major barrier in predicting patient symptoms and disease severity (Lamoril et al., 2001). This makes the establishment of animal models of HCP difficult, but necessary. Here, we report the first murine model of hereditary coproporphyrin, the *Cpxw*<sup>+W373X</sup> mouse strain, with biochemical parallels to the human disease and a haematopoietic phenotype. This mutant model would be beneficial in studies of the molecular basis of porphyrinogenic triggers and haem biosynthesis, and also for the testing of future treatment options to improve the clinical management of the acute hepatic porphyrias.

## MATERIALS AND METHODS

### Mice

A G1 pedigree (RBC16; *Cpox*<sup>W373X</sup>) displaying microcytosis was identified in an ENU mutagenesis screen as described previously (Brown et al., 2013). *Cpox*<sup>W373X</sup> mice were genotyped by PCR amplification of the region spanning the W373X mutation using genomic DNA and the primers: For (5'-TTC TCT GCT GCC CGT TCT AGG T-3') and Rev (5'-CAG GGG TTG TGC ATA AGA GGT C-3'); followed by sequencing using the Big Dye Terminator reagents to identify the point mutation. All animal experiments were approved by the Animal Ethics Committee of the Alfred Medical and Research Education Precinct and Monash University.

### Gene mapping and next-generation sequencing

Gene mapping, massively parallel sequencing, and bioinformatics of RBC16 was performed by the Australian Genome Research Facility. Mapping was performed by outcrossing affected heterozygotes with wild-type Balb/c mice. Tail genomic DNA of G2 and subsequent generations were subjected to simple sequence length polymorphism (SSLP)-based genome-wide scanning and SNP fine-mapping. The candidate interval was refined to 56.46-60.98 Mb on chromosome 16. A genomic custom capture array was generated by Roche-NimbleGen to preferentially enrich for the genomic sequence within this range. Genomic DNA was extracted from a liver sample harvested from a presumed RBC16 heterozygote, phenotyped based on low MCV and low MCH on full blood count. Massively parallel sequencing was performed using the Illumina HiSeq platform and assembly of reads to the NCBI37/mm9 C57BL/6 reference sequence, which identified a G-to-A point mutation at position c.1118 of *Cpox* (NM\_007757.2) resulting in a tryptophan to stop codon substitution at amino acid 373.

### Whole blood analysis

Blood was extracted from mice via submandibular vein bleeds and stored in EDTA tubes. Full blood examination was performed on an automated Hemavet (Drew) blood analyser. Whole blood haem was quantified using the BioAssay QuantiChrom Haem Assay Kit performed in a 96-well plate and read on a Multiskan GO (Thermo Fisher Scientific) plate reader. Serum ferritin was measured by the Mouse Ferritin ELISA Kit (Abcam) performed in a 96-well plate and read on a Multiskan GO (Thermo Fisher Scientific) plate reader.

### Real-time Q-PCR

Total RNA was extracted from liver using TRIzol (Invitrogen) according to the manufacturer's instructions, followed by cDNA amplification of 1 µg total RNA using the Reverse Transcription Kit (Promega). Q-PCR was performed on a LightCycler 480II (Roche Diagnostics) using the GoTaq qPCR Master Mix (Promega). Expression of genes was normalised to β-actin and data are presented as relative expression compared with the wild-type controls. Gene-specific primers were as follows: *Cpox*, For: 5'-CGG AGG ACA TGA AGA CCA AGA T-3' and Rev: 5'-TGA TGC CAC CTC CTC CTT CT-3'; *Alas1*, For: 5'-TCT TCC GCA AGG CCA GTC T-3' and Rev: 5'-TGG GCT TGA GCA GCC TCT T-3'.

### Porphyrin and PBG quantification

Mice were housed in individual metabolic cages for the collection of urine and faeces. At least 1 ml urine and 0.5 g faeces was collected from each animal and frozen prior to testing. Urinary porphyrins were measured by a modification of the method of Lim and Peters (1984). Urine (750 µl) was acidified with 50 µl of a solution containing the internal standard deuteroporphyrin. Samples were then vortex mixed, filtered and 60 µl was injected onto a Waters octadecyl reverse-phase column. The samples were run on an Agilent 1200 HPLC system using gradient elution with fluorimetric detection. All porphyrin fraction peaks eluted within 12 min and the total amount was calculated against a six-peak porphyrin calibration standard obtained from Frontier Scientific (Utah, USA). Faecal porphyrins were measured by a modification of the method of Lockwood et al. (1985). A small sample of faeces was homogenised in concentrated HCl and then extracted with ether to remove interfering coloured compounds. On addition of water, carotenoid and chlorophyll derivatives and other coloured

compounds move into the ether phase leaving the porphyrins in the acid aqueous phase. The aqueous phase was then scanned on a Varian Cary Spectrophotometer between 350 and 450 nm and the porphyrin concentration of the extract is proportional to the height of the Soret peak which, along with the percentage dry weight of the faeces, was used to calculate the amount of total faecal porphyrin present. PBG was measured as per Blake et al. (1992), where an anion exchange resin was used for the clean-up of urine specimens, followed by the addition of Ehrlich's reagent prior to spectrophotometric absorbance measurement at 553 nm.

### Red cell half-life

Red cell half-life was studied *in vivo* using EZ-Link NHS-Biotin (Thermo Fisher Scientific). Mice were injected intravenously with biotin diluted in a 10% DMSO/90% saline solution at a concentration of 30 mg/kg body weight. Tail bleeds were performed on subsequent days and analysed by flow cytometry. 1-2 µl of blood was stained with FITC-Ter119 and Streptavidin-PE, and the percentage of biotin-positive cells was calculated as a fraction of the total biotin-positive cells on day 1. All antibodies were purchased from BD Sciences and flow cytometry was performed on FACSCalibur (BD Sciences).

### Phenobarbital treatment

Phenobarbital methods were adapted from Johansson et al. (2003). Female mice underwent overnight fasting prior to treatment for 15 h, followed by four daily intraperitoneal injections of phenobarbital (in the form of phenobarbitone) (Aspen Pharma) at increasing concentrations (75, 80, 85, 90 mg/kg body weight). Mice were housed in metabolic cages during treatment for urine and faeces collection, and were sacrificed 4 h after the last dose on day 4 for RNA extraction.

### Statistical analysis

Where applicable, results are expressed as mean±s.d. For statistical analysis, a two-tailed Student's *t*-test was employed, unless stated otherwise; \**P*<0.05, or as defined in the figure legends.

### Acknowledgements

We would like to thank Rust Turakulov and Matthew Tinning at the Australian Genome Research Facility (AGRF) for their contributions to gene sequencing and bioinformatics, as well as support from the Australian Phenomics Network. Thank you also to David Spiteri and the Diabetic Complications Unit (Baker Heart and Diabetes Institute) for metabolic animal caging services, to Alana Auden for embryo dissections, and also to the Animal Research Laboratory (Monash University) and its technicians for animal husbandry.

### Competing interests

The authors declare no competing or financial interests.

### Author contributions

Conceptualization: A.J.C., F.C.B., B.T.K., S.M.J., D.J.C.; Methodology: A.J.C., F.C.B., R.O.F., B.T.K.; Validation: A.J.C., F.C.B., S.M.J., D.J.C.; Formal analysis: A.J.C., D.J.C.; Investigation: A.J.C., F.C.B., R.O.F., B.T.K., D.J.C.; Resources: R.O.F., B.T.K., S.M.J., D.J.C.; Data curation: A.J.C., D.J.C.; Writing - original draft: A.J.C.; Writing - review & editing: F.C.B., B.T.K., S.M.J., D.J.C.; Visualization: B.T.K., S.M.J., D.J.C.; Supervision: F.C.B., S.M.J., D.J.C.; Project administration: B.T.K., S.M.J., D.J.C.; Funding acquisition: S.M.J., D.J.C.

### Funding

This work was supported in part by a Project Grant (382900) from the Australian National Health and Medical Research Council (NHMRC) awarded to S.M.J. and D.J.C. and a Viertel Senior Medical Research Fellowship awarded to D.J.C.

### References

- Allen, K. R., Whatley, S. D., Degg, T. J. and Barth, J. H. (2005). Hereditary coproporphyrinuria: comparison of molecular and biochemical investigations in a large family. *J. Inher. Metab. Dis.* **28**, 779-785.
- Anderson, K. E., Bloomer, J. R., Bonkovsky, H. L., Kushner, J. P., Pierach, C. A., Pimstone, N. R. and Desnick, R. J. (2005). Recommendations for the diagnosis and treatment of the acute porphyrias. *Ann. Intern. Med.* **142**, 439-450.
- Andersson, C., Innala, E. and Bäckström, T. (2003). Acute intermittent porphyria in women: clinical expression, use and experience of exogenous sex hormones. A population-based study in northern Sweden. *J. Intern. Med.* **254**, 176-183.

- Besur, S., Hou, W., Schmeltzer, P. and Bonkovsky, H. L. (2014). Clinically important features of porphyrin and heme metabolism and the porphyrias. *Metabolites* **4**, 977-1006.
- Bissell, D. M. and Wang, B. (2015). Acute hepatic porphyria. *J. Clin. Transl. Hepatol.* **3**, 17.
- Blake, D., Poulos, V. and Rossi, R. (1992). Diagnosis of porphyria—recommended methods for peripheral laboratories. *Clin. Biochem. Rev.* **13**, S1-S24.
- Brown, F. C., Scott, N., Rank, G., Collinge, J. E., Vadolas, J., Vickaryous, N., Whitelaw, N., Whitelaw, E., Kile, B. T., Jane, S. M. et al. (2013). ENU mutagenesis identifies the first mouse mutants reproducing human  $\beta$ -thalassaemia at the genomic level. *Blood Cells Mol. Dis.* **50**, 86-92.
- Handschin, C., Lin, J., Rhee, J., Peyer, A. K., Chin, S., Wu, P.-H., Meyer, U. A. and Spiegelman, B. M. (2005). Nutritional regulation of hepatic heme biosynthesis and porphyria through PGC-1 $\alpha$ . *Cell* **122**, 505-515.
- Hitotsumachi, S., Carpenter, D. A. and Russell, W. L. (1985). Dose-repetition increases the mutagenic effectiveness of N-ethyl-N-nitrosourea in mouse spermatogonia. *Proc. Natl Acad. Sci. USA* **82**, 6619-6621.
- Homedan, C., Schmitt, C., Laafi, J., Gueguen, N., Desquiret-Dumas, V., Lenglet, H., Karim, Z., Gouya, L., Deybach, J. C., Simard, G. et al. (2015). Mitochondrial energetic defects in muscle and brain of a Hmbs $^{-/-}$  mouse model of acute intermittent porphyria. *Hum. Mol. Genet.* **24**, 5015-5023.
- Iolascon, A., De Falco, L. and Beaumont, C. (2009). Molecular basis of inherited microcytic anemia due to defects in iron acquisition or heme synthesis. *Haematologica* **94**, 395-408.
- Johansson, A., Möller, C., Fogh, J. and Harper, P. (2003). Biochemical characterization of porphobilinogen deaminase-deficient mice during phenobarbital induction of heme synthesis and the effect of enzyme replacement. *Mol. Med.* **9**, 193.
- Kauppinen, R. (2005). Porphyrias. *The Lancet* **365**, 241-252.
- Keel, S. B., Doty, R. T., Yang, Z., Quigley, J. G., Chen, J., Knoblauch, S., Kingsley, P. D., De Domenico, I., Vaughn, M. B., Kaplan, J. et al. (2008). A heme export protein is required for red blood cell differentiation and iron homeostasis. *Science* **319**, 825-828.
- Lamoril, J., Puy, H., Whately, S. D., Martin, C., Woolf, J. R., Da Silva, V., Deybach, J.-C. and Elder, G. H. (2001). Characterization of mutations in the CPO gene in British patients demonstrates absence of genotype-phenotype correlation and identifies relationship between hereditary coproporphyrin and harderoporphyria. *Am. J. Hum. Genet.* **68**, 1130-1138.
- Lim, C. K. and Peters, T. J. (1984). Urine and faecal porphyrin profiles by reversed-phase high-performance liquid chromatography in the porphyrias. *Clin. Chim. Acta* **139**, 55-63.
- Lindberg, R. L., Porcher, C., Grandchamp, B., Ledermann, B., Bürki, K., Brandner, S., Aguzzi, A. and Meyer, U. A. (1996). Porphobilinogen deaminase deficiency in mice causes a neuropathy resembling that of human hepatic porphyria. *Nat. Genet.* **12**, 195-199.
- Lockwood, W. H., Poulos, V., Rossi, E. and Curnow, D. H. (1985). Rapid procedure for fecal porphyrin assay. *Clin. Chem.* **31**, 1163-1167.
- Medlock, A. E., Meissner, P. N., Davidson, B. P., Corrigan, A. V. and Dailey, H. A. (2002). A mouse model for South African (R59W) variegate porphyria: construction and initial characterization. *Cell. Mol. Biol. (Noisy-le-grand)* **48**, 71-78.
- Nakano, K., Yamamoto, S., Kutsukake, G., Ogawa, H., Nakajima, A. and Takano, E. (1960). Hereditary cataract in mice. *Jpn. J. Clin. Ophthalmol.* **14**, 1772-1776.
- Phillips, J. D., Kushner, J. P., Bergonia, H. A. and Franklin, M. R. (2011). Uroporphyrin in the Cyp1a2 $^{-/-}$  mouse. *Blood Cells Mol. Dis.* **47**, 249-254.
- Richard, E., Robert-Richard, E., Ged, C., Moreau-Gaudry, F. and Verneuil, H. D. (2008). Erythropoietic porphyrias: animal models and update in gene-based therapies. *Curr. Gene Ther.* **8**, 176-186.
- Siegesmund, M., van Serooskerken, A. M. V. T., Poblete-Gutiérrez, P. and Frank, J. (2010). The acute hepatic porphyrias: current status and future challenges. *Best Pract. Res. Clin. Gastroenterol.* **24**, 593-605.
- Singal, A. K., Parker, C., Bowden, C., Thapar, M., Liu, L. and McGuire, B. M. (2014). Liver transplantation in the management of porphyria. *Hepatology* **60**, 1082-1089.
- Yasuda, M., Gan, L., Chen, B., Kadirvel, S., Yu, C., Phillips, J. D., New, M. I., Liebow, A., Fitzgerald, K., Querbes, W. et al. (2014). RNAi-mediated silencing of hepatic Alas1 effectively prevents and treats the induced acute attacks in acute intermittent porphyria mice. *Proc. Natl Acad. Sci. USA* **111**, 7777-7782.

---

## CHAPTER FOUR

### **Bone marrow transplantation corrects haemolytic anaemia in a novel ENU mutagenesis mouse model of TPI deficiency**

The following chapter describes the second (of three) complete set of results obtained for this thesis, which were submitted in the form of a research article in a peer-reviewed scientific journal during enrolment (see *Thesis including published works*), and recognises the leading author as Ashlee J. Conway. The hypotheses, aims, and expected outcomes of this thesis are each discussed in this chapter, and additional content specific to the article (methods, references, etc) are also supplied. Since thesis submission to examiners, the article has been published in a peer-reviewed journal, and has therefore been collated in this thesis in its published format.

## RESEARCH ARTICLE

# Bone marrow transplantation corrects haemolytic anaemia in a novel ENU mutagenesis mouse model of TPI deficiency

Ashlee J. Conway<sup>1</sup>, Fiona C. Brown<sup>1</sup>, Elinor J. Hortle<sup>2</sup>, Gaetan Burgio<sup>2</sup>, Simon J. Foote<sup>2</sup>, Craig J. Morton<sup>3</sup>, Stephen M. Jane<sup>4</sup> and David J. Curtis<sup>1,5,\*</sup>

## ABSTRACT

In this study, we performed a genome-wide N-ethyl-N-nitrosourea (ENU) mutagenesis screen in mice to identify novel genes or alleles that regulate erythropoiesis. Here, we describe a recessive mouse strain, called RBC19, harbouring a point mutation within the housekeeping gene, *Tpi1*, which encodes the glycolysis enzyme, triosephosphate isomerase (TPI). A serine in place of a phenylalanine at amino acid 57 severely diminishes enzyme activity in red blood cells and other tissues, resulting in a macrocytic haemolytic phenotype in homozygous mice, which closely resembles human TPI deficiency. A rescue study was performed using bone marrow transplantation of wild-type donor cells, which restored all haematological parameters and increased red blood cell enzyme function to wild-type levels after 7 weeks. This is the first study performed in a mammalian model of TPI deficiency, demonstrating that the haematological phenotype can be rescued.

**KEY WORDS:** Erythropoiesis, N-ethyl-N-nitrosourea, Anaemia, TPI deficiency, Transplantation

## INTRODUCTION

Triosephosphate isomerase (TPI, or TIM) is an anaerobic glycolysis enzyme encoded by the *TPI1* gene at chromosomal position 12p13 in humans (Ralser et al., 2008). It is responsible for the reversible conversion of dihydroxyacetone phosphate (DHAP) to D-glyceraldehyde 3-phosphate (GAP) and is ubiquitously expressed in all cells (Orosz et al., 2009; Orosz et al., 2006). Homozygous or compound heterozygous mutations within the *TPI1* gene result in the rare enzymopathy, TPI deficiency, which presents clinically with chronic haemolytic anaemia, cardiomyopathy, increased susceptibility to infections, neurodegeneration and death in early childhood (Sarper et al., 2013; Rosa et al., 1985; Fermo et al., 2010). Of the various glycolytic enzymopathies, TPI deficiency is considered the most severe in clinical presentation.

Of the ~13 pathological *TPI1* mutations identified in humans so far, the Glu104Asp substitution has been the most commonly identified variant, believed to be responsible for up to 80% of all reported cases of TPI deficiency (Arya et al., 1997; Schneider and

Cohen-Solal, 1996). This mutation is believed to cause impaired dimerisation of the enzyme, which is crucial for its catalytic activity, while other variants can also impair substrate binding to the active site (Ralser et al., 2006; Mainfroid et al., 1996; Oliver and Timson, 2017). Heterozygous carriers appear asymptomatic and maintain at least 50% TPI activity in all cells, while the loss of enzyme function in the erythrocytes, platelets or lymphocytes of homozygotes is more profound and ranges between zero and 30% of that of normal activity (Valentin et al., 2000; Hollán et al., 1993). Congenital mutations within glycolytic enzymes, such as TPI, have a particularly detrimental effect on the lifespan and function of red blood cells, which rely exclusively on anaerobic glycolysis for ATP production (Van Wijk and van Solinge, 2005; McMullin, 1999). Nonspherical haemolytic anaemia therefore manifests in all patients with TPI deficiency as a result of rapid red blood cell exhaustion and turnover, and poses a significant burden to health (Clay et al., 1982). Currently, no treatment is available nor has been trialled for TPI deficiency, likely owing to its rarity and fast mortality.

Models resembling TPI deficiency in experimental animals have been established previously. The *TPI<sup>sugarkill</sup> (sgk; Tpi<sup>sgk-1</sup>)* *Drosophila*, generated through ethyl methanesulfonate (EMS) mutagenesis, demonstrated reduced enzyme function and central brain pathology contributing to locomotive degeneration; a phenotype vaguely analogous to the neurodegenerative traits of human TPI deficiency (Palladino et al., 2002; Celotto et al., 2006). In a mammalian system, the *Tpi<sup>a-m6Neu</sup>* chemical mutagenesis mutant was the first viable homozygous mouse model, which presented with reduced enzyme activity in multiple tissues and evidence of haemolytic anaemia (Pretsch, 2009). While rescue studies in the *sgk* mutant were partially successful in restoring fly lifespan, locomotion and glycolytic output (Hrizo and Palladino, 2010), attempts to rescue the haematological phenotype in a mammalian model have not yet been trialled. Here, we describe a novel homozygous mouse model of TPI deficiency, called RBC19, which was generated in a genome-wide N-ethyl-N-nitrosourea (ENU) mutagenesis screen for defects in erythropoiesis. Whole-exome sequencing (WES) identified a missense mutation resulting in a phenylalanine-to-serine substitution at amino acid 57 of exon 1 (F57S). RBC19 homozygotes were viable and fertile, and presented with a macrocytic haemolytic anaemia, which closely paralleled the human disease. A bone marrow transplant was performed using wild-type donor cells to correct the haemolytic phenotype in RBC19 mice, restoring all red blood cell parameters and erythrocyte glycolytic function. This investigation represents the first rescue study of TPI deficiency in a mammalian model.

## RESULTS

### Characterisation of a homozygous mouse strain with macrocytic haemolytic anaemia

In an ENU mutagenesis screen designed to identify novel genes or alleles regulating erythropoiesis, we identified a mouse with

<sup>1</sup>Australian Centre for Blood Diseases, Central Clinical School, Monash University, Melbourne 3004, Australia. <sup>2</sup>The John Curtin School of Medical Research, Australian National University, Canberra 0200, Australia. <sup>3</sup>Australian Cancer Research Foundation Rational Drug Discovery Centre, St. Vincent's Institute of Medical Research, Fitzroy 3065, Australia. <sup>4</sup>The Alfred Hospital, Melbourne 3004, Australia. <sup>5</sup>Central Clinical School, Monash University, Melbourne 3004, Australia.

\*Author for correspondence (david.curtis@monash.edu)

 D.J.C., 0000-0001-9497-0996

This is an Open Access article distributed under the terms of the Creative Commons Attribution License (<http://creativecommons.org/licenses/by/3.0>), which permits unrestricted use, distribution and reproduction in any medium provided that the original work is properly attributed.

macrocytic red blood cells, named RBC19. When crossed with wild-type (SJL) mice, ~50% of progeny displayed macrocytosis and increased reticulocytes, indicating that the phenotype was fully penetrant. Mating two macrocytic mutants generated a third cohort of progeny at a ratio of ~25% (data not shown). This presumed homozygous (m/m) population had more profound macrocytosis, a reduced red blood cell count and elevated reticulocytes (14.6%), compared with the heterozygous mice (Table 1). White blood cell and platelet indices were normal in all cohorts.

Peripheral blood smears of RBC19 homozygotes (m/m) revealed a homogenous population of macrocytic red blood cells with mild pallor but normal shape (Fig. 1A). Significant polychromasia was visible in the blood smear, consistent with the elevated reticulocyte numbers. Increased spleen size was seen in homozygous, but not heterozygous, mice (Fig. 1B). Flow cytometric analysis of spleen cells identified a marked expansion of early Ter-119<sup>+</sup> CD71<sup>hi</sup> (Ly76<sup>+</sup> Tfrc<sup>hi</sup>; *hi*, high) erythroblasts in the homozygous cohort, consistent with stress erythropoiesis (Fig. 1C). Histological sections of spleens revealed a dense, crowded red pulp packed with proliferating erythroid precursors (Fig. 1D). Biotinylation was employed to measure *in vivo* red blood cell half-life, as previously described (Conway et al., 2017), which demonstrated a significantly reduced half-life of RBC19 homozygous red blood cells (8 days), compared with wild-type red blood cells (17 days) (Fig. 1E). Total serum bilirubin was also markedly elevated in homozygotes compared with wild-type controls, but normal in the heterozygotes (Fig. 1F). Taken together, the results indicated that the RBC19 homozygous mutant mouse presented with a macrocytic red blood cell phenotype, with evidence of haemolytic anaemia.

### RBC19 mice harbour a missense mutation in the glycolysis enzyme gene, *Tpi1*

The ENU-induced mutation was identified using WES, as previously described (Brown et al., 2013). Two samples of genomic DNA extracted from presumed RBC19 homozygotes, based on high mean corpuscular volume (MCV), were subjected to massively paralleled sequencing using the Illumina HiSeq platform. Reads were assembled against the SJL genomic sequence and subsequent bioinformatics identified a T→C base-pair mutation at position c170 in the first exon of *Tpi1*. This resulted in a predicted phenylalanine-to-serine substitution at amino acid 57 (F57S).

**Table 1. Full blood examination of the RBC19 mutant mouse strain**

	SJL <i>n</i> =18	+/m <i>n</i> =14	m/m <i>n</i> =24
RCC (×10 <sup>12</sup> /l)	9.68±1.0	9.45±1.3	7.12±0.3*
Hb (g/dl)	13.7±1.0	13.5±1.3	12.5±0.9
HCT (%)	49.0±4.9	46.6±4.7	38.3±1.8*
MCV (fl)	46.1±2.1	50.8±1.8*	53.8±0.9*
MCH (pg)	14.0±0.8	14.5±0.7	16.2±0.8*
MCHC (g/dl)	32.8±2.5	30.1±1.2	29.7±1.0
RDW (%)	19.6±1.5	19.1±1.5	18.7±1.3
WBC (×10 <sup>9</sup> /l)	9.32±1.1	8.32±2.5	9.77±3.4
Platelets (×10 <sup>9</sup> /l)	1332±489	1128±250	1360±186
MPV (fl)	5.8±0.2	5.8±0.3	6.3±0.35
Reticulocytes (%)	5.0%±2.2	10.2±2.7*	14.6%±1.9*

Blood parameters obtained from 7-week-old wild-type (SJL), heterozygous (+/m) and homozygous (m/m) RBC19 mice. Data are mean±s.d. Two-tailed Student's *t*-test was used for statistical analysis; \**P*<0.05 compared with wild type. Hb, haemoglobin; HCT, haematocrit; MCH, mean corpuscular haemoglobin; MCHC, mean corpuscular haemoglobin concentration; MCV, mean corpuscular volume; MPV, mean platelet volume; RCC, red blood cell count; RDW, red blood cell distribution width; WBC, white blood cell count.

Sanger sequencing of complementary DNA (cDNA) generated from the bone marrow of RBC19 homozygous mice (herein referred to as *Tpi1*<sup>F57S/F57S</sup>) confirmed the presence of the base-pair mutation (Fig. 2A). Quantitative real-time polymerase chain reaction (RT-PCR), performed on bone marrow, showed no significant differences in *Tpi1* mRNA expression levels between *Tpi1*<sup>F57S/F57S</sup> and wild-type mice (Fig. 2B); however, western blots revealed a significant reduction of TPI protein in the bone marrow lysates of homozygotes compared with wild-type samples, while heterozygous cells showed a ~50% reduction in protein levels (Fig. 2C). This suggested that the F57S mutation had a detrimental effect on protein stability.

Computer modelling was used to help predict how the F57S mutation would affect TPI enzyme conformation and activity. In a three-dimensional (3D) model of the dimer's crystal structure, the F57 side chain was shown to be buried in a hydrophobic pocket, suggesting that it had an important role in stabilisation of the TIM 'barrel' configuration of the protein (Fig. 2D). In a contact map of the mutation site, it was further demonstrated that F57 played a central role in amino acid interactions via the packing of its aromatic side chain (Fig. 2E). Replacing this hydrophobic amino acid with a polar, hydrophilic amino acid (serine) is expected to disrupt those interactions, resulting in a misfolded protein and degradation. This likely explained the normal expression of *Tpi1* mRNA but markedly reduced levels of TPI protein.

### *Tpi1*<sup>F57S/F57S</sup> mice display haematological parallels to TPI deficiency

Reduced erythrocyte TPI enzyme activity, in combination with nonspherical haemolytic anaemia, is a key diagnostic indicator of TPI deficiency. To examine the parallels between the *Tpi1*<sup>F57S/F57S</sup> mouse strain and the human condition, TPI enzyme function was analysed in lysates made of peripheral red blood cells and various other tissues (Table 2). In the homozygous population, the lowest enzyme activity was seen in red blood cells (10% of that of wild type), followed by brain (12%), bone marrow-derived macrophages (BMMs) (13%), and unsorted bone marrow (16%). Heterozygotes, which lacked a haemolytic phenotype, had a partial loss of enzyme activity in red blood cells (53% of that of wild type) and bone marrow cells (77%). Additionally, the end products of glycolysis, pyruvate (Fig. 3A) and lactic acid (Fig. 3B), were significantly reduced in the serum of *Tpi1*<sup>F57S/F57S</sup> mice compared with wild types, demonstrating the detrimental effect of the loss of TPI activity on the glycolysis pathway. Together, this indicated that the *Tpi1*<sup>F57S/F57S</sup> mutant is a novel model of TPI deficiency, and mimics the haematological and molecular defects typically observed in humans. Heterozygotes represented asymptomatic carriers.

No neurological phenotype was identified in the *Tpi1*<sup>F57S/F57S</sup> strain. Mice showed no loss of mobility or grip strength with age (data not shown), and histology of the brain did not reveal any pathological changes in 9-month-old mice (Fig. 3C). Serological tests of glycolytic metabolites typically identified in TPI-deficient patients with neurodegenerative symptoms, such as DHAP (Fig. 3D) and HbA1c – as an indirect measurement of methylglyoxal (Fig. 3E) – were also normal compared with wild-type serum values. These data suggest that the F57S mutation is not a catalyst of the neurodegenerative phenotypes often associated with TPI deficiency.

### Bone marrow transplantation rescues red blood cell defects in *Tpi1*<sup>F57S/F57S</sup> mice

To determine whether the erythroid phenotype in *Tpi1*<sup>F57S/F57S</sup> mice could be rescued, bone marrow transplants were performed using wild-type (SJL) mice. *Tpi1*<sup>F57S/F57S</sup> recipients, reconstituted with

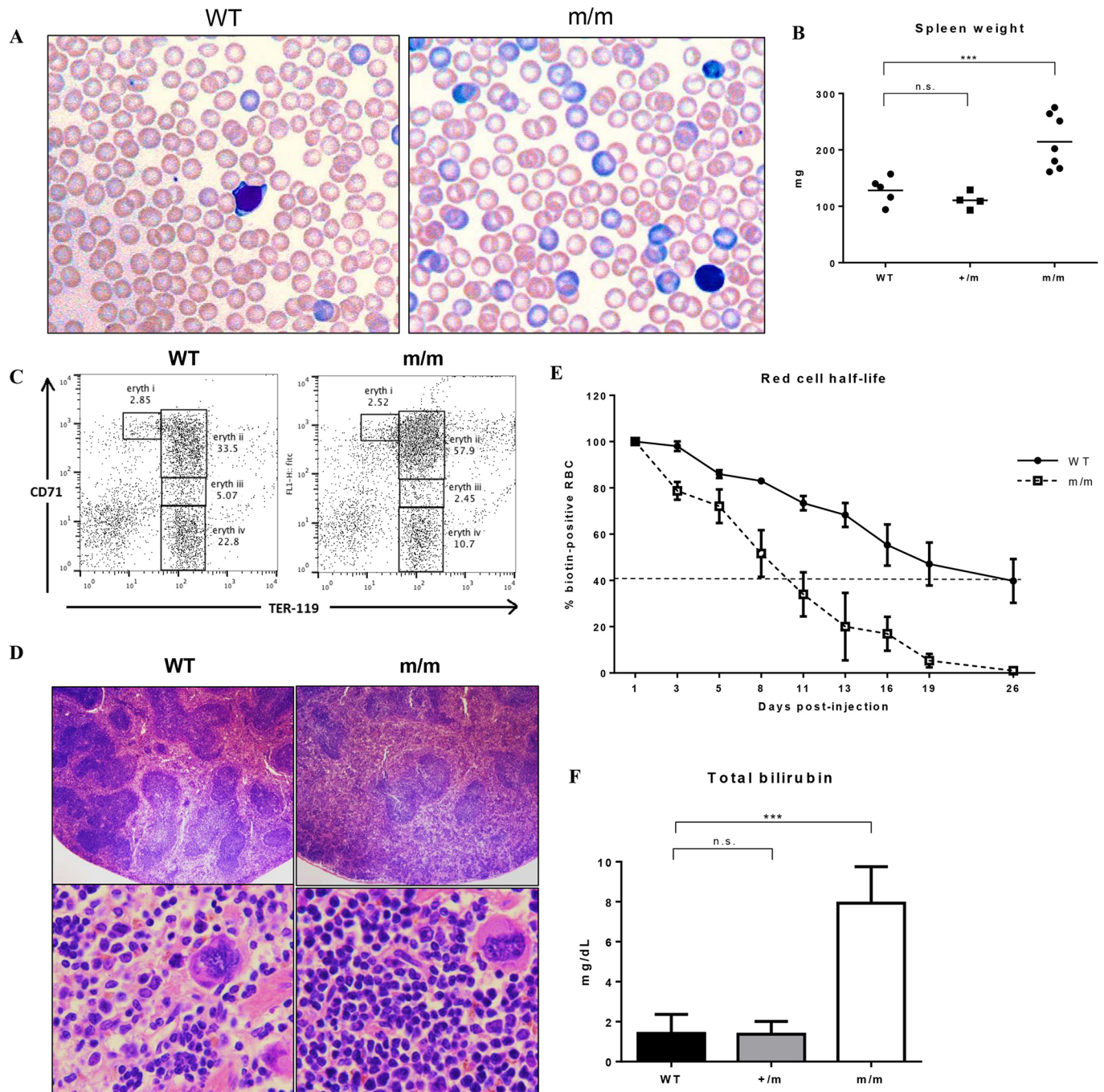


**Fig. 1. Phenotype of the RBC19 mutant mouse.** (A) Peripheral blood smears of 7-week-old wild-type (WT) and RBC19 homozygous (m/m) mice, stained with May-Grünwald Giemsa. Macrocytic red blood cells and a high degree of polychromasia (blue) are seen in the homozygous film. (B) Wet spleen weights of wild-type (WT), heterozygous (+/m), and homozygous (m/m) mice. Individual values are shown, along with the mean (solid line). (C) Fluorescence-activated cell sorting (FACS) plot of live spleen cells stained with Ter-119 and CD71. There is a significant increase in early Ter-119<sup>+</sup> CD71<sup>hi</sup> cells (eryth ii) in the homozygotes. eryth i, proerythroblasts; eryth ii, basophilic erythroblasts; eryth iii, chromatophilic erythroblasts; eryth iv, orthochromic normoblasts. (D) Hematoxylin and Eosin (H&E) staining of sectioned spleens harvested from 2-month-old WT and m/m mice, photographed at low (×40) and high (×200) magnification. (E) Red blood cell half-life measured *in vivo* using biotinylation, showing a more rapid rate of red blood cell turnover in the homozygotes; *n*=4. Error bars represent s.d. (F) Total serum bilirubin quantification of WT, +/m and m/m mice. Data are mean±s.d.; *n*=6. \*\*\**P*<0.0001, n.s., not significant.

wild-type bone marrow, showed restoration of all peripheral red blood cell parameters after 7 weeks' recovery, including reduced MCV (Fig. 4A) and reduced reticulocytes (Fig. 4B), with levels comparable to those of the wild-type control cohort (SJL). The *in vivo* red blood cell half-life, measured by biotinylation, was identical to that of wild-type red blood cells (Fig. 4C). In addition, TPI enzyme activity within peripheral red blood cells had returned to

100% of wild-type activity levels (Fig. 4D). In contrast, *Tpi1*<sup>F57S/F57S</sup> mice reconstituted with *Tpi1*<sup>F57S/F57S</sup> bone marrow showed persistent macrocytosis, shortened red blood cell half-life, and reduced red blood cell TPI activity at 7 weeks (Fig. 4A-D). Thus, the macrocytic haemolytic anaemia in the *Tpi1*<sup>F57S/F57S</sup> mutant strain, being intrinsic to haematopoiesis, could be rescued using bone marrow transplantation.

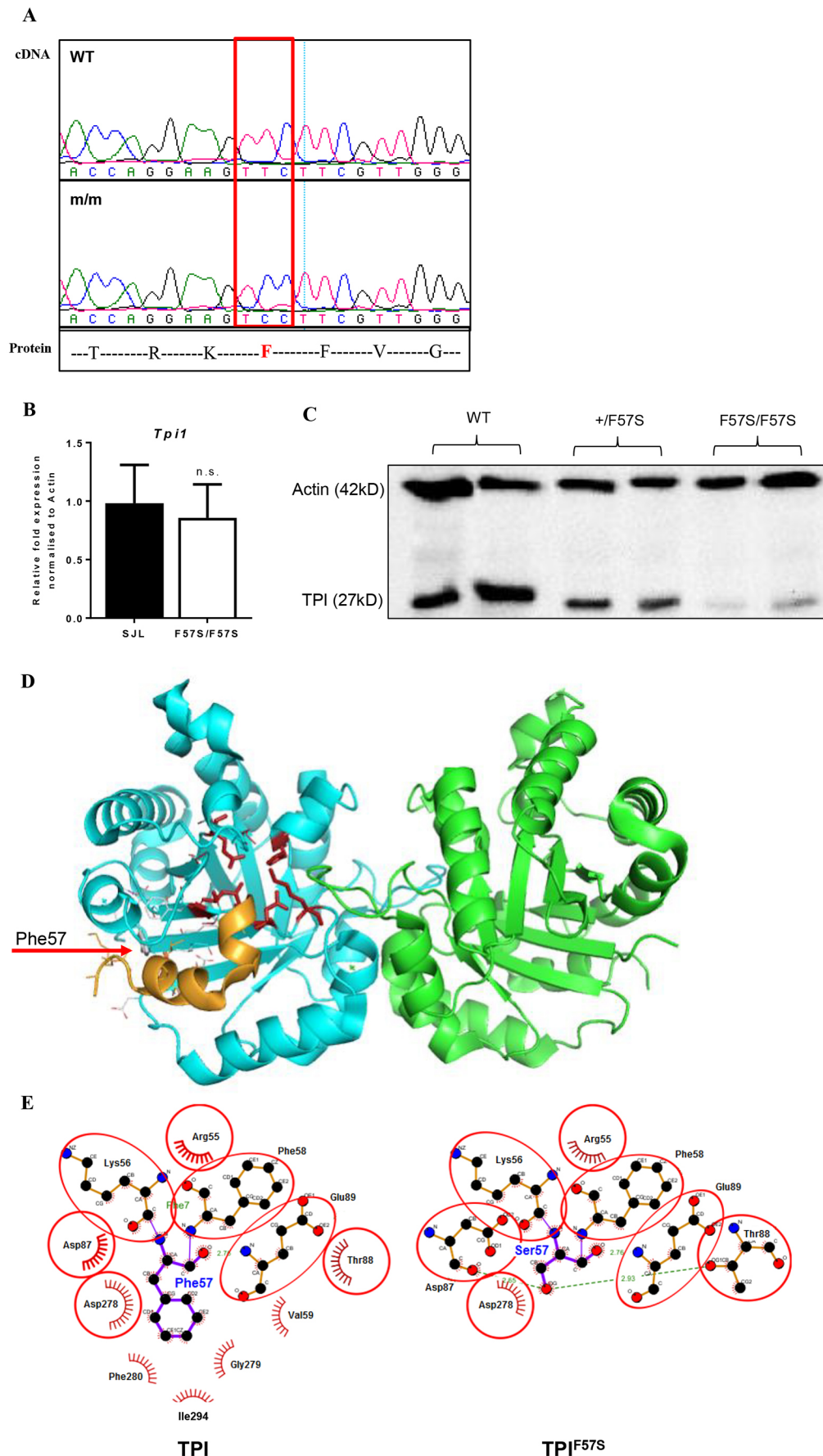


**Fig. 2. Characterisation of the F57S mutation.** (A) Sanger sequencing of RBC19 homozygous cDNA shows a T→C substitution in *Tpi1*, resulting in a phenylalanine (F) to serine (S) amino acid change. (B) Quantitative RT-PCR for relative *Tpi1* mRNA expression in the bone marrow of wild-type (WT) and homozygous (F57S/F57S) mice. Data are mean±s.d.; *n*=4. (C) Western blot of the TPI protein from bone marrow lysates of WT, heterozygous (+/F57S) and homozygous (F57S/F57S) mice. (D) 3D protein modelling of the murine TPI dimer in ribbons (blue and green), showing the enzyme active site (red sticks). The location of F57 is highlighted (red arrow to grey stick), as well as its adjacent binding helix (orange ribbon). (E) 2D contact map of the F57 site and its surrounding amino acids in both the WT (TPI) and mutant (TPI<sup>F57S</sup>) forms. In the mutant, the F57S substitution is predicted to distort surrounding amino acid interactions and subsequently induce conformational changes to the protein.

**Table 2. TPI enzyme activity in blood cells and tissues**

	+F57S	F57S/F57S
Red blood cells	53±2.3	10±1.0
Bone marrow	77±3.9	16±2.2
Spleen	–	85±3.9
Liver	–	19±0.4
Skeletal muscle	–	48±5.3
Brain	–	12±0.8
BMM	–	13±1.1

Measured TPI enzyme activity of various cell populations obtained from heterozygous (+F57S) and homozygous (F57S/F57S) mice, shown as a percentage (%) of the respective wild-type (SJL) value. BMM, bone marrow macrophages. Data are mean±s.d.; n=6 for all populations.

## DISCUSSION

In the present study, we have described a novel ENU mutagenesis mouse strain harbouring a homozygous loss-of-function mutation in the *Tpi1* gene, resulting in a macrocytic haemolytic phenotype that closely resembles human TPI deficiency. A phenylalanine-to-serine substitution at amino acid 57 severely reduced enzyme activity in multiple tissues, particularly those with a high dependence on anaerobic glycolysis, such as red blood cells, bone marrow and neurons. This novel model of TPI deficiency was utilised to demonstrate that the haematological phenotype could be rescued by transplantation using wild-type donor bone marrow. Transplantation successfully eliminated macrocytosis and haemolytic anaemia, improved the *in vivo* red blood cell lifespan, and increased red blood cell TPI enzyme activity to wild-type levels. This study is the first to recognise that the haematological defects associated with TPI deficiency can be rescued by bone marrow transplantation.

The glycolytic housekeeping protein, TPI, is a ubiquitously expressed enzyme responsible for maintaining equilibrium of the metabolic intermediates DHAP and GAP (Ralser et al., 2008; Orosz et al., 2009; Sarper et al., 2013). Homozygous or compound heterozygous mutations occurring in the *TPI1* gene cause the rare enzymopathy TPI deficiency. Approximately 13 mutations spanning less than 50 reported cases of the disease have been identified in humans so far (Schneider, 2000), each demonstrating variable degrees of enzyme deficiency, anaemia and neurodegeneration (Fermo et al., 2010; Hollán et al., 1993). Nonspherical haemolytic anaemia is a hallmark of TPI deficiency, often identified at birth, and has a chronic effect on patient health (Sarper et al., 2013; Clay et al., 1982). No treatment options have been established for TPI deficiency to date, and no incidence of transplantation or similar trial has been recorded in humans or a mammalian model of the disease. Patients rarely survive beyond childhood, prompting the need to generate more effective long-term clinical management strategies for this devastating disease.

The haematological phenotype identified in the ENU-generated RBC19 (*Tpi1*<sup>F57S/F57S</sup>) mouse strain closely matched the human condition, presenting with a haemolytic phenotype, nonspherical red blood cells, and evidence of erythropoietic stress on extramedullary organs. Despite a slightly elevated MCV and peripheral reticulocyte numbers, heterozygous *Tpi1*<sup>+F57S</sup> mice did not display the characteristics of haemolytic anaemia and were therefore excluded from most tests. This heterozygous population resembled the silent carriers frequently described in human cases, typically associated with a residual enzyme activity of >50% in all cells (Schneider, 2000). Otherwise, the degree of residual TPI enzyme function observed in the erythrocytes of homozygotes fell within the range reported in human case studies (Valentin et al.,

2000; Hollán et al., 1993). Enzyme activity of peripheral blood cells is the gold standard for identifying TPI deficiency. The variation in enzyme function observed in other tissues was likely related to the rate of protein synthesis occurring in those cells. Ultimately, bone marrow transplantation of wild-type donor cells eliminated the macrocytic haemolytic phenotype in *Tpi1*<sup>F57S/F57S</sup> recipients within 7 weeks. The restored red blood cell half-life and peripheral red blood cell TPI activity were key indicators of the transplant's effectiveness, the results of which might prove to be translatable to the treatment of TPI deficiency in humans.

The neurological symptoms often associated with TPI deficiency vary in onset and severity, but do not appear to have a direct correlation to enzyme activity (Ralser et al., 2008; Ahmed et al., 2003). A genotype-phenotype relationship has been suggested, as specific mutant alleles, particularly those that disrupt TPI protein dimerisation, have been shown to correlate with more severe neurodegenerative phenotypes in patients (Orosz et al., 2006; Roland et al., 2016). Compounding genetic factors affecting other metabolic pathways, particularly glyoxal pathways, have also been suggested to play a role in the accumulation of potentially neurotoxic metabolic intermediates, such as DHAP or methylglyoxal (Ahmed et al., 2003; Oláh et al., 2005). On a genetic level, the *Tpi1*<sup>F57S</sup> mutation does not represent a known variant observed in humans. Additionally, 3D protein modelling revealed that the mutational site is unlikely to directly impact protein dimerisation, based on its position in the context of TPI's well-characterised crystal structure (Mainfroid et al., 1996). Physiologically, the mutant mouse does not show any loss of motor function with age, nor any histological evidence of neuropathy. Taken together, we conclude that the *Tpi1*<sup>F57S/F57S</sup> mouse strain presents exclusively as a model of the haematological defects associated with TPI deficiency.

This study is an example of the power of forward-genetics screens in the development of animal models that accurately recapitulate rare human diseases, and subsequently the use of those models in trialling new therapeutic options with clinical translatability. The ENU-generated *Tpi1*<sup>F57S/F57S</sup> mouse strain, a novel model of TPI deficiency, was found to harbour the key haematological characteristics of the human disease, which are targetable by bone marrow transplantation. Our studies of this model hopefully bridge a significant gap in the clinical management and treatment of this rare haemolytic enzymopathy.

## MATERIALS AND METHODS

### Mice

A G1 pedigree (RBC19; *Tpi1*<sup>F57S</sup>) displaying macrocytosis was identified in an ENU mutagenesis screen on an SJL background, as described previously (Brown et al., 2013; Bauer et al., 2015). Mice were genotyped by PCR amplification of the region spanning the F57S mutation using cDNA and the primers: Forward (5'-AGAGAGCCGTGCGTTTGTGA-3') and Reverse (5'-GCCCCATTGGTCACTTTGTGA-3'); followed by sequencing using the Big Dye Terminator™ reagents (Australian Genome Research Facility) to identify the point mutation. All animal experiments were approved by Monash University and the Animal Ethics Committee (AEC) of the Alfred Medical and Research Education Precinct. Animals were used and cared for in accordance with AEC guidelines.

### Next-generation sequencing

Massively parallel sequencing (whole exome) was performed on the Illumina HiSeq platform (Australian Genome Research Facility) using the genomic DNA of G<sub>2</sub> homozygous mice, determined by high MCV. Reads were assembled against the SJL reference sequence, which identified a point mutation at position c170 of *Tpi1* (NC\_000072.6), resulting in a phenylalanine to serine substitution at amino acid 57 (F57S).

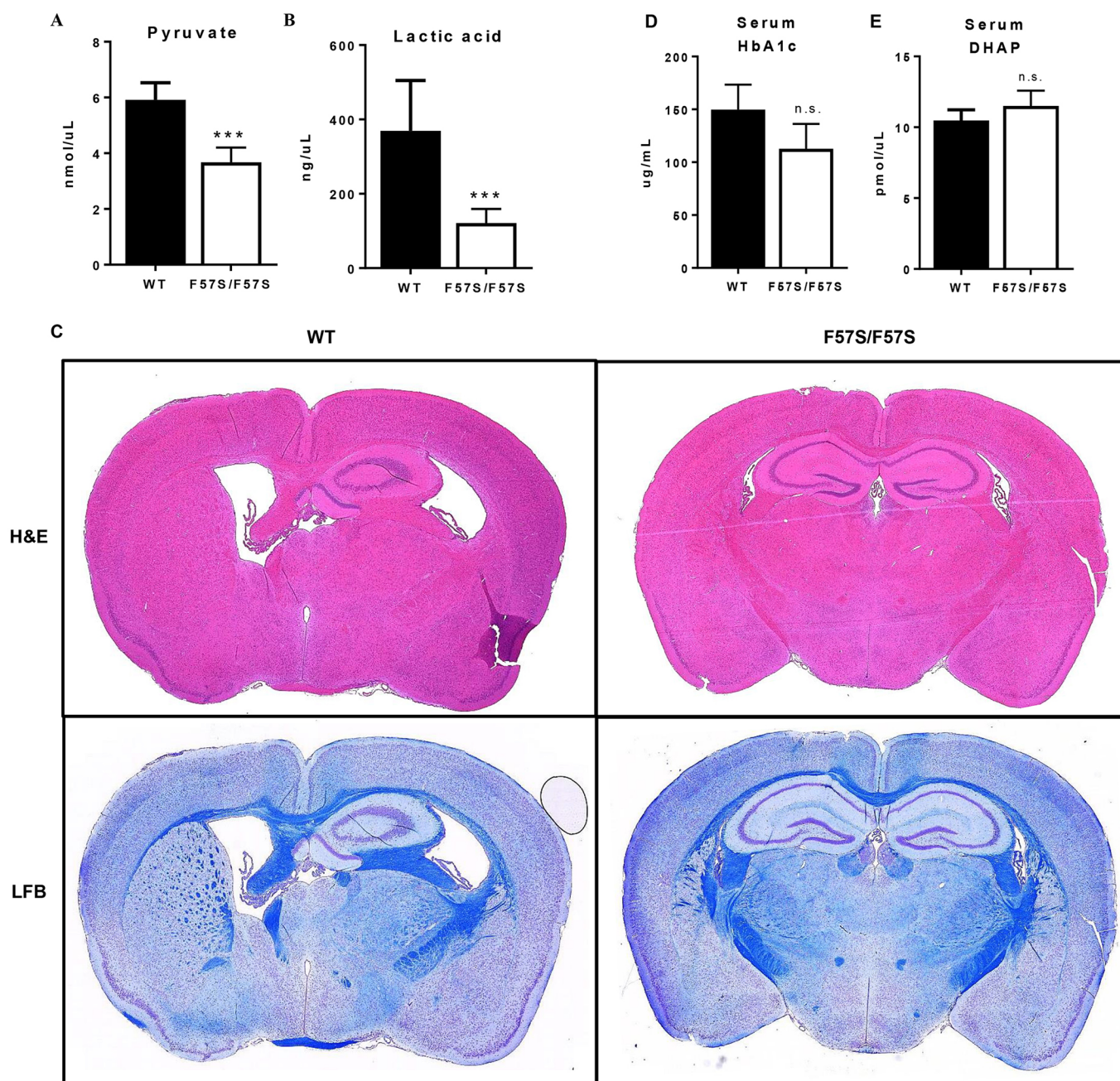


**Fig. 3.** *Tpi1*<sup>F57S/F57S</sup> mice display a TPI deficiency-like phenotype without neuropathy. (A,B) Pyruvate (A) and lactic acid (B) measured in the serum of wild-type (WT) and homozygous (F57S/F57S) mice. Data are mean±s.d.; *n*=6. (C) Sectioned brains of 9.5-month-old WT and F57S/F57S mice, stained with H&E (upper) and Luxol Fast Blue (LFB) (lower). (D,E) DHAP (D) and HbA1c (E) measured in the serum of WT and F57S/F57S mice. Data are mean±s.d.; *n*=5. \*\*\**P*<0.0001, n.s., not significant.

### Computer modelling

The 3D structure of wild-type TPI1 (PDB entry 4POC) was modified to introduce the F57S substitution using Coot (Emsley et al., 2010). The two-dimensional (2D) contact map for the wild-type and F57S residue was generated using LogiPlot+ (Laskowski and Swindells, 2011). Structures were inspected and figures were generated using PyMOL (version 2.0.3).

### Enzyme assays

TPI enzyme activity was measured colorimetrically using a kit from BioVision (Milpitas, CA, USA). For red blood cell measurements, EDTA-treated blood samples were centrifuged at 4000 *g* for 15 min and the packed red blood cell volume was diluted in dH<sub>2</sub>O to a 1:20 dilution, followed by three freeze-thaw cycles with intermittent vortexing to ensure complete

lysis. Other tissues were collected in PBS (pH 7.0–7.4) and separated using a 40- $\mu$ m cell strainer (Stem Cell). Lysates were made in TPI enzyme kit diluent containing a protease inhibitor cocktail ('cOmplete', Sigma-Aldrich, MO, USA) followed by three freeze-thaw cycles. Prior to testing, all cell lysates were centrifuged at 4000 *g* for 5 min to allow collection of the supernatant. Activity was measured using a Multiskan<sup>TM</sup> microplate photometer (Thermo Fisher Scientific, Scoresby, Australia) in kinetic mode at 37°C for a maximum of 40 min.

### Serum assays

Bilirubin and lactate were measured colorimetrically in 96-well plates using assay kits obtained from Sigma-Aldrich, and absorbance was read on the Multiskan<sup>TM</sup> microplate photometer (Thermo Fisher Scientific).

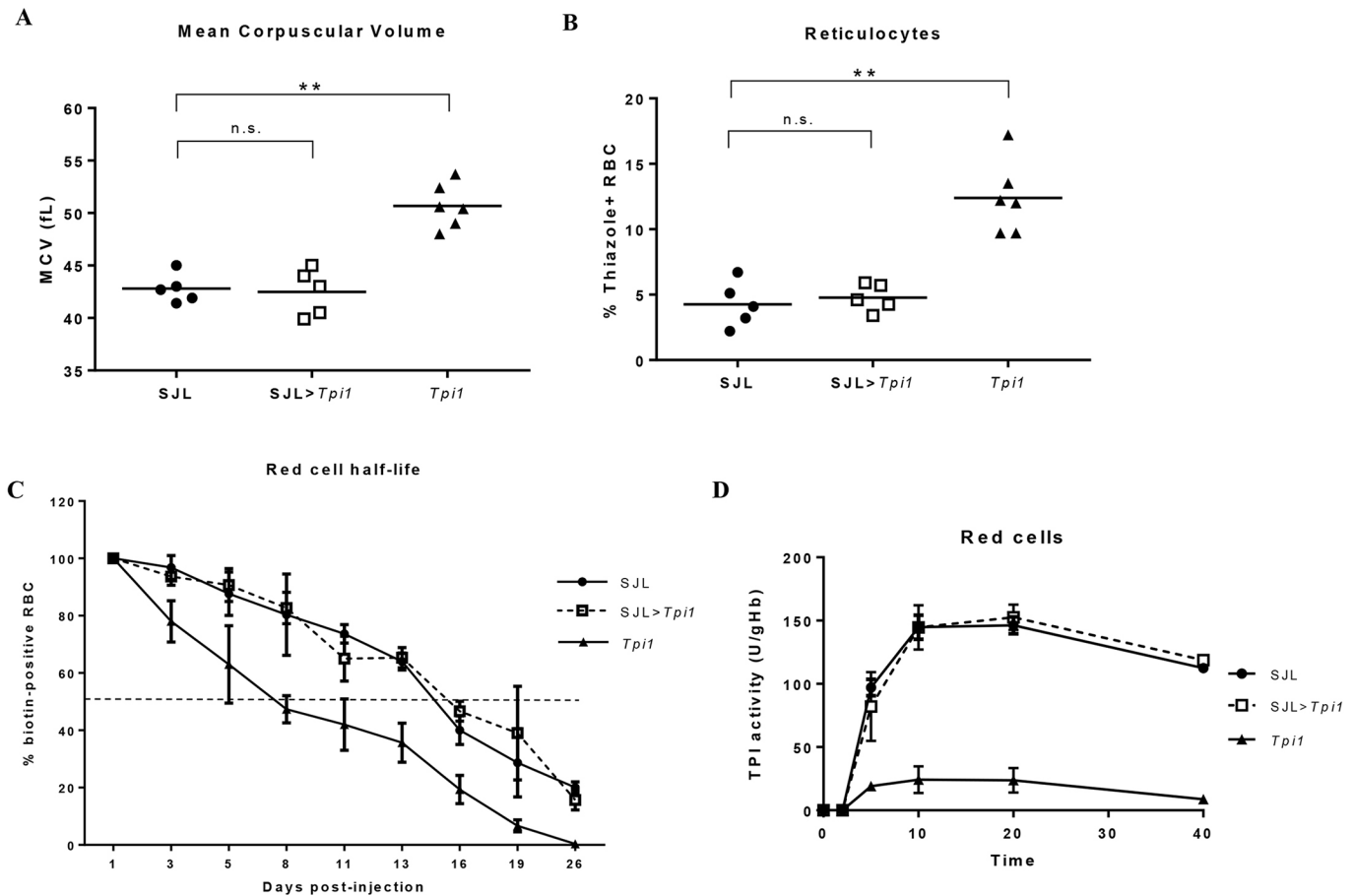


**Fig. 4. Bone marrow transplantation corrects macrocytosis and haemolysis.** (A,B) Red blood cell mean corpuscular volume (MCV) (A) and circulating reticulocytes (B), measured in the peripheral blood of 7-week post-transplanted mice. Individual values are shown, along with the mean (solid line). (C) Red blood cell half-life measured *in vivo* in 7-week post-transplanted mice using biotinylation, demonstrating the increased half-life of circulating red blood cells in the transplanted (SJL>Tpi1) cohort;  $n=4$ . Error bars represent s.d. (D) Kinetic assay showing TPI enzyme activity, measured in the peripheral red blood cells of 7-week post-transplanted mice over a time-course of 40 min. Enzyme activity within the red blood cells of the transplanted cohort (SJL>Tpi1) shows equal catalytic function to the wild-type enzyme;  $n=3$ . Error bars represent s.d.  $**P<0.001$ , n.s.: not significant.

DHAP was measured fluorometrically using a PicoProbe™ assay kit (BioVision), and analysed on a FLUOstar OPTIMA (BMG Labtech, Victoria, Australia) on fluorescent intensity mode with an excitation wavelength of 544 nm and an emission wavelength of 590 nm. HbA1c was measured by enzyme-linked immunosorbent assay (ELISA) (MyBioSource, San Diego, CA, USA), and absorbance was read on the Multiskan™ microplate photometer.

### Statistical analysis

Where applicable, results are expressed as mean±s.d. For statistical analysis, a two-tailed Student's *t*-test was employed, unless stated otherwise.  $P<0.05$  was considered statistically significant.

### Acknowledgements

We thank Rust Turakolov and Matthew Tinning at the Australian Genome Research Facility for their contributions to gene sequencing and bioinformatics; the Australian Phenomics Network for providing support; Raelene Pickering of the Baker Heart and Diabetes Institute for culturing macrophages; and the Animal Research Laboratory (Monash University) and its technicians for animal husbandry.

### Competing interests

The authors declare no competing or financial interests.

### Author contributions

Conceptualization: E.J.H., G.B., S.J.F., S.M.J., D.J.C.; Methodology: A.J.C., F.C.B., E.J.H., G.B., S.J.F.; Software: C.J.M.; Validation: A.J.C.; Formal analysis: A.J.C.;

Investigation: A.J.C., F.C.B., E.J.H., G.B., S.J.F., C.J.M.; Resources: F.C.B., E.J.H., G.B., S.J.F., C.J.M., S.M.J., D.J.C.; Data curation: A.J.C., C.J.M.; Writing - original draft: A.J.C.; Writing - review & editing: A.J.C., F.C.B., C.J.M., S.M.J., D.J.C.; Supervision: F.C.B., S.M.J., D.J.C.; Project administration: S.M.J., D.J.C.; Funding acquisition: S.M.J., D.J.C.

### Funding

This work was supported by the National Health and Medical Research Council (382900 to S.M.J. and D.J.C.) and the Sylvia and Charles Viertel Charitable Foundation (Senior Medical Research Fellowship to D.J.C.).

### References

- Ahmed, N., Battah, S., Karachalias, N., Babaei-Jadidi, R., Horányi, M., Baróti, K., Hollan, S. and Thornalley, P. J. (2003). Increased formation of methylglyoxal and protein glycation, oxidation and nitrosation in triosephosphate isomerase deficiency. *Biochim. Biophys. Acta.* **1639**, 121-132.
- Arya, R., Lalloz, M. R. A., Bellingham, A. J. and Layton, D. M. (1997). Evidence for founder effect of the Glu104Asp substitution and identification of new mutations in triosephosphate isomerase deficiency. *Hum. Mutat.* **10**, 290.
- Bauer, D. C., McMorran, B. J., Foote, S. J. and Burgio, G. (2015). Genome-wide analysis of chemically induced mutations in mouse in phenotype-driven screens. *BMC Genomics* **16**, 866.
- Brown, F. C., Scott, N., Rank, G., Collinge, J. E., Vadolas, J., Vickaryous, N., Whitelaw, N., Whitelaw, E., Kile, B. T., Jane, S. M. et al. (2013). ENU mutagenesis identifies the first mouse mutants reproducing human  $\beta$ -thalassaemia at the genomic level. *Blood Cells Mol. Dis.* **50**, 86-92.

- Celotto, A. M., Frank, A. C., Seigle, J. L. and Palladino, M. J.** (2006). Drosophila model of human inherited triosephosphate isomerase deficiency glycolytic enzymopathy. *Genetics* **174**, 1237-1246.
- Clay, S. A., Shore, N. A. and Landing, B. H.** (1982). Triosephosphate isomerase deficiency: a case report with neuropathological findings. *Am. J. Dis. Child.* **136**, 800-802.
- Conway, A. J., Brown, F. C., Fullinlaw, R. O., Kile, B. T., Jane, S. M. and Curtis, D. J.**, (2017). A mouse model of hereditary coproporphyrinemia identified in an ENU mutagenesis screen. *Dis. Models Mech.* **10**, 1005-1013.
- Emsley, P., Lohkamp, B., Scott, W. G. and Cowtan, K.** (2010). Features and development of Coot. *Acta Crystallogr. D Biol. Crystallogr.* **66**, 486-501.
- Fermo, E., Bianchi, P., Vercellati, C., Rees, D. C., Marcello, A. P., Barcellini, W. and Zanella, A.** (2010). Triose phosphate isomerase deficiency associated with two novel mutations in TPI gene. *Eur. J. Haematol.* **85**, 170-173.
- Hollán, S., Fujii, H., Hirono, A., Hirono, K., Karro, H., Miwa, S., Harsányi, V., Gyódi, É. and Insekt-Kovács, M.** (1993). Hereditary triosephosphate isomerase (TPI) deficiency: two severely affected brothers one with and one without neurological symptoms. *Hum. Genet.* **92**, 486-490.
- Hrizo, S. L. and Palladino, M. J.** (2010). Hsp70- and Hsp90-mediated proteasomal degradation underlies TPI sugar-kill pathogenesis in Drosophila. *Neurobiol. Dis.* **40**, 676-683.
- Laskowski, R. A. and Swindells, M. B.** (2011). Logiplot+: multiple ligand-protein interaction diagrams for drug discovery. *J. Chem. Info. Model.* **51**, 2778-2786.
- Mainfroid, V., Terpstra, P., Beaugard, M., Frère, J.-M., Mande, S. C., Hol, W. G. J., Martial, J. A. and Goraj, K.** (1996). Three hTIM mutants that provide new insights on why TIM is a dimer. *J. Mol. Biol.* **257**, 441-456.
- McMullin, M. F.** (1999). The molecular basis of disorders of red cell enzymes. *J. Clin. Pathol.* **52**, 241.
- Oláh, J., Orosz, F., Puskás, L. G., Hackler, L., Horányi, M., Polgár, L., Hollán, S. and Ovádi, J.**, (2005). Triosephosphate isomerase deficiency: consequences of an inherited mutation at mRNA, protein and metabolic levels. *Biochem. J.* **392**, 675-683.
- Oliver, C. and Timson, D. J.**, (2017). In silico prediction of the effects of mutations in the human triose phosphate isomerase gene: Towards a predictive framework for TPI deficiency. *Eur. J. Med. Genet.* **60**, 289-298.
- Orosz, F., Oláh, J. and Ovádi, J.** (2006). Triosephosphate isomerase deficiency: facts and doubts. *IUBMB Life* **58**, 703-715.
- Orosz, F., Oláh, J. and Ovádi, J.** (2009). Triosephosphate isomerase deficiency: new insights into an enigmatic disease. *Biochim Biophys Acta.* **1792**, 1168-1174.
- Palladino, M. J., Hadley, T. J. and Ganetzky, B.** (2002). Temperature-sensitive paralytic mutants are enriched for those causing neurodegeneration in Drosophila. *Genetics* **161**, 1197-1208.
- Pretsch, W.** (2009). Triosephosphate isomerase activity-deficient mice show haemolytic anaemia in homozygous condition. *Genet. Res.* **91**, 1-4.
- Ralsler, M., Heeren, G., Breitenbach, M., Lehrach, H. and Krobitsch, S.** (2006). Triose phosphate isomerase deficiency is caused by altered dimerization—not catalytic inactivity—of the mutant enzymes. *PLoS One* **1**, e30.
- Ralsler, M., Nebel, A., Kleindorp, R., Krobitsch, S., Lehrach, H., Schreiber, S., Reinhardt, R. and Timmermann, B.** (2008). Sequencing and genotypic analysis of the triosephosphate isomerase (TPI1) locus in a large sample of long-lived Germans. *BMC Genet.* **9**, 38.
- Roland, B. P., Zeccola, A. M., Larsen, S. B., Amrich, C. G., Talsma, A. D., Stuchul, K. A., Heroux, A., Levitan, E. S., VanDemark, A. P. and Palladino, M. J.** (2016). Structural and genetic studies demonstrate neurologic dysfunction in triosephosphate isomerase deficiency is associated with impaired synaptic vesicle dynamics. *PLoS Genet.* **12**, e1005941.
- Rosa, R., Prehu, M.-O., Calvin, M.-C., Badoual, J., Alix, D. and Girod, R.**, (1985). Hereditary triose phosphate isomerase deficiency: seven new homozygous cases. *Hum. Genet.* **71**, 235-240.
- Sarper, N., Zengin, E., Jakobs, C., Salomons, G. S., Wamelink, M. M., Ralsler, M., Kurt, K. and Kara, B.**, (2013). Mild hemolytic anemia, progressive neuromotor retardation and fatal outcome: a disorder of glycolysis, triose-phosphate isomerase deficiency. *Turk. J. Pediatr.* **55**, 198-202.
- Schneider, A. S.** (2000). Triosephosphate isomerase deficiency: historical perspectives and molecular aspects. *Baillieres Best Pract. Res. Clin. Haematol.* **13**, 119-140.
- Schneider, A. and Cohen-Solal, M.** (1996). Hematologically important mutations: triosephosphate isomerase. *Blood Cells Mol. Dis.* **22**, 82-84.
- Valentin, C., Pissard, S., Martin, J., Héron, D., Labrune, P., Livet, M. O., Mayer, M., Gelbart, T., Schneider, A., Max-Audit, I. et al.** (2000). Triose phosphate isomerase deficiency in 3 French families: two novel null alleles, a frameshift mutation (TPI Alfortville) and an alteration in the initiation codon (TPI Paris). *Blood* **96**, 1130-1135.
- Van Wijk, R. and van Solinge, W. W.** (2005). The energy-less red blood cell is lost: erythrocyte enzyme abnormalities of glycolysis. *Blood* **106**, 4034-4042.

---

## CHAPTER FIVE

### **Characterization of *Tfrc*-mutant mice with microcytic phenotypes**

The following chapter describes the third (of three) complete set of results obtained for this thesis, which were submitted in the form of a research article in a peer-reviewed scientific journal during enrolment (see *Thesis including published works*), and recognises the leading author as Ashlee J. Conway. The hypotheses, aims, and expected outcomes of this thesis are each discussed in this chapter, and additional content specific to the article (methods, references, etc) are also supplied. Since thesis submission to examiners, the article has been published in a peer-reviewed journal, and has therefore been collated in this thesis in its published format.

# Characterization of *Tfrc*-mutant mice with microcytic phenotypes

Ashlee J. Conway,<sup>1</sup> Fiona C. Brown,<sup>1</sup> Gerhard Rank,<sup>2</sup> Benjamin T. Kile,<sup>3,4</sup> Craig J. Morton,<sup>5</sup> Stephen M. Jane,<sup>6</sup> and David J. Curtis<sup>1,7</sup>

<sup>1</sup>Australian Centre for Blood Diseases, Central Clinical School, Monash University, Melbourne, Australia; <sup>2</sup>Rotary Bone Marrow Research Laboratory, Royal Melbourne Hospital, Melbourne, Australia; <sup>3</sup>The Walter and Eliza Hall Institute of Medical Research, Melbourne, Australia; <sup>4</sup>Anatomy and Developmental Biology, Monash Biomedicine Discovery Institute, Monash University, Melbourne, Australia; <sup>5</sup>Australian Cancer Research Foundation Rational Drug Discovery Centre, St. Vincent's Institute of Medical Research, Fitzroy, Australia; <sup>6</sup>The Alfred Hospital, Melbourne, Australia; and <sup>7</sup>Department of Clinical Haematology, Central Clinical School, Monash University, Melbourne, Australia

## Key Points

- Novel *Tfrc*-mutant mouse identified in ENU mutagenesis screen with stable receptor expression.
- Flow imaging cytometry demonstrates microcytosis in mutants derives from dysfunctional receptor-mediated endocytosis of Tf-TfR complex.

To identify novel regulators of erythropoiesis, we performed independent forward genetic screens using the chemical mutagen ENU in mice. Among progeny displaying microcytic red-cell phenotypes, 7 independent mouse strains harboring mutations within the transferrin receptor gene *Tfrc* were identified. Six of the mutants, including the previously described red blood cell 6 (RBC6) strain, displayed reduced erythroblast CD71 expression and midgestation lethality of homozygotes (E12.5-E14.5), and 1 novel strain, RBC21, displayed a variable phenotype with sustained CD71 expression and late homozygous lethality (E18.5). Standard iron studies were normal in the RBC21 mutant, but intracellular ferritin was significantly reduced. The microcytic phenotype seen in the RBC21 strain was the result of impaired binding of transferrin to the receptor. Neither RBC6 nor RBC21 responded to iron replacement therapy. These studies describe how point mutations of the transferrin receptor can cause a microcytic anemia that does not respond to iron therapy and would not be detected by routine iron studies, such as serum ferritin.

## Introduction

The transferrin receptor (TfR, TfR1, CD71), encoded by the *TFRC* gene in humans, is an integral component of iron metabolism and erythrocyte production.<sup>1</sup> The highest expression of TfR is seen in the bone marrow on developing erythroblasts, which require intake of circulating iron for hemoglobin synthesis.<sup>2,3</sup> The 2 key ligands of TfR are transferrin (Tf) and the hemochromatosis protein (HFE), which both play prominent roles in iron metabolism and regulation, respectively.<sup>4</sup> These ligands directly compete for overlapping binding sites within the ectopic helical domain of the receptor, composed of N-terminal amino acids 607 to 760 (mouse equivalent, 610-763) within exons 17 to 19.<sup>5</sup> The binding affinities and conformational relationships of both ligands to TfR have been previously described.<sup>6,7</sup> As a homodimer, TfR has 2 binding sites for the acceptance of 2 molecules of either Tf or HFE, or it can form a ternary structure with both simultaneously at a 1:1:1 ratio, but ultimately, the receptor has a much higher affinity for Tf, specifically iron-bound Tf (Fe-Tf), at biological potential of hydrogen (pH).<sup>5</sup> This is due to the enclosed conformational change that Tf undergoes when iron is captured from the circulation. In contrast, TfR has a weak affinity for iron-free Tf, the conformation of which is more open and reduces the number of binding sites accessible by the receptor. After the binding of Tf to the membrane-bound receptor, the Tf-TfR complex undergoes receptor-mediated endocytosis within a clathrin-coated pit, facilitated by endocytic mediators, such as dynamin 2 (*Dnm2*).<sup>8</sup> A reduction in endosomal pH (~5.5) allows iron to disassociate from its carrier protein without disturbing Tf-TfR binding, and subsequently, iron enters the cell through the DMT-1 portal, where it can be used in the synthesis of heme or stored intracellularly in the form of ferritin.<sup>9</sup> The iron-free Tf-TfR complex is then recycled to the cell surface, where Tf is released back into the circulation.

TfR-HFE interactions also play an important role in maintaining iron homeostasis.<sup>10</sup> As the concentration of serum iron increases, so does Fe-Tf, which subsequently outcompetes HFE for TfR binding positions. Displaced HFE initiates a negative feedback loop by prompting the formation of an iron-regulatory complex

**Table 1. List of *Tfrc*-mutant mouse strains generated by ENU mutagenesis**

Mutant	Nucleotide mutation, cDNA	Amino acid change	Mean heterozygote MCV	Homozygote phenotype	CD71 expression, heterozygote
BL/6	NA	NA	46	NA	Normal
RBC1	T1849C	Y617H	42	Lethal (E10.5-E12.5)	Reduced
RBC4	T2048A	Y686Stop	42	Lethal (E10.5-E12.5)	Reduced
RBC5	T1925G	L642R	41	Lethal (E10.5-E12.5)	Reduced
RBC6*	T1934G	L645R	43	Lethal (E10.5-E12.5)	Reduced
RBC8, RBC17	A2105G	H702R	41	Lethal (E10.5-E12.5)	Reduced
RBC21	G1961A	R654H	37	Lethal (E16.5-E18.5)	Normal

Mouse mutants with autosomal-dominant microcytic phenotypes, identified in independent ENU mutagenesis screens, were deemed RBC mutants, by order of discovery. Mutants were phenotyped by their mean corpuscular volume (MCV), calculated by an automated blood analyzer (Hemavet, Drew Scientific). Timed pregnancy studies determined embryonic lethality in each mutant strain. CD71 expression was determined by flow cytometry, performed on live Ter-119<sup>+</sup> bone marrow erythroblasts, which compared CD71 intensity with that of WT littermates in each cohort.

NA, not applicable.

around the liver-specific homolog TfR2.<sup>11</sup> This complex involves the recruitment of proteins such as hemojuvelin (HJV) and BMP-6, which require HFE for stabilization. The regulatory complex initiates downstream signaling through TfR2 and other iron-sensing receptors and ultimately triggers production of the peptide hormone hepcidin.<sup>11</sup> Hepcidin inhibits excessive iron from entering the circulation via blockage and degradation of ferroportin. At low iron concentrations, TfR is thought to sequester HFE to prevent it from inappropriately enacting on TfR2.<sup>10,12</sup> In addition to regulation, TfR2 is also important for erythropoietic development through its cooperation with the erythropoietin receptor; however, the phenotypes of experimental animals lacking TfR2 are strikingly different to those with TfR defects.<sup>13</sup>

Inheritable mutations within genes encoding HFE, TfR2, or HJV are known to cause iron overload, or hemochromatosis.<sup>11</sup> In contrast, there have been no definitive reported cases of red-cell diseases resulting from inherited mutations in *TFRC* in humans. Genome-wide association studies previously identified a homozygous mutation in the C-terminal cytoplasmic domain of TfR, resulting in primary immunodeficiency,<sup>14</sup> but no erythroid-specific diseases resulting from mutations in *TFRC* have been confirmed to date. However, microcytic anemia with iron deficiency-like characteristics, often unresponsive to iron therapy, is a recognized clinical finding in humans, and many cases go unresolved.<sup>15</sup> It is therefore possible that congenital mutations within other key proteins of the iron metabolism pathway, such as TfR, do exist in the population but go undetected. The generation of experimental animals harboring *Tfrc* mutations, particularly mice, typically results in iron-deficient erythropoiesis with various degrees of anemia and liver iron overload,<sup>1,8,16</sup> but the pathological role of aberrant TfR endocytic cycling in iron therapy-resistant microcytic anemia and its clinical relevance remain poorly characterized. In a series of genome-wide ENU mutagenesis screens, we identified a collection of mutant mice with dominant microcytic red-cell phenotypes, all harboring *Tfrc* mutations within the Tf/HFE binding domain. Detailed phenotypical analyses of these mutant strains have offered greater insight into the key characteristics of TfR-mediated microcytic anemia and the molecular mechanisms underpinning red-cell pathologies.

## Materials and methods

### Mice

Dominant ENU mutagenesis screens were performed in mice as described previously.<sup>17</sup> G<sub>1</sub> pedigrees displaying microcytosis were

identified from 7 individual founder mice. Gene mapping followed by whole-exome sequencing was performed on each strain,<sup>8</sup> which identified each mutation in the *Tfrc* gene, as listed in Table 1. Genotyping of the strains red blood cell 6 (RBC6; *Tfrc*<sup>+L645R</sup>) or RBC21 (*Tfrc*<sup>+R654H</sup>) was performed using bone marrow complementary DNA (cDNA) and the primers forward (5'-CAC ACC TGG CTT TCC TTC TT-3') and reverse (5'-ATG AGG AAC CAG ACC GTT ATG-3'), followed by sequencing using BigDye Terminator reagents. All animal experiments were approved by the animal ethics committees of the Alfred Medical and Research Education Precinct and Monash University.

### Blood and serum studies

Full blood examinations were performed on EDTA-treated whole blood collected from submandibular venepuncture and processed by the Hemavet automated blood analyzer (Drew Scientific, Miami Lakes, FL). Tf and ferritin assays were performed by enzyme-linked immunosorbent assay (ALPCO Diagnostics, Salem, MA). Serum iron and Tf saturation were quantified using a total iron binding capacity reagent set (Pointe Scientific, Inc., Canton, MI). Liver iron was assayed using an iron assay kit (Abcam, Cambridge, MA).

### Tf uptake assay and flow imaging

Single-cell flow imaging was performed on whole bone marrow stained with conjugated antibodies Ter-119 and CD71 (BD Biosciences, San Jose, CA) on the Amins ImageStreamX Mark II flow cytometer (Merck, Darmstadt, Germany). A minimum of 2000 erythroblast (Ter-119<sup>+</sup>) events were captured for each run. Compensation and analysis were performed using Amnis IDEAS software (Merck). Early proerythroblasts and late erythroid cell subtypes were excluded from analysis based on Ter-119 expression. Focused cells were chosen based on a bright field intensity gradient of >40, followed by elimination of debris and doublets by the bright field aspect ratio vs area dot plot. Colocalization analysis generated a median bright intensity score for the fluorescent intensities of Ter-119 and CD71, where higher score indicated greater overlap of the 2 probes. Internalization analysis generated the mean internalization erode score using Ter-119 as the mask probe, where a score equal to 1.0 indicated the probe was membrane bound, and a score >1.0 correlated with increased internalization of the probe. Using these parameters, Tf uptake was assessed on bone marrow additionally stained with 5 mg/mL

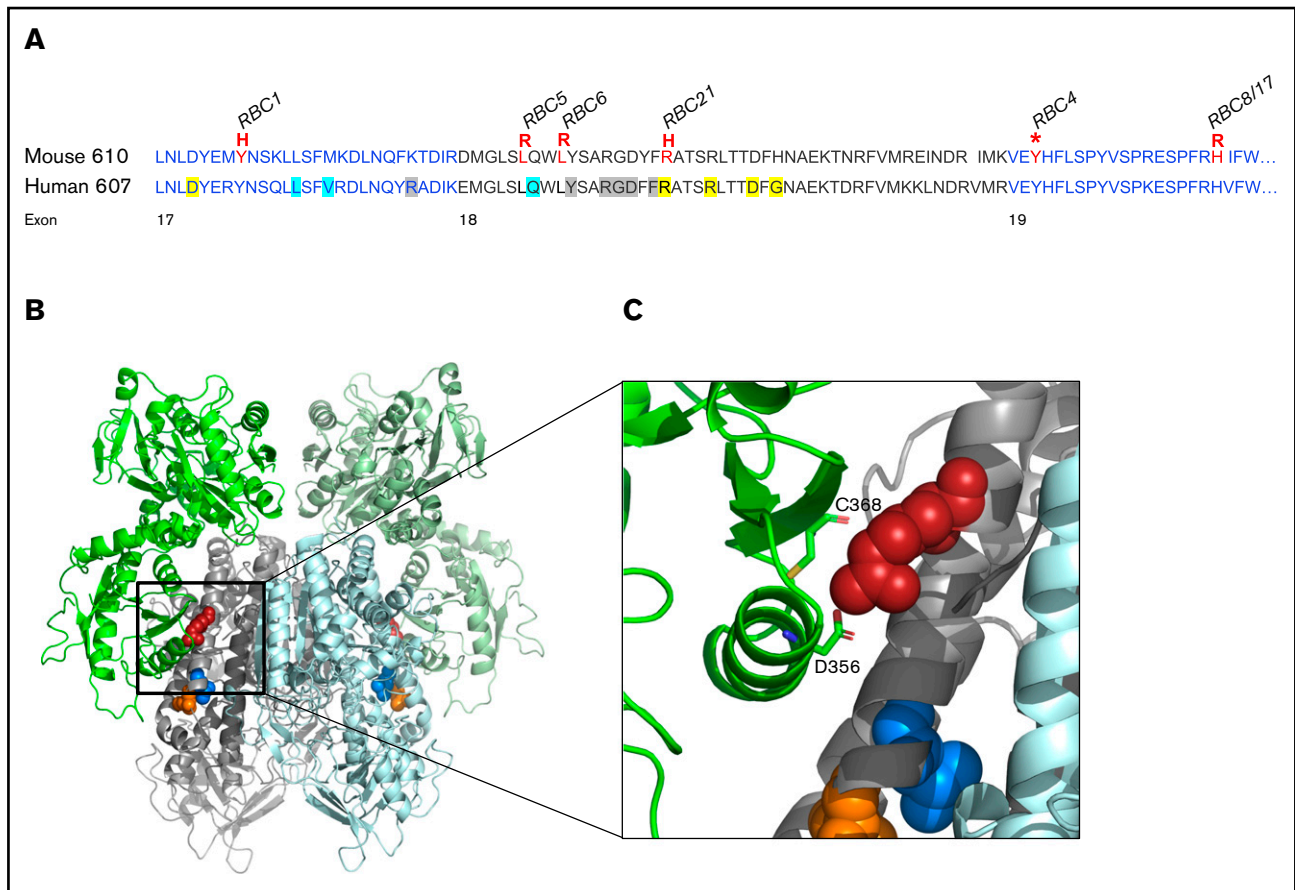


**Figure 1. Distribution of *Tfrc* mutations identified in ENU mutagenesis screens.** (A) Amino acid sequence of the mouse (upper) and human (lower) ectopic helical domain of the *Tfrc* gene. Mutations identified in murine ENU mutagenesis screens are highlighted (red), with their corresponding RBC mutant strain. Known ligand binding positions include Tf binding (yellow), HFE binding (blue), and sites with overlapping Tf/HFE binding (gray). (B) Three-dimensional structure of the murine TfR-Tf complex (PD entry 3S9L) inspected by PyMOL (version 2.0.3). A cluster of *Tfrc* mutations (RBC5, orange; RBC6, blue; RBC21, red) is highlighted. (C) Closer inspection of the RBC21 mutation and its positioning within the TfR-Tf complex. The R654 amino acid (human equivalent, R651) is shown to have a direct Tf binding role via interactions with Tf amino acids C368 and D356. Other mutation sites (RBC5, RBC6) are suggested to play structural roles within the receptor.

of Tf–Alexa Fluor 647 conjugate (Life Technologies, Scoresby, Australia) for 45 minutes at 4°C in the dark. Uptake was initiated by incubating cells at 37°C and halted at desired time points by placing cells in ice. Cells were then briefly acid washed (150 mmol/L of sodium chloride, 20 mmol/L of calcium dichloride, 20 mmol/L of sodium acetate; pH, 4.6) before cytometric analysis and imaging. Tf uptake was calculated at each time point by dividing the relative intensity of internalized Tf by the 0-minute noninternalized unwashed control.

### Quantitative real-time polymerase chain reaction

Total RNA was extracted from liver using TRIzol (Invitrogen) according to the manufacturer's instructions, followed by cDNA amplification of 1 µg total RNA using a reverse transcription kit (Promega). Quantitative real-time polymerase chain reaction was performed on a LightCycler 480II (Roche Diagnostics) using the GoTaq qPCR Master Mix (Promega). Expression of genes was normalized to β-actin, and data are presented as relative expression compared with WT controls. Gene-specific primers were as follows: *Hamp-1*: forward (5'-AAG CAG GGC AGA CAT TGC GAT-3') and reverse (5'-CAG GAT GTG GCT CTA GGC TAT GT-3'); β-Actin: forward (5'-CTG TCC

CTG TAT GCC TCT G-3') and reverse (5'-ATG TCA CGC ACG ATT TCC-3').

### Statistical analysis

Where applicable, results are expressed as mean ± standard deviation. For statistical analysis, a 2-tailed Student *t* test was employed, unless stated otherwise, where *P* < .05 indicated significance (or as defined in the figure legends).

## Results

### Identification of microcytic mouse strains with dominant *Tfrc* mutations

A series of independent genome-wide ENU mutagenesis screens were performed in mice to identify novel genes or alleles regulating erythropoiesis, as previously described.<sup>17,18</sup> Seven G<sub>1</sub> progeny exhibiting a reduced MCV >3 standard deviations below the average population were isolated. Further breeding demonstrated the phenotype was fully penetrant and autosomal dominant in inheritance. Pedigrees were termed the RBC mutants, numbered in order of discovery (Table 1).

To identify the genetic mutation responsible for the microcytic phenotypes observed, gene mapping or whole-exome sequencing was used as previously described<sup>8,17</sup> and confirmed by Sanger sequencing on bone marrow cDNA. Mutations within the *Tfrc* gene on chromosome 16 were identified in each pedigree. Two mutants were genetically identical (RBC8 and RBC17), resulting in 6 different *Tfrc* mouse strains (Table 1), including the previously reported RBC6 mouse (*Tfrc*<sup>+L645R</sup>).<sup>8</sup> Five of the 6 unique alleles were missense substitutions, and 1 was a premature stop codon (RBC4). All mutations were localized within exon 17, 18, or 19, resulting in substitutions of conserved amino acids (Figure 1A). Three-dimensional modeling of the murine TfR dimer, in the context of the Fe-Tf complex, showed several *Tfrc* mutations (RBC5, RBC6, RBC21) to be within the helical binding domain, either at or adjacent to known Tf/HFE binding sites (Figure 1B). Modeling predicted that many mutational sites played important structural and conformational roles within TfR, such as providing hydrophobic packing for the helical bundle (RBC5, RBC6), or otherwise produced an unstable truncated form (RBC4). One mutation, R654H (RBC21), was found to be directly involved in securing Tf to the receptor (Figure 1C) and was the only substitution predicted not to distort protein conformation, instead affecting the ligand binding capacity of Tf.

### TfR mutants with distinct phenotypes

Mice carrying the RBC21 allele (denoted *Tfrc*<sup>R654H</sup>) displayed a unique phenotype among the RBC mutants and therefore became the major focus of our investigations. Similar to other *Tfrc* mutants described here and previously,<sup>17</sup> *Tfrc*<sup>+R654H</sup> mice displayed significantly reduced MCV, hemoglobin, and hematocrit, as well as increased red-cell count and red-cell distribution width, in comparison with WT littermates (Table 2). White-cell and platelet values were unchanged. Peripheral blood smears revealed microcytic red cells with unremarkable morphology in heterozygotes (Figure 2A). Surprisingly, serum ferritin and serum Tf, typically used to diagnose iron deficiency in humans, were normal in both *Tfrc*<sup>+L645R</sup> and *Tfrc*<sup>+R654H</sup> mice (Table 3). Total liver iron was also normal. However, red-cell ferritin concentrations were significantly reduced in both strains, indicating an intracellular iron deficit in both the *Tfrc*<sup>+L645R</sup> and *Tfrc*<sup>+R654H</sup> mutants (Table 3).

A key difference observed in the *Tfrc*<sup>+R654H</sup> strain was increased expression of CD71 (TfR) on the surface of Ter-119<sup>+</sup> bone marrow erythroblasts (Figure 2B). In all other *Tfrc*-mutant RBC strains, such as *Tfrc*<sup>+L645R</sup>, CD71 expression was significantly reduced compared with WT littermates (Figure 2B). These data, combined with the 3-dimensional modeling, suggested that *Tfrc*<sup>R654H</sup> erythroblasts express a structurally stable mutant TfR protein at the cell surface.

In contrast to other strains, *Tfrc*<sup>R654H/R654H</sup> embryos displayed notably delayed homozygous lethality (Table 1). *Tfrc*<sup>R654H/R654H</sup> embryos had an anemic phenotype detectable at E14.5 and died between E16.5 and E18.5 (Figure 2C). E14.5 *Tfrc*<sup>R654H/R654H</sup> embryos showed severe pallor, edema, and underdeveloped craniofacial structures and had significantly fewer fetal liver cells compared with WT littermates (Figure 2D). Despite this, CD71 expression on Ter-119<sup>+</sup> cells harvested from E14.5 *Tfrc*<sup>R654H/R654H</sup> fetal livers was increased (Figure 2E). To determine which mutant allele was dominant, we intercrossed *Tfrc*<sup>+L645R</sup> and *Tfrc*<sup>+R654H</sup> heterozygous mice to generate *Tfrc*<sup>L645R/R654H</sup> compound heterozygotes. Double-heterozygous embryos were found to be phenotypically identical to *Tfrc*<sup>R654H/R654H</sup> embryos, with embryonic lethality observed between days E16.5 and E18.5 (Figure 2C).

**Table 2. Full blood examination of the *Tfrc*<sup>+R654H</sup> strain**

	Mean ± SD		P
	WT (n = 22)	<i>Tfrc</i> <sup>+R654H</sup> (n = 18)	
RBCs, × 10 <sup>12</sup> /L	9.57 ± 0.7	11.21 ± 1.2	<.0001
Hb, g/L	14.2 ± 1.2	13.4 ± 1.4	<.05
HCT, %	45.9 ± 2.5	41.3 ± 4.6	<.0001
MCV, fL	47.6 ± 1.7	36.9 ± 2.5	<.0001
MCH, pg	14.9 ± 0.4	12.0 ± 0.7	<.0001
MCHC, g/dL	31.3 ± 1.3	32.6 ± 1.9	n.s.
RDW, %	18.7 ± 1.1	19.7 ± 1.0	<.05
WBCs, × 10 <sup>9</sup> /L	8.69 ± 1.8	7.63 ± 2.5	n.s.
Platelets, × 10 <sup>9</sup> /L	972 ± 190	1057 ± 385	n.s.
Reticulocytes, %	5.2 ± 1.6	4.0 ± 2.0	n.s.

Blood parameters obtained from 7-week-old WT and heterozygous (*Tfrc*<sup>+R654H</sup>) mice using automated blood analyzer (Hemavet). Two-tailed Student *t* test was used.

Hb, hemoglobin; HCT, hematocrit; MCH, mean corpuscular hemoglobin; MCHC, mean corpuscular hemoglobin concentration; n.s., not significant; RDW, red-cell distribution width; SD, standard deviation; WBC, white blood cell.

Thus, the *Tfrc*<sup>R654H</sup> mutation retained partial function and was able to rescue the loss-of-function *Tfrc*<sup>+L645R</sup>-mutant allele.

Given that the *Tfrc*<sup>R654H</sup> mutation was germ line and affected all tissues requiring iron intake, fetal liver transplantations were performed to establish whether embryonic lethality in homozygotes was due to erythropoietic defects. WT or *Tfrc*<sup>R654H/R654H</sup> fetal liver cells from E14.5 embryos were transplanted into lethally irradiated adult WT mice. Survival of the transplanted recipients was tracked over time (Figure 2F), and peripheral blood was analyzed after 7-week recovery (Table 4). As expected, WT fetal liver cells were able to rescue lethally irradiated mice, with complete donor reconstitution of all hematopoietic lineages. However, a majority of mice transplanted with *Tfrc*<sup>R654H/R654H</sup> fetal liver cells died within 2 weeks as a result of severe anemia (Figure 2F). Furthermore, blood analysis of the single surviving *Tfrc*<sup>R654H/R654H</sup> recipient demonstrated severe microcytic, hypochromic anemia (Table 4). Thus, the lethality of homozygous embryos could be attributed to an intrinsic defect in red-cell production.

### *Tfrc*<sup>R654H</sup> mutation inhibits Tf binding and internalization

The reduced intracellular iron, despite elevated CD71 expression, suggested that the *Tfrc*<sup>R654H</sup> mutation affected interactions with Tf. The binding capacity and internalization of Tf and TfR were analyzed in erythroblasts using the Amnis ImageStreamX flow imaging cytometer. We first validated CD71 expression levels on Ter-119<sup>+</sup> erythroblasts harvested from each cohort using single-cell fluorescent imaging (Figure 3A). In comparison with WT cells, CD71 expression on *Tfrc*<sup>+L645R</sup> erythroblasts was significantly reduced and displayed a lower CD71/Ter-119 overlap score (1.56 compared with 1.81 in WT; *P* = .01), indicating reduced CD71 expression. In *Tfrc*<sup>+R654H</sup> erythroblasts, however, the median CD71/Ter-119 overlap was greater than the WT ratio (1.96; *P* = .01), consistent with the increased CD71 surface expression observed by flow cytometry (Figure 2B). Erythroblasts from WT, *Tfrc*<sup>+L645R</sup>, and *Tfrc*<sup>+R654H</sup> mice were subsequently stained with a Tf-Alexa Fluor conjugate for flow imaging to analyze Tf-TfR binding and internalization. After incubation with the ligand, both WT and

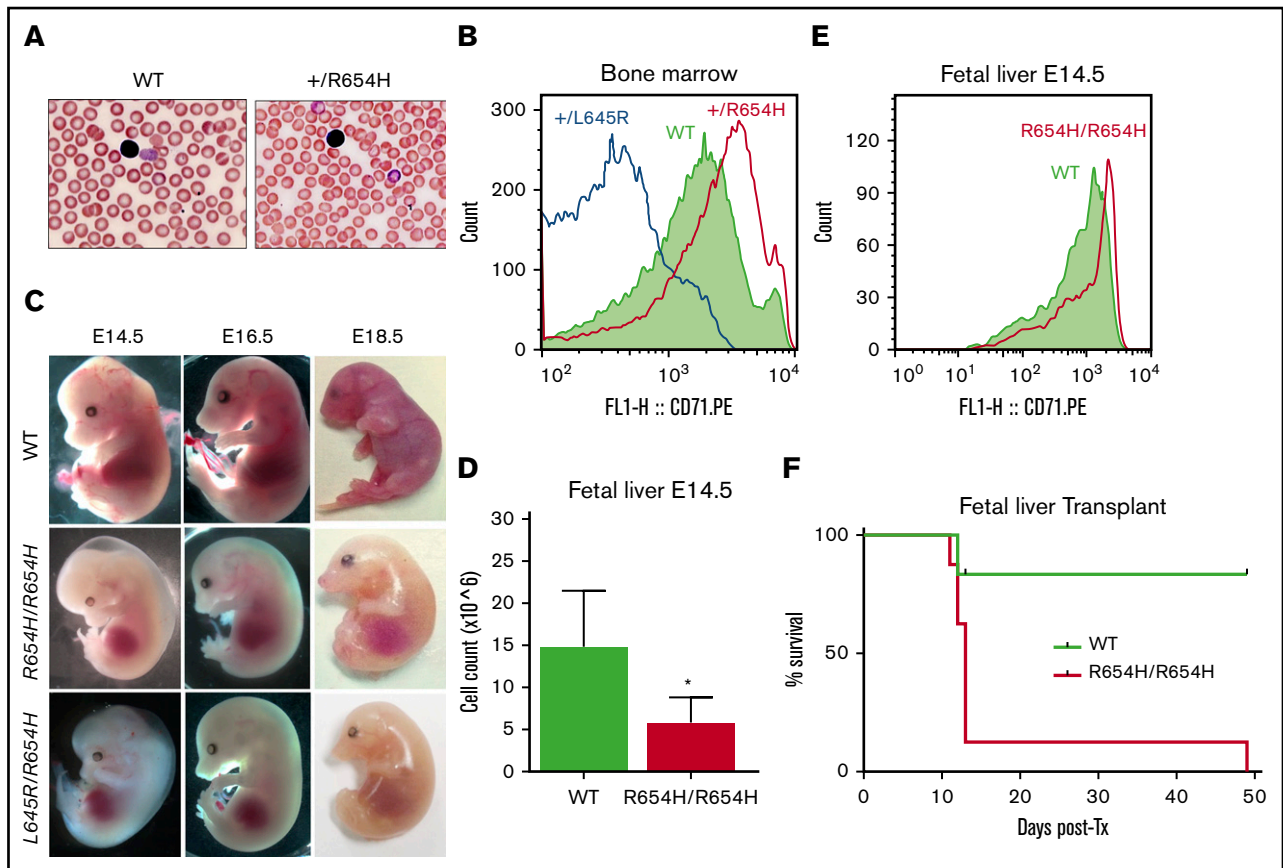


**Figure 2. Phenotype of the RBC21 mouse.** (A) Peripheral blood smears of 7-week-old WT and RBC21 heterozygous ( $Tfrc^{+/R654H}$ ) mice (original magnification  $\times 400$ ; hematoxylin and eosin stain). Heterozygotes show microcytic red cells with mild pallor. (B) Flow cytometric analysis of CD71 expression levels, performed on live Ter-119<sup>+</sup> bone marrow erythroblasts of WT, RBC6 ( $Tfrc^{+L645R}$ ), and RBC21 ( $Tfrc^{+/R654H}$ ) mice. (C) Timed pregnancies showing WT, RBC21 homozygous ( $Tfrc^{R654H/R654H}$ ), and RBC6/RB21 double-heterozygous ( $Tfrc^{L645R/R654H}$ ) embryos, dissected at embryonic days 14.5, 16.5, and 18.5. (D) Fetal liver live cell counts performed on WT and RBC21 homozygous ( $Tfrc^{R654H/R654H}$ ) embryos at embryonic day 14.5 ( $n = 4$ ). (E) Flow cytometric analysis of CD71 expression levels, performed on live Ter-119<sup>+</sup> fetal liver cells of WT and RBC21 homozygous ( $Tfrc^{R654H/R654H}$ ) embryos at embryonic day 14.5. (F) Survival curve of irradiated adult mice transplanted with WT or RBC21 homozygous ( $Tfrc^{R654H/R654H}$ ) fetal liver cells, extracted from E14.5 embryos. Median survival of homozygous cohort, 13 days ( $n = 12$ ). \* $P < .05$ . Tx, treatment.

$Tfrc^{+/L645R}$  erythroblasts showed an average of 20% Tf saturation across membrane-bound CD71 (Figure 3B). In contrast,  $Tfrc^{+/R654H}$  erythroblasts demonstrated significantly reduced Tf conjugation to CD71 at the cell surface, despite increased CD71 expression (13.8%;  $P = .045$ ), indicating that the  $Tfrc^{R654H}$  mutation reduced Tf binding to TfR.

To investigate whether reduced Tf binding resulted in less intracellular Tf uptake, TfR uptake through receptor-mediated endocytosis was assessed by flow imaging over time using a Tf–Alexa Fluor conjugate. Internalization of Tf was quantified by the mean internalization erode score, which positively correlates with the percentage of endocytosed Tf. At 0 minutes (Figure 3C), Tf was detectable exclusively at the cell membrane in all 3 cohorts, resulting in a low internalization score ( $\sim 1.03$ ). After 5 minutes (Figure 3D), a significant proportion of Tf was internalized by receptor-mediated endocytosis in WT erythroblasts (1.23), correlating with Tf uptake of 46% (Figure 3E).  $Tfrc^{+/L645R}$ -mutant erythroblasts had a similar internalization erode score (1.19;  $P = .09$ ) and Tf uptake of 42% (Figure 3E). In contrast,  $Tfrc^{+/R654H}$ -mutant erythroblasts showed significantly reduced internalization

(1.06;  $P = .02$ ) and endocytosis of Tf (21%; Figure 3E) after 5 minutes.

Tf and HFE have a number of overlapping binding sites for TfR; however, based on the helical domain sequence (Figure 1A),<sup>6</sup> the  $Tfrc^{L645R}$  and  $Tfrc^{R654H}$  mutations were not predicted to affect HFE binding. To confirm the mutations did not interfere with HFE binding to the receptor, we measured liver *Hamp-1* messenger RNA expression as an indirect readout of the HFE–TfR interaction. Liver *Hamp-1* expression was normal in both  $Tfrc^{+/L645R}$  and  $Tfrc^{+/R654H}$  mice compared with WT controls (Figure 3F). These results indicated the HFE binding regions on TfR were unaffected, and the red-cell phenotypes observed in these mice were not the result of increased hepcidin production.

### ***Tfrc*-mutant mice are resistant to iron therapy**

To determine if *Tfrc* mutations respond to iron therapy, we treated  $Tfrc^{+/L645R}$  and  $Tfrc^{+/R654H}$  mice with iron dextran and reevaluated iron parameters 3 weeks later. Despite the significant increases that occurred to serum Tf, serum ferritin, and liver iron after administration, iron dextran treatment was unable to restore red-cell ferritin

**Table 3. Iron studies of *Tfrc*<sup>+L645R</sup> and *Tfrc*<sup>+R654H</sup> mice**

	Mean ± SD		
	WT (n = 9)	<i>Tfrc</i> <sup>+L645R</sup> (n = 6)	<i>Tfrc</i> <sup>+R654H</sup> (n = 5)
Serum Tf, g/L	3.80 ± 1.2	4.24 ± 0.68	3.99 ± 0.87
Serum ferritin, µg/L	1021 ± 130.6	905 ± 228.8	908 ± 125.2
RBC ferritin, µg/L	60.43 ± 9.54	17.22 ± 1.21*	28.70 ± 8.65*
Serum iron, µmol/L	47.21 ± 2.23	38.09 ± 9.29*	47.90 ± 27.6
TIBC, µmol/L	115.84 ± 11.7	106.68 ± 6.82	95.92 ± 15.7*
Tf saturation, %	48.95 ± 2.59	35.85 ± 2.16*	55.75 ± 2.33*
Liver iron, nmol/kg	1.89 ± 0.25	1.64 ± 0.34	1.62 ± 0.46

Serum and tissue iron parameters obtained from 10-week-old WT, RBC6 (*Tfrc*<sup>+L645R</sup>), and RBC21 (*Tfrc*<sup>+R654H</sup>) mice. Two-tailed Student *t* test was used to compare values with WT.

TIBC, total iron binding capacity.

\**P* < .05.

concentrations in either mutant strain (Table 5). Consequently, the reduced MCV and mean corpuscular hemoglobin persisted in both *Tfrc*<sup>+L645R</sup> and *Tfrc*<sup>+R654H</sup> mice (Table 5). Taken together, these results indicate that microcytic, hypochromic anemia caused by *Tfrc* mutations is nonresponsive to iron replacement therapy, regardless of CD71 expression (*Tfrc*<sup>+L645R</sup>) or endocytic function (*Tfrc*<sup>+R654H</sup>).

## Discussion

We conducted a genome-wide ENU mutagenesis screen to identify novel regulators of erythropoiesis in mice. Here, we describe a series of autosomal-dominant mutations of the *Tfrc* gene. The phenotype in each case was microcytic hypochromic anemia. Of the 6 unique *Tfrc* mutants identified, the RBC21 strain (*Tfrc*<sup>+R654H</sup>) displayed a distinct phenotype, including sustained erythroblast CD71 expression and delayed homozygous lethality. This study offers a broader examination of hematological and developmental phenotypes caused by autosomal-dominant *Tfrc* mutations, as well proposed pathological mechanisms underlying those phenotypes.

Receptor-mediated endocytosis of the Tf-TfR complex is the key mechanism by which cells, particularly erythroblasts, obtain iron. Extensive studies in vitro have identified key motifs within the extracellular helical domain of the receptor (exons 17-19) that are indispensable for ligand binding and function.<sup>5,6</sup> Studies of microcytic mice harboring point substitutions and deletions within *Tfrc*, including those identified in ENU mutagenesis screens,<sup>1,8,16</sup> or mutations in upstream factors regulating TfR transcription<sup>19,20</sup> typically reported a microcytic, hypochromic phenotype because of haploinsufficiency of the receptor. Through crystal structure modeling and CD71 flow cytometry, we found the *Tfrc*<sup>+R654H</sup> mouse strain expressed a stable mutant protein at the cell surface. This provided a unique opportunity to study the consequences of defective TfR ligand binding and its effect on erythropoiesis and development in vivo.

The R654 amino acid (human equivalent, R651) is a key Tf binding hotspot within the TfR, the loss of which has been shown to severely diminish the Tf, but not HFE, binding affinity of the receptor.<sup>1,10</sup> The use of novel cytometric tools, such as the Amnis ImageStreamX flow imager, provided visual and quantitative evidence of the importance of this binding site in iron transport and metabolism and

**Table 4. Full blood examination of fetal liver-transplanted mice**

	Mean ± SD	
	WT	<i>Tfrc</i> <sup>R654H/R654H</sup>
RBCs, × 10 <sup>12</sup> /L	11.72 ± 1.4	4.46
Hb, g/dL	15.4 ± 0.7	6.6
HCT, %	52.6 ± 3.2	17.5
MCV, fL	45.1 ± 2.9	35.9
MCH, pg	13.6 ± 1.3	14.8
MCHC, g/dL	30.1 ± 1.5	37.7
RDW, %	19.5 ± 1.6	20.0
<b>WBCs, × 10<sup>9</sup>/L</b>	9.80 ± 0.9	5.66
Lymphocytes, %	78.9 ± 2.4	62.7
Platelets, × 10 <sup>9</sup> /L	970 ± 269	>2972

Blood parameters obtained from mice 7 weeks posttransplantation after lethal irradiation and transplantation with either WT or homozygous (*Tfrc*<sup>R654H/R654H</sup>) E14.5 fetal liver cells.

ultimately demonstrated how a microcytic phenotype could persist in the *Tfrc*<sup>+R654H</sup> mutant despite sustained CD71 expression levels. Interestingly, the pattern of ineffective Tf-TfR uptake observed in *Tfrc*<sup>+R654H</sup> erythroblasts was comparable to a mouse model harboring a *Dnm2* mutation, displaying defects in endocytosis.<sup>8</sup> This suggested both Tf binding and receptor internalization were disrupted by the *Tfrc*<sup>R654H</sup> mutation; however, there may be additional disruptions to intracellular mechanisms contributing to the phenotype of the animal. Indeed, other aspects of receptor-mediated endocytosis and endosomal iron transport could be further investigated using this method, because many intracellular erythroid metabolic programs remain poorly described.

Surprisingly, and in contrast to other mutants described here, *Tfrc*<sup>R654H/R654H</sup> embryos survived until late embryogenesis, enabling the study of the requirements of *Tfrc* during development. Early embryonic lethality of homozygotes previously prevented these observations.<sup>8,16,20</sup> Aside from the profound anemia and tissue hypoxia, gross malformations of the brain and craniofacial regions seen in E14.5 to E18.5 homozygotes and double *Tfrc*<sup>L645R/R654H</sup> heterozygous embryos are consistent with previous reports that TfR cycling has a prominent role in neurological development.<sup>1</sup> The opportunity to perform fetal liver transplantations using *Tfrc*<sup>R654H/R654H</sup> cells allowed further assessment of the function of this *Tfrc* allele in adult hematopoiesis. Although homozygosity of the *Tfrc*<sup>R654H</sup> mutation was ultimately incompatible with life, blood values of the long-surviving transplant recipient suggested reconstitution of nonerythroid cell lineage populations was still possible in the absence of TfR cycling. Lymphocyte development, for instance, may use alternative uptake pathways when TfR-mediated endocytosis is inefficient, given the observed role of iron in lymphoid maturation.<sup>21</sup>

Iron studies performed on *Tfrc*<sup>+R654H</sup> and *Tfrc*<sup>+L645R</sup> mice were normal except for Tf saturation, which was slightly elevated in the *Tfrc*<sup>+R654H</sup> strain. This may be linked to CD71 expression status. Red-cell ferritin proved to be the most informative indicator of an iron metabolic defect in *Tfrc* mutants, which did not respond to iron dextran administration. Red-cell ferritin is frequently used to identify cellular iron deficits in microcytic mice when serum markers appear normal<sup>8,22</sup> and has been shown to be more informative

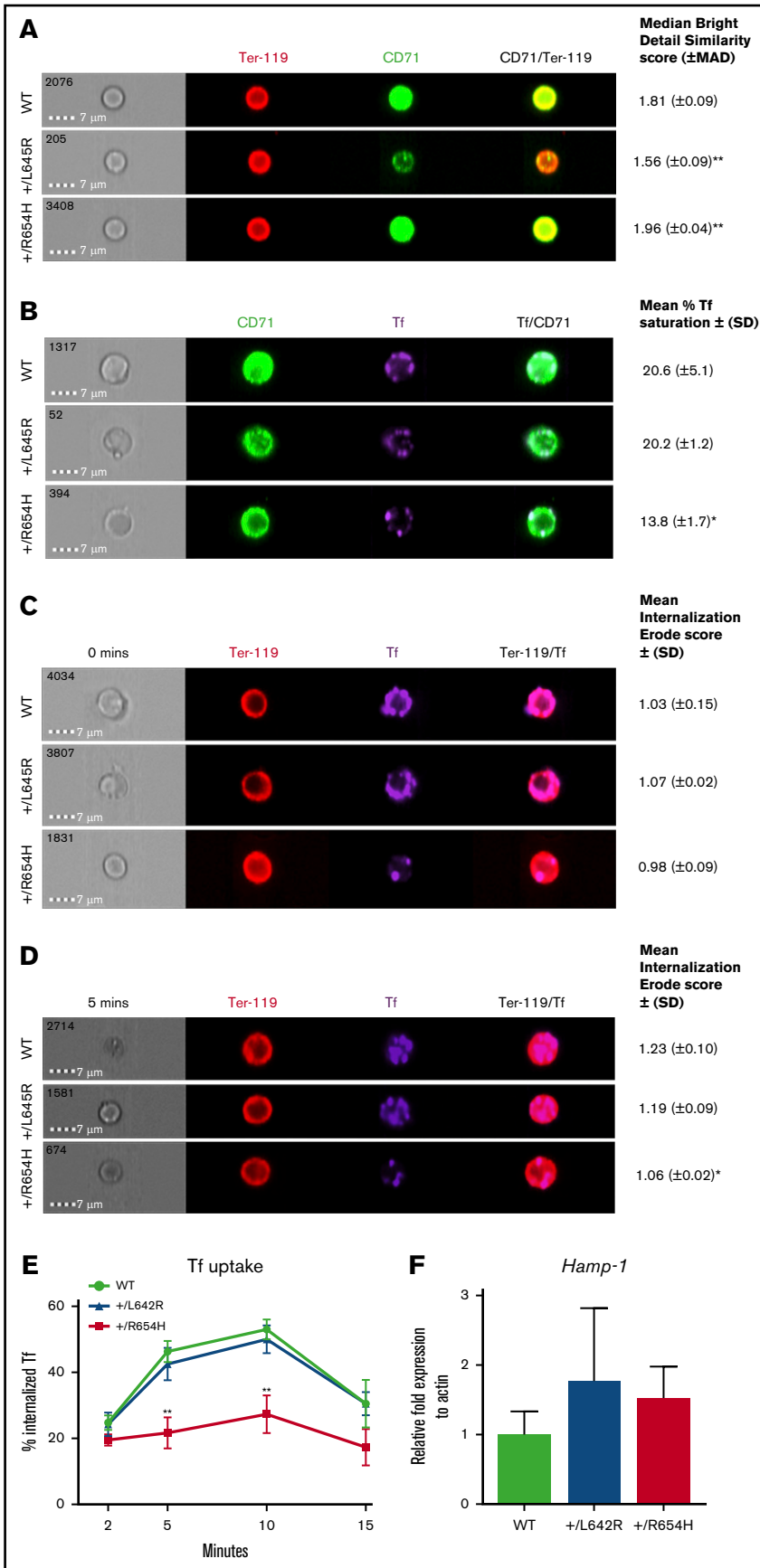


**Figure 3. Analysis of TfR binding and internalization using Amnis flow imaging cytometry.** (A) CD71/Ter-119 colocalization imaging of erythroblasts obtained from the bone marrow of WT, RBC6 (*Tfrc*<sup>+/L645R</sup>), and RBC21 (*Tfrc*<sup>+/R654H</sup>) mice. Intensity of CD71/Ter-119 overlap (yellow) generates the median bright detail similarity score. (B) Tf/CD71 colocalization imaging of erythroblasts from the 3 cohorts. Intensity of Tf/CD71 overlap (pale blue) generates the median bright detail similarity score, which is normalized to generate the mean percentage of Tf saturation. (C) Tf/Ter-119 internalization imaging of erythroblasts from each cohort at 0 minutes (before initiation of endocytosis). The mean internalization erode score of Tf uses Ter-119 as the mask. (D) Tf/Ter-119 internalization imaging of erythroblasts from each cohort at 5 minutes postinitiation of endocytosis. All scores represent 2000 Ter-119<sup>+</sup> events captured in each cohort. (E) Total time course of Tf uptake, via endocytosis, calculated in Ter-119<sup>+</sup> erythroblasts from each cohort. Mean  $\pm$  (SD) shown in error bars. (F) Quantitative real-time polymerase chain reaction of liver *Hamp-1* messenger RNA expression in each cohort. Mean  $\pm$  (SD) shown (n = 6). \**P* < .05, \*\**P* < .01. MAD, median average deviation.

**Table 5. Iron studies of *Tfrc*<sup>+ /L645R</sup> and *Tfrc*<sup>+ /R654H</sup> mice after iron (dextran) treatment**

	Mean ± SD		
	WT	<i>Tfrc</i> <sup>+ /L645R</sup>	<i>Tfrc</i> <sup>+ /R654H</sup>
Serum Tf, g/L	9.33 ± 2.44	8.22 ± 0.55	8.23 ± 3.90
Serum ferritin, µg/L	3427 ± 445	3220 ± 315	3939 ± 567
RBC ferritin, µg/L	148.2 ± 3.68	27.80 ± 7.9*	38.64 ± 5.63*
Serum iron, µmol/L	83.90 ± 9.91	77.03 ± 17.4	78.80 ± 2.59
TIBC, µmol/L	89.06 ± 12.1	79.04 ± 21.4	86.73 ± 15.6
Tf saturation, %	71.28 ± 15.1	64.2 ± 19.8	82.37 ± 19.8
Liver iron, nmol/kg	2.81 ± 0.73	3.72 ± 1.37	2.69 ± 0.54
MCV, fL	48.0 v 2.5	39.5 ± 1.5*	35.7 ± 1.6*
MCH, pg	14.7 ± 0.42	12.4 ± 0.51*	11.2 ± 0.25*

Blood and tissue iron parameters obtained from 10-week-old WT, RBC6 (+/L645R), and RBC21 (+/R654H) mice, 3 weeks after a single intraperitoneal injection of iron dextran. Two-tailed Student *t* test was used to compare values with the WT.

\**P* < .05.

than ZnPP/heme ratios, for example.<sup>8</sup> However, intraerythrocytic ferritin is not a typical clinical test of iron deficiency anemia.<sup>23</sup> Despite the obvious defect in iron uptake by red cells, the predominant red-cell phenotype was microcytosis in the absence of hypochromia. This suggests that isolated microcytosis may be due to inherited defects in the TfR. Although mutations within the *TFRC* gene have not yet been associated with microcytosis in humans, the inclusion of intracellular iron measurements may prove to be highly valuable in the search for congenital mutations within iron internalization pathways, particularly in cases when iron therapy has failed. A greater understanding of the phenotypical characteristics associated with congenital iron metabolic defects in animal models, along with the development of novel tools and markers of iron deficiency, will progressively contribute to better clinical

## References

1. Levy JE, Jin O, Fujiwara Y, Kuo F, Andrews NC. Transferrin receptor is necessary for development of erythrocytes and the nervous system. *Nat Genet.* 1999;21(4):396-399.
2. Marsee DK, Pinkus GS, Yu H. CD71 (transferrin receptor): an effective marker for erythroid precursors in bone marrow biopsy specimens. *Am J Clin Pathol.* 2010;134(3):429-435.
3. Chen K, Liu J, Heck S, Chasis JA, An X, Mohandas N. Resolving the distinct stages in erythroid differentiation based on dynamic changes in membrane protein expression during erythropoiesis. *Proc Natl Acad Sci USA.* 2009;106(41):17413-17418.
4. West AP Jr, Bennett MJ, Sellers VM, Andrews NC, Enns CA, Bjorkman PJ. Comparison of the interactions of transferrin receptor and transferrin receptor 2 with transferrin and the hereditary hemochromatosis protein HFE. *J Biol Chem.* 2000;275(49):38135-38138.
5. Giannetti AM, Bjorkman PJ. HFE and transferrin directly compete for transferrin receptor in solution and at the cell surface. *J Biol Chem.* 2004;279(24):25866-25875.
6. Cheng Y, Zak O, Aisen P, Harrison SC, Walz T. Structure of the human transferrin receptor-transferrin complex. *Cell.* 2004;116(4):565-576.
7. Aisen P. Transferrin receptor 1. *Int J Biochem Cell Biol.* 2004;36(11):2137-2143.
8. Brown FC, Collett M, Tremblay CS, et al. Loss of dynamin 2 GTPase function results in microcytic anaemia. *Br J Haematol.* 2017;178(4):616-628.
9. Ponka P, Lok CN. The transferrin receptor: role in health and disease. *Int J Biochem Cell Biol.* 1999;31(10):1111-1137.
10. Schmidt PJ, Toran PT, Giannetti AM, Bjorkman PJ, Andrews NC. The transferrin receptor modulates Hfe-dependent regulation of hepcidin expression. *Cell Metab.* 2008;7(3):205-214.
11. Gao J, Chen J, Kramer M, Tsukamoto H, Zhang AS, Enns CA. Interaction of the hereditary hemochromatosis protein HFE with transferrin receptor 2 is required for transferrin-induced hepcidin expression. *Cell Metab.* 2009;9(3):217-227.

management strategies for patients with unresolved microcytic anemias.

## Acknowledgments

The authors thank Rust Turakolov and Matthew Tinning at the Australian Genome Research Facility for their contributions to gene sequencing and bioinformatics, as well as support from the Australian Phenomics Network. The authors also thank Eva Orlowski and Alfred Medical Research and Education Precinct FlowCore for cytometry services and the Animal Research Laboratory (Monash University) and its technicians for animal husbandry.

This work was supported in part by Project Grant #382900 (S.M.J. and D.J.C.) and Program Grant #1016647 (B.T.K.) and Independent Research Institutes Infrastructure Support Scheme Grant #361646 (B.T.K.) from the Australian National Health and Medical Research Council and a Viertel Senior Medical Research Fellowship (D.J.C.).

## Authorship

Contribution: A.J.C., F.C.B., B.T.K., and D.J.C. designed and performed experiments; G.R. designed mutagenesis screens; C.J.M. prepared structural models; A.J.C., F.C.B., S.M.J., and D.J.C. prepared the manuscript; and all authors reviewed the manuscript.

Conflict-of-interest disclosure: The authors declare no competing financial interests.

ORCID profiles: A.J.C., 0000-0002-9000-7366; F.C.B., 0000-0001-9711-9769; B.T.K., 0000-0002-8836-8947; C.J.M., 0000-0001-5452-5193; S.M.J., 0000-0002-1045-0481; D.J.C., 0000-0001-9497-0996.

Correspondence: David J. Curtis, Australian Centre for Blood Diseases, Central Clinical School, Monash University, Level 1, Alfred Centre, 99 Commercial Rd, Melbourne, VIC 3004, Australia; e-mail: david.curtis@monash.edu.

12. Fleming RE. Iron sensing as a partnership: HFE and transferrin receptor 2. *Cell Metab.* 2009;9(3):211-212.
13. Forejtíková H, Vieillevoye M, Zermati Y, et al. Transferrin receptor 2 is a component of the erythropoietin receptor complex and is required for efficient erythropoiesis. *Blood.* 2010;116(24):5357-5367.
14. Jabara HH, Boyden SE, Chou J, et al. A missense mutation in TFRC, encoding transferrin receptor 1, causes combined immunodeficiency. *Nat Genet.* 2016;48(1):74-78.
15. Hershko C, Camaschella C. How I treat unexplained refractory iron deficiency anemia. *Blood.* 2014;123(3):326-333.
16. Lelliott PM, McMorrán BJ, Foote SJ, Burgio G. Erythrocytic iron deficiency enhances susceptibility to plasmodium chabaudi infection in mice carrying a missense mutation in transferrin receptor 1. *Infect Immun.* 2015;83(11):4322-4334.
17. Brown FC, Scott N, Rank G, et al. ENU mutagenesis identifies the first mouse mutants reproducing human  $\beta$ -thalassemia at the genomic level. *Blood Cells Mol Dis.* 2013;50(2):86-92.
18. Rank G, Sutton R, Marshall V, et al. Novel roles for erythroid ankyrin-1 revealed through an ENU-induced null mouse mutant. *Blood.* 2009;113(14):3352-3362.
19. Galy B, Ferring D, Minana B, et al. Altered body iron distribution and microcytosis in mice deficient in iron regulatory protein 2 (IRP2). *Blood.* 2005;106(7):2580-2589.
20. Zhu BM, McLaughlin SK, Na R, et al. Hematopoietic-specific Stat5-null mice display microcytic hypochromic anemia associated with reduced transferrin receptor gene expression. *Blood.* 2008;112(5):2071-2080.
21. Ned RM, Swat W, Andrews NC. Transferrin receptor 1 is differentially required in lymphocyte development. *Blood.* 2003;102(10):3711-3718.
22. Brown RG. Determining the cause of anemia. General approach, with emphasis on microcytic hypochromic anemias. *Postgrad Med.* 1991;89(6):161-164, 167-170.
23. Lopez A, Cacoub P, Macdougall IC, Peyrin-Biroulet L. Iron deficiency anaemia. *Lancet.* 2016;387(10021):907-916.

---

## Discussion and future directions

This thesis focused on the characterisation and phenotypic investigations of ENU mutagenesis mouse strains harbouring inheritable defects in erythropoiesis. Three unique mouse models were characterised in this study: RBC16, RBC19, and RBC21. Each harboured a random, chemically-induced mutation in a gene that was shown to be vital for red blood cell development or function, resulting in either a microcytic or macrocytic red cell phenotype. Through next-generation sequencing, particularly WES, we successfully identified the causative mutation in each strain and demonstrated its pathological role in the observed phenotypes of these RBC mutants. Lastly, we investigated the possible clinical relevance of these mutant mice and made a number of translatable observations which could impact the future diagnosis and treatment of human red cell diseases.

Three unique research articles, either published or in submission to peer-reviewed scientific journals, were generated from this thesis, each of which addressed this project's hypotheses, aims, and expected outcomes. These articles demonstrated the power of forward genetics in the identification of novel genes or alleles governing biological systems, such as erythropoiesis, and also validated ENU as a suitable tool for the generation of animal models that recapitulate human diseases. Two models of human congenital red cell defects were generated through this project, one of which proved to be the first of its kind described in literature (RBC16, reference 54), and another for which no treatment or rescue study had been previously trialled *in vivo* (RBC19, reference 55). Future investigations of these models may result in the identification of novel therapeutic targets or clinical treatments for their respective diseases, both of which (hereditary coproporphyrinuria, and TPI

deficiency, respectively) currently lack adequate long-term management strategies for patients. The heterogeneity of HCP and the lack of genotype-phenotype relationship in patients remains a significant hurdle in developing suitable therapies that effectively target the haem synthesis pathway. Animal models that recapitulate the biochemical abnormalities of the human condition, as witnessed in the RBC16 strain, will be instrumental in measuring the effectiveness of novel drugs or inhibitors that will likely emerge in the near future. In the case of TPI deficiency, the severity and lethality of the disease highlights the immediate need to invest in translatable research using adequate animal models. RBC19 provided the fundamental evidence that transplantation may be a viable treatment option for patients, which is yet to be explored clinically. The third mutant (RBC21, reference 56), while not a model of a known human disease, offered new insights into the phenotypic variations that we now know exist amongst mice harbouring *Tfrc* mutations. Since iron deficiency is the most prevalent cause of microcytosis in the global population, understanding the complex intracellular mechanisms of the iron metabolism pathway is key to improving the diagnosis of non-dietary causes of iron deficiency in patients. To date, many intracellular red cell pathways, such as the internalisation and trafficking of iron, remain poorly explored. The wider incorporation of new technologies (Amnis) will also improve our understanding of these elusive molecular mechanisms.

The completed investigations outlined in this thesis, demonstrated in the form of three unique published/submitted articles, collectively demonstrate significant additions to our understanding of the genetic regulators of erythropoiesis, as well as the underlying molecular mechanisms of selective human red cell diseases. As congenital red cell defects remain a substantial global health burden, the establishment of animal models that phenotypically recapitulate human diseases, through methods such as ENU mutagenesis, will continue to play a vital role in the understanding of disease pathogenesis and erythroid developmental pathways.

---

## References

*Note: To avoid repetition, references cited within the published articles included in this thesis have been omitted from this section.*

1. Ema H, Morita Y, Suda T. Heterogeneity and hierarchy of hematopoietic stem cells. *Exp. Hematol.* 2014 Feb 28;42(2):74-82.
2. Crisan M, Dzierzak E. The many faces of hematopoietic stem cell heterogeneity. *Development.* 2016 Dec 15;143(24):4571-81.
3. An X, Schulz VP, Li J, Wu K, Liu J, Xue F, Hu J, Mohandas N, Gallagher PG. Global transcriptome analyses of human and murine terminal erythroid differentiation. *Blood.* 2014 May 29;123(22):3466-77.
4. Iscove NN, Sieber F, Winterhalter KH. Erythroid colony formation in cultures of mouse and human bone marrow: analysis of the requirement for erythropoietin by gel filtration and affinity chromatography on agarose-concanavalin A. *J. Cell Physiol.* 1974 Apr 1;83(2):309-20.
5. Moura IC, Hermine O, Lacombe C, Mayeux P. Erythropoiesis and transferrin receptors. *Curr. Opin. Hematol.* 2015 May 1;22(3):193-8.
6. Medvinsky AL, Dzierzak EA. Development of the definitive hematopoietic hierarchy in the mouse. *Dev. Comp. Immunol.* 1998 May 1;22(3):289-301.
7. Baron MH, Isern J, Fraser ST. The embryonic origins of erythropoiesis in mammals. *Blood.* 2012 May 24;119(21):4828-37.
8. Sankaran VG, Xu J, Ragozy T, Ippolito GC, Walkley CR, Maika SD, Fujiwara Y, Ito M, Groudine M, Bender MA, Tucker PW. Developmental and species-divergent globin switching are driven by BCL11A. *Nature.* 2009 Aug 27;460(7259):1093-7.
9. Bauer A, Tronche F, Wessely O, Kellendonk C, Reichardt HM, Steinlein P, Schütz G, Beug H. The glucocorticoid receptor is required for stress erythropoiesis. *Genes Dev.* 1999 Nov 15;13(22):2996-3002.

10. Pietrangelo A. Hereditary hemochromatosis—a new look at an old disease. *N. Engl. J. Med.* 2004 Jun 3;350(23):2383-97.
11. Clark SF. Iron deficiency anemia. *Nutr. Clin. Pract.* 2008 Apr;23(2):128-41.
12. Kosman DJ. Redox cycling in iron uptake, efflux, and trafficking. *J. Biol. Chem.* 2010 Aug 27;285(35):26729-35.
13. Mohandas N, Gallagher PG. Red cell membrane: past, present, and future. *Blood.* 2008 Nov 15;112(10):3939-48.
14. Muñoz M, Villar I, García-Erce JA. An update on iron physiology. *World J. Gastroenterol.* 2009 Oct 7;15(37):4617.
15. Cheng Y, Zak O, Aisen P, Harrison SC, Walz T. Structure of the human transferrin receptor-transferrin complex. *Cell.* 2004 Feb 20;116(4):565-76.
16. Goswami T, Andrews NC. Hereditary hemochromatosis protein, HFE, interaction with transferrin receptor 2 suggests a molecular mechanism for mammalian iron sensing. *J. Biol. Chem.* 2006 Sep 29;281(39):28494-8.
17. Ganz T. Heparin, a key regulator of iron metabolism and mediator of anemia of inflammation. *Blood.* 2003 Aug 1;102(3):783-8.
18. Jung G., Nemeth E. The erythroid factor erythroferrone and its role in iron homeostasis. *Blood.* 2013; 122(21): 4.
19. Muckenthaler MU, Galy B, Hentze MW. Systemic iron homeostasis and the iron-responsive element/iron-regulatory protein (IRE/IRP) regulatory network. *Annu. Rev. Nutr.* 2008 Aug 21;28:197-213.
20. Akin M, Atay E, Oztekin O, Karadeniz C, Karakus YT, Yilmaz B, Erdogan F. Responsiveness to parenteral iron therapy in children with oral iron-refractory iron-deficiency anemia. *Pediatr. Hematol. Oncol.* 2014 Feb 1;31(1):57-61.
21. Ponka P. Tissue-specific regulation of iron metabolism and heme synthesis: distinct control mechanisms in erythroid cells. *Blood.* 1997 Jan 1;89(1):1-25.
22. Moore MR. Biochemistry of porphyria. *Int. J. Biochem.* 1993 Oct 1;25(10):1353-68.
23. Mustajoki P, Nordmann Y. Early administration of heme arginate for acute porphyric attacks. *Arch. Internal Med.* 1993 Sep 13;153(17):2004-8.

24. Yasuda M, Gan L, Chen B, Kadirvel S, Yu C, Phillips JD, New MI, Liebow A, Fitzgerald K, Querbes W, Desnick RJ. RNAi-mediated silencing of hepatic *Alas1* effectively prevents and treats the induced acute attacks in acute intermittent porphyria mice. *Proc. Natl. Acad. Sci.* 2014 May 27;111(21):7777-82.
25. Stamatoyannopoulos G. Control of globin gene expression during development and erythroid differentiation. *Exp. Hematol.* 2005 Mar 31;33(3):259-71.
26. Weatherall DJ. The inherited diseases of hemoglobin are an emerging global health burden. *Blood.* 2010 Jun 3;115(22):4331-6.
27. Rees DC, Williams TN, Gladwin MT. Sickle-cell disease. *The Lancet.* 2010 Dec 17;376(9757):2018-31.
28. Mercer RW, Dunham PB. Membrane-bound ATP fuels the Na/K pump. Studies on membrane-bound glycolytic enzymes on inside-out vesicles from human red cell membranes. *J. Gen. Physiol.* 1981 Nov 1;78(5):547-68.
29. Sheetz MP, Singer SJ. On the mechanism of ATP-induced shape changes in human erythrocyte membranes. I. The role of the spectrin complex. *J. Cell Biol.* 1977 Jun 1;73(3):638-46.
30. Koralkova P, Solinge WW, Wijk R. Rare hereditary red blood cell enzymopathies associated with hemolytic anemia—pathophysiology, clinical aspects, and laboratory diagnosis. *International journal of laboratory hematology.* 2014 Jun 1;36(3):388-97.
31. Lunt SY, Vander Heiden MG. Aerobic glycolysis: meeting the metabolic requirements of cell proliferation. *Annu. Rev. Cell Dev. Biol.* 2011 Nov 10;27:441-64.
32. Cappellini MD, Fiorelli GE. Glucose-6-phosphate dehydrogenase deficiency. *The Lancet.* 2008 Jan 11;371(9606):64-74.
33. Orosz F, Oláh J, Ovádi J. Triosephosphate isomerase deficiency: new insights into an enigmatic disease. *Biochim. Biophys. Acta.* 2009 Dec 31;1792(12):1168-74.
34. Sazawal S, Dhingra U, Dhingra P, Dutta A, Shabir H, Menon VP, Black RE. Efficiency of red cell distribution width in identification of children aged 1-3 years with iron deficiency anemia against traditional hematological markers. *BMC Pediatr.* 2014 Jan 15;14(1):8.
35. Sankaran VG, Ghazvinian R, Do R, Thiru P, Vergilio JA, Beggs AH, Sieff CA, Orkin SH, Nathan DG, Lander ES, Gazda HT. Exome sequencing identifies *GATA1* mutations resulting in Diamond-Blackfan anemia. *J. Clin. Investig.* 2012 Jul 2;122(7):2439.

36. Chinwalla AT, Cook LL, Delehaunty KD, Fewell GA, Fulton LA, Fulton RS, Graves TA, Hillier LW, Mardis ER, McPherson JD, Miner TL. Initial sequencing and comparative analysis of the mouse genome. *Nature*. 2002 Dec 5;420(6915):520-62.
37. Capecchi MR. Targeted gene replacement. *Sci. Am.* 1994 Mar 1;270(3):52-9.
38. Russell WL, Kelly EM, Hunsicker PR, Bangham JW, Maddux SC, Phipps EL. Specific-locus test shows ethylnitrosourea to be the most potent mutagen in the mouse. *Proc. Natl. Acad. Sci.* 1979 Nov 1;76(11):5818-9.
39. Cattanach BM, Burtenshaw MD, Rasberry C, Evans EP. Large deletions and other gross forms of chromosome imbalance compatible with viability and fertility in the mouse. *Nat. Gen.* 1993 Jan 1;3(1):56-61.
40. Justice MJ, Noveroske JK, Weber JS, Zheng B, Bradley A. Mouse ENU mutagenesis. *Hum. Mol. Genet.* 1999 Jan 1;8(10):1955-63.
41. Takahasi KR, Sakuraba Y, Gondo Y. Mutational pattern and frequency of induced nucleotide changes in mouse ENU mutagenesis. *BMC Mol. Biol.* 2007 Jun 20;8(1):52.
42. Toye AA, Moir L, Hugill A, Bentley L, Quarterman J, Mijat V, Hough T, Goldsworthy M, Haynes A, Hunter AJ, Browne M. A new mouse model of type 2 diabetes, produced by N-ethyl-nitrosourea mutagenesis, is the result of a missense mutation in the glucokinase gene. *Diabetes*. 2004 Jun 1;53(6):1577-83.
43. Lewis MA, Quint E, Glazier AM, Fuchs H, De Angelis MH, Langford C, Van Dongen S, Abreu-Goodger C, Piipari M, Redshaw N, Dalmay T. An ENU-induced mutation of miR-96 associated with progressive hearing loss in mice. *Nat. Gen.* 2009 May 1;41(5):614-8.
44. Greth A, Lampkin S, Mayura-Guru P, Rodda F, Drysdale K, Roberts-Thomson M, McMorran BJ, Foote SJ, Burgio G. A novel ENU-mutation in ankyrin-1 disrupts malaria parasite maturation in red blood cells of mice. *PLoS One*. 2012 Jun 19;7(6):e38999.
45. Aigner B, Rathkolb B, Klempt M, Wagner S, Michel D, Klaften M, Laufs J, Schneider B, Sedlmeier R, De Angelis MH, Wolf E. Generation of N-ethyl-N-nitrosourea-induced mouse mutants with deviations in hematological parameters. *Mamm. Genome*. 2011 Oct 1;22(9-10):495.
46. Oliver PL, Davies KE. Analysis of human neurological disorders using mutagenesis in the mouse. *Clin. Sci.* 2005 May 1;108(5):385-97.

47. Kiernan AE, Erven A, Voegelings S, Peters J, Nolan P, Hunter J, Bacon Y, Steel KP, Brown SD, Guénet JL. ENU mutagenesis reveals a highly mutable locus on mouse Chromosome 4 that affects ear morphogenesis. *Mamm. Genome*. 2002 Mar 1;13(3):142-8.
48. Davis AP, Woychik RP, Justice MJ. Effective chemical mutagenesis in FVB/N mice requires low doses of ethylnitrosourea. *Mamm. Genome*. 1999 Mar 21;10(3):308-10.
49. Rank G, Sutton R, Marshall V, Lundie RJ, Caddy J, Romeo T, Fernandez K, McCormack MP, Cooke BM, Foote SJ, Crabb BS. Novel roles for erythroid Ankyrin-1 revealed through an ENU-induced null mouse mutant. *Blood*. 2009 Apr 2;113(14):3352-62.
50. Brown FC, Scott N, Rank G, Collinge JE, Vadolas J, Vickaryous N, Whitelaw N, Whitelaw E, Kile BT, Jane SM, Curtis DJ. ENU mutagenesis identifies the first mouse mutants reproducing human  $\beta$ -thalassaemia at the genomic level. *Blood Cells Mol. Dis*. 2013 Feb 28;50(2):86-92.
51. Brown, F.C., Collett, M., Tremblay, C.S., Rank, G., De Camilli, P., Booth, C.J., Bitoun, M., Robinson, P.J., Kile, B.T., Jane, S.M. and Curtis, D.J., 2017. Loss of Dynamin 2 GTPase function results in microcytic anaemia. *British Journal of Haematology*.
52. Brown FC, Conway AJ, Cerruti L, Collinge JE, McLean C, Wiley JS, Kile BT, Jane SM, Curtis DJ. Activation of the erythroid K-Cl cotransporter Kcc1 enhances sickle cell disease pathology in a humanized mouse model. *Blood*. 2015 Dec 24;126(26):2863-70.
53. Tremblay CS, Brown FC, Collett M, Saw J, Chiu SK, Sonderegger SE, Lucas SE, Alserihi R, Chau N, Toribio ML, McCormack MP. Loss-of-function mutations of Dynamin 2 promote T-ALL by enhancing IL-7 signalling. *Leukemia*. 2016 Oct 1;30(10):1993-2001.
54. Conway AJ, Brown FC, Fullinaw RO, Kile BT, Jane SM, Curtis DJ. A mouse model of hereditary coproporphyrinemia identified in an ENU mutagenesis screen. *Dis. Models Mech*. 2017 Aug 1;10(8):1005-13.
55. Conway AJ, Brown FC, Burgio G, Morton CJ, Jane SM, Curtis DJ. Bone marrow transplantation corrects haemolytic anaemia in a novel ENU mutagenesis model of TPI deficiency. *Disease Models and Mechanisms*, 2018 Apr 18 11(5).
56. Conway AJ, Brown FC, Rank G, Kile BT, Morton CJ, Jane SM, Curtis DJ. Characterization of *Tfr*-mutant mice with microcytic phenotypes. *Blood Advances*, 2018 Aug 9 2(15).

57. Socolovsky, M., Nam, H.S., Fleming, M.D., Haase, V.H., Brugnara, C. and Lodish, H.F., 2001. Ineffective erythropoiesis in Stat5a<sup>-/-</sup> 5b<sup>-/-</sup> mice due to decreased survival of early erythroblasts. *Blood*, 98(12), pp.3261-3273.